

Department of Precision and Microsystems Engineering

Incorporating AM-specific Manufacturing Constraints into Topology Optimization

M. Reuben Serphos

Report no : EM 2014.011
Coaches : Dr.ir. M. Langelaar (TU Delft)
: Dr. J. Fatemi, MSc (Dutch Space)
Professor : Prof.dr.ir. F. van Keulen (TU Delft)
Specialisation : Engineering Mechanics
Type of report : MSc Thesis
Date : 30 May 2014

Incorporating AM-specific Manufacturing Constraints into Topology Optimization

MASTER OF SCIENCE THESIS

For the degree of Master of Science in Mechanical Engineering at Delft
University of Technology

M. Reuben Serphos

May 30, 2014

Faculty of Mechanical, Maritime and Materials Engineering (3mE) · Delft University of
Technology

About the cover:

A close up of a lightweight titanium lattice ball manufactured using the Additive Manufacturing or 3D printing process. This design is a good example of AM capabilities: these hollow balls possessing a complex external geometry could not have been manufactured in a single part using a conventional manufacturing process. But they are incredibly light while also stiff, opening up possibilities for future space applications.

Photo and description: ESA



The work in this thesis was supported by Dutch Space B.V. Their cooperation is hereby gratefully acknowledged.



Engineering Mechanics
All rights reserved.

Copyright © Precision and Microsystems Engineering -

Abstract

Designs to be manufactured by Additive Manufacturing (AM) are subject to geometrical restrictions which are necessary to guarantee successful production. This makes it necessary to modify the obtained topology optimized design such that it is manufacturable. By doing this the optimality of the structure can be reduced. To achieve a manufacturable design directly from the topology optimization requires the incorporation of such a geometrical restriction directly into the optimization process. This research has been carried out to develop a method to do so.

The manufacturing constraint being implemented is that a structure should be self-supporting. For this to be the case overhanging features in the design must be at an angle of at least 45 degrees with respect to the base plate.

Three approaches have been formulated and investigated: (1) a multiple objective, (2) global constraint and (3) a density filter. A global measure has been formulated for the multiple objective and the global constraint and a filtering scheme for the density filter. The three approaches have been implemented into a 2D optimization code written in MATLAB. Three predictable reference models have been used to test the suitability of each method.

The results show that the multiple objective and the global constraint remain potential candidates but further investigation is needed to determine proper parameter values. The topologies obtained with these approaches were modified to partially meet the manufacturing constraint but remained with overhanging features. The filtering method produced topologies that had no overhanging features. The design was a compromise between slight alterations and the introduction of support structures. This approach however showed instabilities that are directly linked to the proposed filtering scheme. True convergence was not achieved with any of the approaches.

The filtering approach provides a proof of concept for the inclusion of the 45 degree overhang restriction but further development is needed. The other two approaches are also potential candidates for inclusion of the restriction.

Table of Contents

Preface	xi
Acknowledgments	xiii
1 Introduction	1
1-1 The Antenna - Articulated Deployment System (A-ADS)	1
1-2 Benefiting from AM	2
1-3 Topology optimization	3
2 Problem and hypothesis	7
2-1 Problem description	7
2-2 A-ADS hinge-bracket	9
2-3 Summary	10
3 Method	11
3-1 Current status of commercial software	11
3-1-1 Hyperworks Optistruct	12
3-1-2 Simulia ATOM	12
3-2 Description 88-line MATLAB code	14
3-3 Set-up	14
3-4 Reference models	15
3-4-1 Cantilever beams	15
3-4-2 Tension beam	16

4	Formulation of the overhang restriction	19
4-1	Using the continuous nature of TO	19
4-2	Using the discrete nature of TO	20
4-3	Pragmatic approach	22
4-4	Restriction method	24
4-5	Local constraints	24
4-6	Multiple objective and global constraint	25
4-6-1	Multiple Objective	25
4-6-2	Multiple objective function sensitivities	28
4-6-3	Global constraint	30
4-7	Filter	30
4-7-1	Modification by sequential scanning	31
5	Validation	33
5-1	Validation of the multiple objective and global constraint	33
5-1-1	Parameters M , δ and p_n	34
5-1-2	Sensitivity check	41
5-2	Verification of filter formulation	44
5-2-1	Modification by sequential scanning	44
6	Notes on implementation	49
6-1	Element selection	49
6-2	Ghost-layers	50
6-3	Invalid values	50
6-4	Constraint in MMA	50
7	Final results	53
7-1	Multiple Objective	53
7-1-1	Cantilever beam corner-load	53
7-1-2	Cantilever beam mid-load	55
7-1-3	Tension beam	55
7-2	Global constraint	57
7-2-1	Cantilever beam corner-load	58
7-2-2	Cantilever beam mid-load	58
7-2-3	Tension beam	59
7-3	Filter	60
8	Discussion	63
8-1	Modification of strut orientation	63
8-2	Stalactites in multiple objective method and global constraint method	64
8-3	Erratic objective values, instability and Ω_{fac}	64
8-4	Lowered volume fraction and high compliance	65
8-5	Additional considerations	66

9 Conclusion	69
10 Recommendations	71
A A-ADS hinge-bracket	73
A-1 Design requirements	73
A-2 Circular in-plane torque	75
A-3 Circular out-of-plane torque	75
A-4 Hinge-bracket	76
B Another filter approach	79
B-1 Formulation of the filter - Modification by supportivity matrix	79
B-2 Validation - Modification by supportivity matrix	82
C Results	85
C-1 Multiple objective	85
C-1-1 Corner-loaded cantilever beam	85
C-1-2 Mid-loaded cantilever beam	89
C-1-3 Tension beam	92
C-2 Global constraint	96
C-2-1 Corner-loaded cantilever beam	96
C-2-2 Mid-loaded cantilever beam	99
C-2-3 Tension beam	102
C-3 Filter	105
C-3-1 Corner-loaded cantilever beam	105
C-3-2 Mid-loaded cantilever beam	105
C-3-3 Tension beam	105
Glossary	109
List of Acronyms	109
List of Symbols	109

List of Figures

1-1	A-ADS	2
1-2	Benefiting from AM	2
1-3	Schematic representation of the SLM process; Source: [1]	3
2-1	Schematic of overhanging surface	8
2-2	Various levels of curl occurring as a result of residual stress in increasingly overhanging material; Source: [2]	9
2-3	Sagging of material in vertically built holes; Source: [2]	9
2-4	Concept design produced by topology optimization	9
3-1	Response types Hyperworks Optistruct	12
3-2	Manufacturing constraints Hyperworks Optistruct Member size, stress, fatigue, draw direction, extrusion, symmetry and patterning	12
3-3	Response types Simulia ATOM	13
3-4	Manufacturing constraints Simulia ATOM Member size, draw direction, symmetry	13
3-5	Structured grid mesh	14
3-6	(Left) Load case cantilever beam mid-load and (right) the result with: Iterations: 121; Objective value: 57.17; Volume fraction: 0.418	16
3-7	(Left) Load case cantilever beam corner-load and (right) the result with: Iterations: 191; Objective value: 64.00; Volume fraction: 0.426	16
3-8	(Left) Load case tension beam and (right) the result with: Iterations: 1160; Objective value: 5.49; Volume fraction: 0.474	17
4-1	Gradient of density field	20
4-2	Local gradients in black and white topology represented by blue arrows	21
4-3	Discontinuous aspect of topology optimization showing candidate support elements	21
4-4	Example of P-norm behavior	22

4-5	(Left) Reference model corner-loaded cantilever beam and (right) result pragmatic approach for: mesh: 30x50; volume fraction: 0.5; filter penalization power: 3; radius: 1.5; Obtained objective after 49 iterations: 67.57; volume fraction: 0.421	23
4-6	(Left) Reference model corner-loaded cantilever beam for: mesh: 60x100; imposed volume fraction: ≤ 0.5 ; filter penalization power: 3; radius: 1.5; Obtained objective after 270 iterations: 62.69; volume fraction: 0.404 and (right) result pragmatic approach with: Obtained objective after 38 iterations: 67.23; volume fraction: 0.422	24
4-7	Value ρ_{Δ} with respect to ρ_{max} and ρ_i	26
4-8	Plot of the logistic function with x ranging from -1 to 1	27
4-9	Overhang with $M = 10$ and $\delta = 0,5$	27
4-10	Influenced elements for sensitivities	28
5-1	Standard geometry for verification	33
5-2	Exact OH detection in standard geometry	34
5-3	Approximate OH detection in standard geometry, with $M = 35$, $p_n = 8$ and $\delta = 0.2$	34
5-4	Logistic function for varying values of M	35
5-5	Ω_{tot} for parameter M from 10-100	36
5-6	Ω_{tot} for varying parameter δ	37
5-7	Ω^* for gradient geometry with $\delta = 0$ giving $\Omega_{tot} = 0.223$	38
5-8	Error due to P-norm	39
5-9	Ω_{tot} for varying P-norm power p_n	40
5-10	Minimum detectable ρ difference	42
5-11	Density of arbitrary element (in the center of the ring) is incrementally increased from 0 to 1	42
5-12	Comparison of the calculated and the finite difference sensitivity	43
5-13	Element to be varied and element of which the sensitivity is determined	44
5-14	Filtering the densities by sequential scanning of the elements	45
5-15	Effect of P-norm power on element density directly below overhang	46
5-16	Filtering the corner loaded cantilever beam by sequential scanning of the elements	46
5-17	Filtered densities for varying density of test element	47
5-18	Comparison of calculated and finite difference sensitivity	48
6-1	Candidate support elements for an element under inspection	49
6-2	Ghost-layer	50
7-1	Results multiple objective for cantilever corner-load obtained in 191 iterations	54
7-2	Ω^* multiple objective for cantilever corner-load; Using the following parameter values: $M = 35$; $\delta = 0.2$; $p_n = 8$	55
7-3	Results multiple objective for cantilever mid-load obtained in 121 iterations	56
7-4	Ω^* global constraint for cantilever mid-load; Using the following parameter values: $M = 35$; $\delta = 0.2$; $p_n = 8$	56
7-5	Results multiple objective for tension beam	57

7-6	Ω^* multiple objective for tension beam; Using the following parameter values: $M = 35; \delta = 0.2; p_n = 8$	57
7-7	Results global constraint for cantilever corner-load obtained in 191 iterations . . .	58
7-8	Ω^* global constraint for cantilever corner-load; Using the following parameter values: $M = 35; \delta = 0.2; p_n = 8$	58
7-9	Results cantilever mid-load obtained in 121 iterations	59
7-10	Ω^* global constraint for cantilever mid-load; Using the following parameter values: $M = 35; \delta = 0.2; p_n = 8$	59
7-11	Results tension beam obtained	60
7-12	Ω^* global constraint for tension beam; Using the following parameter values: $M = 35; \delta = 0.2; p_n = 8$	60
7-13	Results filter for cantilever corner-load	61
7-14	Results filter for cantilever mid-load	61
7-15	Results filter for tension beam	62
8-1	Stalactite formation	64
8-2	Cantilever beam corner-load with parameters $\delta = 0.2, M = 8, p_n = 8$ and $\Omega_{fac} = 10^3$	65
8-3	Extracting a black-white topology from the filter result	66
A-1	Schematic representation of the hinge-bracket	74
A-2	Load case circular in-plane torque (left) and result (right)	75
A-3	Load case circular out-of-plane torque (left) and result (right)	75
A-4	Load case of the hinge-bracket	77
A-5	Result of the hinge-bracket	78
B-1	Involved elements in determining the supportivity of an element ρ_0 . Numbers denote element numbers (not corresponding to actual numbering in the MATLAB code).	81
B-2	Filtering the densities using the supportivity matrix	83
B-3	Effect of P-norm power on the density of a element at the top of the structure	83
B-4	Filtering the corner loaded cantilever beam using the supportivity matrix	84

Preface

As long as I can remember I have had a great interest in all types of science, technology and mechanics in general and a desire to put this to practical use. The choice to study mechanical engineering has therefore always been obvious to me. Though besides this broad interest a more specific passion developed after visiting the Kennedy Space Center as a child. Discovering the vastness of what lies beyond Earth fascinated me. This sparked a passion for space exploration and space travel, finding new worlds and expanding humanities knowledge of the universe, which to this day has stuck with me.

This passion is what drove me to apply for a thesis topic at Dutch Space. The opportunity to apply what I had learned during my studies in a space technology oriented environment greatly enthused me.

In discussing possible topics, my supervisor from Dutch Space, Dr. J. Fatemi (MSc), proposed the design of a satellite part which was to be manufactured by Additive Manufacturing (AM). This immediately intrigued me. Taking part in the application of a new developing technology in a space oriented environment was an ideal combination of my interests and I am very grateful Dr. J. Fatemi (MSc) could give me this opportunity.

During the course of my literature survey it became clear that the project was going to be a bit more fundamental than anticipated. The literature survey revealed that design methodologies for AM were underdeveloped. Even though the use of topology optimization as a design tool for AM is widely agreed upon as being the way to go, the approach is not complete. The tool has not been tailored to the advantages and limitations of AM. This realization is what led to the final version of the research goal leading to the thesis that lies before you. It is a small step in the development of design tools specifically for AM and I hope it will lead to further developments in its field.

I am glad I got the opportunity to do this and am thankful to those who helped make it possible.

Acknowledgments

I would like to take the opportunity to thank the following people for helping me with my research and writing. First of all I would like to thank my professor Prof.dr.ir. F. van Keulen for giving me the opportunity to do this research. I am also grateful for the assistance given by Dr. ir. M. Langelaar whose feedback on ideas and drafts has been very valuable. A special thanks goes to Dr. J. Fatemi (MSc) for giving me guidance and providing a critical view of the steps made along the way. Advice given by Dr.ir. G. van der Veen has been a great help. I would like to express my gratitude to Dutch Space B.V for providing the facilities to work on my research at your company. I am thankful for the A-ADS team who welcomed me into the team and were always willing to provide me with information about the A-ADS project. The company of the interns that were part of the 'Skunk Works' group at Dutch Space has been much appreciated.

Finally I would like to thank my friends and family for their support and encouragement throughout this process.

Delft, University of Technology
May 30, 2014

M. Reuben Serphos

Chapter 1

Introduction

Currently Additive Manufacturing (AM) is making a growth spurt in terms of technological developments and its popularity is increasing. Due to the alternative manufacturing method, it introduces new possibilities and allows a new approach to mechanical design.

At Dutch Space B.V. the question has been posed as to whether this new manufacturing technology can be benefited from. It is then the goal to apply this such that new, innovative, superior metal products can be produced that have performance comparable to or exceeding that of the existing products and can then compete with products made of Carbon Fiber Reinforced Polymer (CFRP) in terms of performance and cost.

To investigate this an existing project had been selected for which one of the parts was to be designed with AM in mind. The project selected for this was the so-called Antenna - Articulated Deployment System (A-ADS).

1-1 The A-ADS

The A-ADS is a system designed to deploy large antennae dishes far away from the spacecraft (S/C) body. The system is to be stowed in a compact volume, once in orbit it is deployed by a deployment spring mechanism which locks into place upon full deployment. The system must then be pointed with considerable accuracy and errors due to environmental influences must be minimized (e.g. Thermo-elastic deformation (TED)).

The system consists of tubular CFRP booms which are connected by hinge-brackets that house the spring- and locking mechanism and the synchro-system (a cable system that ensures synchronous deployment of the booms). There will be several hinge-brackets on such a system. Figure 1-1 shows a schematic representation of the A-ADS. In this figure the connection on the far left (u-turn consisting of two 90° hinge-brackets) had originally been selected to serve as a test-case for application of AM. The goal was to design a hinge-bracket that would meet all necessary requirements with AM in mind as manufacturing method.

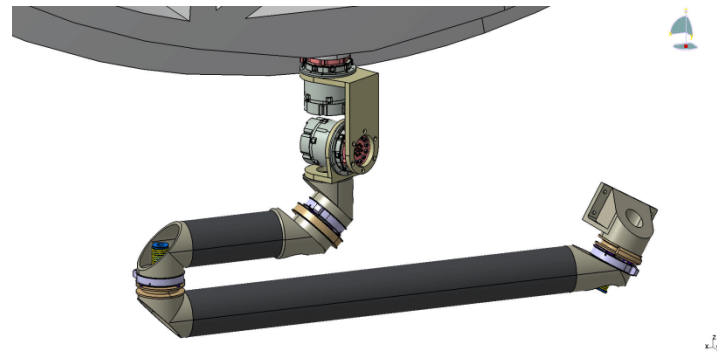


Figure 1-1: A-ADS

1-2 Benefiting from AM

In the literature survey related to this thesis [3] various methods of benefiting from AM were mentioned. A summary of the three most relevant methods for industrial applications is shown in Figure 1-2.

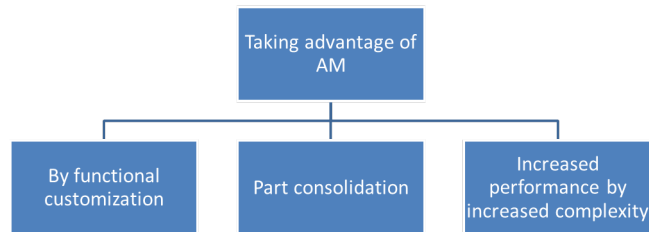


Figure 1-2: Benefiting from AM

Functional customization refers to the customization of designs by varying certain parameters so that the design can be applied in slightly different situations. For example in the case of the hinge-bracket, the same design could be used for a bracket under an angle of 45° instead of 90° . Then without having to make a new mold, as would be the case for a CFRP part, a 3D CAD design could simply be modified and manufactured.

The application of this does not require any drastic changes to the design or design methodology. It can be implemented in the design and manufacturing process in a straightforward manner. It is therefore not treated further in this study.

Part consolidation is the integration of multiple functions into one part. By doing this the number of parts in a product could be reduced resulting in lower assembly costs. By doing this the complexity of the part is increased, which for conventional methods would result in higher manufacturing costs, but for AM this is not the case.

There is no structured or systematic way to choose which components should or shouldn't be integrated.

The last route to take is increasing the performance of a part by increasing the complexity of the structure. Examples of this are using internal/cellular structures to create a lightweight yet stiff structure or the design of complex compliant mechanisms to create materials with mechanical behavior otherwise not found in monolithic materials.

Topology optimization is a method that accommodates this approach particularly well. It exploits the design freedom available to find structures that are optimized for certain behavior (for example a maximum stiffness). Topology optimization provides a systematic way of finding these designs.

In this study attention is focused on this last approach. It provides a measurable and structured means of design which is increasing its popularity in industry. It has been proven to be a promising tool for design and is a natural counterpart of AM.

Various AM methods exist each with their own advantages and disadvantages. A key difference between the various AM methods is the type of materials they can handle and how the material properties compare after manufacture to that of conventional manufacturing techniques. In [3] it was found that for metallic products requiring high mechanical performance the best method is a powder-bed fusion method. A powder-bed fusion method selectively melts or sinters powdered material together in a powder-bed (see Figure 1-3). Dutch Space has access to the powder-bed method Selective Laser Melting (SLM) which fully melts the powdered metal by laser layer-by-layer to form a product. This method has been shown to produce metal parts with the best mechanical properties compared to other AM methods and is therefore the most suitable for the manufacture of end-use parts in industry. For this reason SLM is the method of choice for this research.

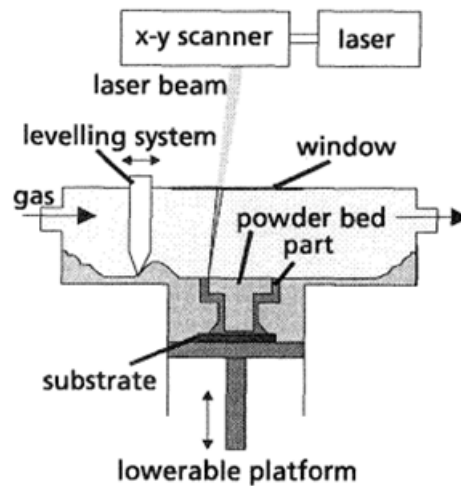


Figure 1-3: Schematic representation of the SLM process; Source: [1]

1-3 Topology optimization

Topology optimization is a computational method that explores various geometrical material lay-outs in a given design space until an optimal value for a given objective and constraints has

been found. This method is free of any geometrical restrictions (apart from the discretization resolution) unless explicitly imposed.

Two main approaches exist: the boundary evolution approach and the material distribution approach. The first takes some initial design as starting point and evolves it by varying the boundaries that describe it. In this case the parameters that describe the curve of the design boundary are the design variables. To be able to introduce holes special mechanisms must be built into the algorithm. Another boundary method that does not have this problem is the level set method. This method defines a so-called level set function which can be manipulated, but the result is only a level set (i.e. isoline) of the function, this way the boundary is manipulated but it is done implicitly.

The material distribution approach on the other hand starts by discretizing the design space and then varying the amount of material in each discretized sub-domain. In this case the variables are the amount of material in each sub-domain. In this approach the problem may be discrete or continuous in the sense that the variable may be limited to no material or maximum material (discrete) or intermediate densities are permitted (continuous). The latter is more common due to the awkwardness of discrete problem solving in numerical methods. Within this category are various methods of topology optimization e.g. ground structure method, varying sheet thickness, homogenization. The most common method used currently is the so-called Solid Isotropic Material Penalization (SIMP) or power-law approach. In this method the elements of the discretized design space are assigned a density which can be varied. The material properties being evaluated (in the case of compliance this would be the modulus of elasticity) are assumed to be proportional to this density.

In practice lay-outs with either full material density or void values are preferred since intermediate densities are difficult to manufacture. For this reason a penalization factor is introduced by raising the density to the power of this penalization factor. By doing this intermediate densities appear less efficient to the optimizer and are thus discouraged. Every iteration the topology is evaluated by a Finite Element Analysis (FEA). The optimization problem can then be solved by applying an optimization algorithm like the method of moving asymptotes, sequential quadratic programming or an optimality criterion update. Compliance minimization is one of the most common optimization problems solved with topology optimization applied for weight saving in various industries. A way to formulate this problem (for the SIMP method) is as follows:

$$\begin{aligned}
 \min_{\boldsymbol{\rho}} \quad & c(\boldsymbol{\rho}) = \mathbf{U}^T \mathbf{K} \mathbf{U} = \sum_{e=1}^N (\rho_e)^p \mathbf{u}_e^T \mathbf{k}_e \mathbf{u}_e \\
 \text{subject to} \quad & \mathbf{K} \mathbf{U} = \mathbf{F} \\
 & \frac{V(\boldsymbol{\rho})}{V_0} = f \\
 & \mathbf{0} < \boldsymbol{\rho}_{min} \leq \boldsymbol{\rho} \leq \mathbf{1}
 \end{aligned} \tag{1-1}$$

Where:

c = Compliance of the material lay-out

\mathbf{U} = Global displacement vector

\mathbf{F} = Force vector

\mathbf{K} = Global stiffness matrix

\mathbf{u}_e = Element displacement vector

\mathbf{k}_e =Element stiffness matrix

$\boldsymbol{\rho}$ =Vector of design variables

$\boldsymbol{\rho}_{min}$ =Vector of minimum relative densities

N =Number of elements used to discretize design domain

p =Penalization power

$V(\boldsymbol{\rho})$ =Material volume

V_0 =Design domain volume

f =Prescribed volume fraction

Loads to which the design will be subjected can be implemented in the force vector while displacement boundary conditions can be incorporated in the displacement vector. The objective function is subject to the constraints listed below it. The first constraint describes the equality condition that the material volume is the prescribed fraction (f) of the total design domain volume, i.e. the amount of volume to be distributed is predetermined. The second constraint is the mechanical equilibrium condition and the final line bounds the density such that it cannot become zero to avoid singularities and limits it to one, since this is of course maximum density.

The design space is discretized into a finite number of elements, which is referred to as the finite element mesh or mesh for short. Varying the number of these elements may have large effects on the obtained result and computation time; mesh-dependency. Mesh-dependence will generally result in increasingly finer structures, microstructures for example, as the mesh is refined. This is due to the fact that in general increasing the perimeter in a design for a fixed volume increases the efficiency (in terms of stiffness) of the material [4]. There are various techniques to limit this, for example [4] name the following techniques:

- Perimeter control, where a constraint is added to the problem limiting the total length of the perimeter of the design.
- Gradient methods, where for example the local density variation is constrained.
- Spatially filtering the density, which limits the density variations in the set of the admissible stiffness tensor, this in turn results in that the stiffness in a point depends on the density of all points in the neighborhood of that point.
- Spatially filtering of the sensitivities, which modifies the design sensitivity of a specific element based on the sensitivities in the area around that element.

Such a filter also prevents so-called checkerboarding. Checkerboarding is the occurrence of checkerboard patterned solutions in the topology. These patterns provide, especially for high penalization power values, a numerical work-around for intermediate densities. By checkerboarding a group of elements, the equivalent of all elements having half-density is achieved. An artificial stiffness is the result, since (depending on element type and mesh) the elements are only connected by their respective corners.

Problem and hypothesis

2-1 Problem description

Currently topology optimization is widely being used in the design process for products to be manufactured with Selective Laser Melting (SLM). Generally the ‘optimal’ design found is modified based on engineering judgment (using design rules and experience with the manufacturing process) such that it can be manufactured, i.e. complies with the manufacturing constraints of SLM. Such modifications are for example orienting the product such that build time is minimized while surface roughness (which is dependent on the orientation of the surface) is acceptable, building support structures to prevent material from sagging (due to melt pool properties, see Figure 2-3) or curling (due to residual stresses, see Figure 2-2) and ensuring that minimum achievable dimensions are not exceeded. Such factors as surface roughness and number of supports can have a large influence on the final cost of the product since these factors increase post-processing.

It has been suggested by [2] that to minimize post-processing designs should be self-supporting structures.

Some design rules for SLM are suggested by [2], a selection is presented here:

1. Minimum member size;/minimum wall thickness
2. Minimum slot size
3. Maximum member size
4. Restrict closed surfaces (to allow powder removal)
5. Overhang ≥ 45 degrees
6. Cost minimization by encouraging low build height
7. Cost minimization by minimizing the amount of support structures needed

The choice of the selection of rules above has been based on the observation that these rules form the basis for the other (non-selected) rules, e.g. allowable chamfer angle, adapted radii and holes. The maximum member size (3) does not originate directly from the design rules/criteria, but is rather based on a statement made in [5], namely that limiting the maximum member thickness could lead to an increase in the amount of members which would then result in less overhanging structures. Possibly, depending on the chosen parameters, this could also lead to the formation of cellular (lattice) structures, which might prove useful for lightweight structures.

As mentioned before (and can be found in [3]) structural elements where sagging or curling may occur require support structures. Such structural elements are referred to as overhang or an overhanging surface and is defined in this text as follows:

Overhang

When a surface is facing down and parallel to or inclined at an angle with respect to the base-plate.

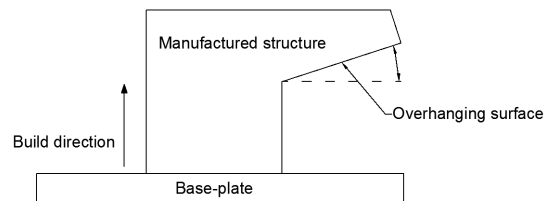


Figure 2-1: Schematic of overhanging surface

Up to an angle of 45° additional support-structures are needed. Thus in the design process overhanging structures inclined at an angle lower than 45° should either be avoided or support-structures will be needed. Alternatively support-structures may be incorporated in the design such that these do not need to be removed afterwards. Additionally the design could be oriented differently in the build chamber to alter the relative angles.

It is rather difficult, when dealing with complex designs, to judge whether the design should be modified (maybe resulting in lower performance) to be self-supporting, re-oriented, to introduce support-structures or some combination of this. The ability to do this well is limited by the creativity and experience of the engineer designing the product. There exists no guide as to when to choose one option or the other, while this restriction can have an extremely large influence on the topology of the design.

It is therefore the goal of this study to *incorporate this overhang restriction into the topology optimization*, thereby eliminating the variable of engineering experience and creativity offering a structured approach for the design for additive manufacturing (DfAM). By doing this the design process is also further streamlined since the step of design modification for Additive Manufacturing (AM) is eliminated.

There is even reason to believe that incorporating the restriction into the topology optimization may yield a design with superior performance to that found when not including the restriction. This behavior was seen to occur in [6] where the incorporation of a draw direction for casting resulted in a stiffer structure than the unrestricted optimization. Including a restriction may force the optimizer out of one local minimum into another or maybe even into a global minimum.

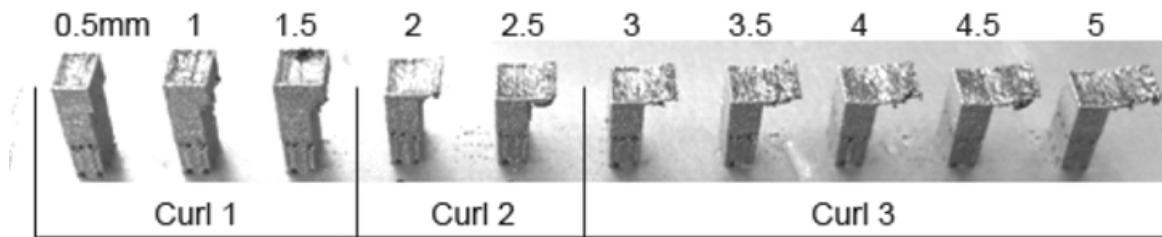


Figure 2-2: Various levels of curl occurring as a result of residual stress in increasingly overhanging material; Source: [2]

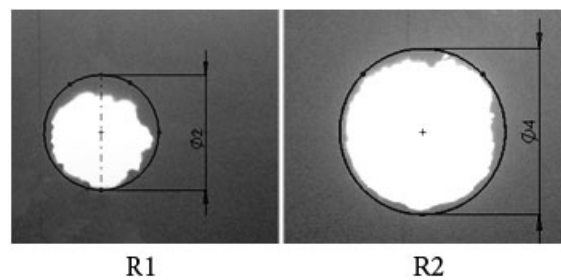


Figure 2-3: Sagging of material in vertically built holes; Source: [2]

2-2 A-ADS hinge-bracket

A simplified topology optimization problem was set-up to generate a concept for the Antenna - Articulated Deployment System (A-ADS) hinge-bracket. The objective was to minimize compliance. A description of the development of the problem can be found in Appendix A. The results are shown in Figure 2-4. In this figure only elements with a density of 0.9 or higher are shown to improve visibility. The wire frame box around the part indicates the design domain, the right image shows a cross-section of the part.

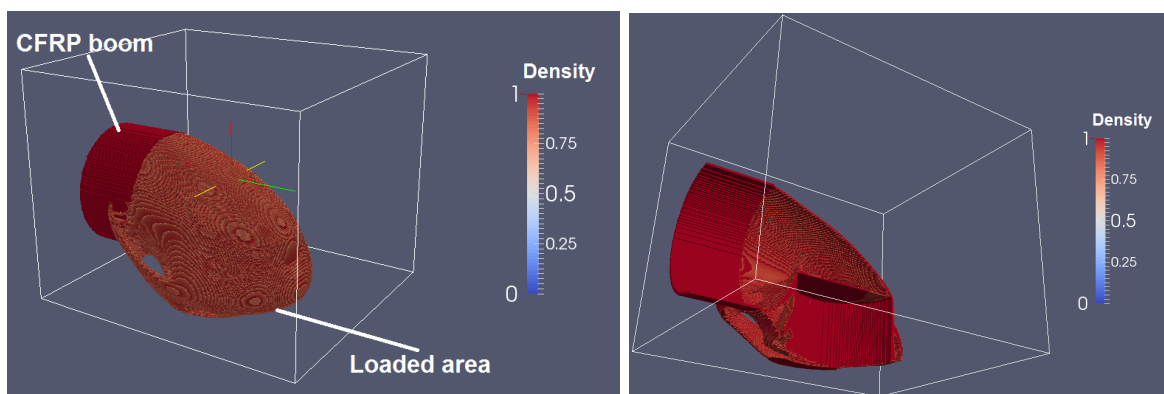


Figure 2-4: Concept design produced by topology optimization

This result must only be viewed as a conceptual suggestion for a design and by far does not represent a final design.

A tubular structure can be recognized connecting the loaded area with the section of Carbon Fiber Reinforced Polymer (CFRP) boom. Some additional internal structure is seen as well as external reinforcements.

Even though the resulting design is not overly complex it requires some thought as to how it would need to be oriented in the build chamber and whether modifications are necessary for printing.

Since both circular ends of the hinge-bracket must interface with other parts of the A-ADS system sufficient geometrical precision must be guaranteed in these areas. For the best results the build direction would need to be along the axis of the ring. Due to the inherent 90° angle of the part this could not be possible for both ends of the hinge-bracket. A compromise would therefore need to be made. Orienting the part such that the axes of the circular ends are at an angle of 45° with respect to the base plate would be a possible solution for this, however by doing this the external reinforcements and the upper section of the tubular wall would now need support.

On the other hand the design could be modified slightly so that the supports are not necessary, reducing post-processing. Another alternative could be to include supporting structures which would not need removing, for example that connect the external reinforcements to the rest of the structure under such an angle that the result is self-supporting.

The above mentioned alternatives illustrate some of the considerations that need to be made for a design to be manufacturable by AM. Besides this the issue of cost is introduced by the possible post-processing needed to remove support structures.

One can imagine that for more complex design conditions these decisions become increasingly difficult to motivate.

2-3 Summary

The problem The design that follows from the current design process is degraded from a supposed optimal design (from topology optimization) to a likely sub-optimal design by modification for manufacturability.

There is no way of knowing if the design has been modified in the best way and modification is limited by the experience and creativity of the engineer.

Research goal It is the goal of this study to find a way to incorporate the 45° overhang restriction into the topology optimization to provide a more structured approach for the design of products for AM that is not limited by the experience and creativity of the engineer.

Hypothesis The overhang restriction can be incorporated into the topology optimization, which can then be used to find designs optimized specifically for the AM method SLM possibly even yielding designs with better performance than an unrestricted optimization.

Chapter 3

Method

A variety of commercial topology optimization software is available on the market that can assist engineers in concept generation of designs. It would be preferable to incorporate the overhang restriction directly into one of these commercial software packages presenting an industry-ready solution for the inclusion of the overhang restriction. To do this the commercial software must allow enough freedom to manipulate the software to achieve this goal. In this section the capabilities of some commercial software packages are discussed and their usefulness for this research is assessed.

It is found that the commercial software does not meet the needs of this research. It is not the goal of this study to re-invent a topology optimizer and thus use is made of a publicly available topology optimizer written in MATLAB code. The basic idea behind the code and the key aspects of it are presented. This code is in 2D and is not sufficient to model the 3D loads of the industrial problem from which this study emerged. This research is thus limited to testing the concept of implementation of the overhang restriction.

Finally a section is devoted to the general framework of the research.

3-1 Current status of commercial software

Most commercial software allows the use of multiple objectives and is able to define various constraints, but the extent to which this is possible must be researched. Besides this it must be checked whether the interface of the available software will allow custom defined constraints/objectives and if enough freedom and access to the underlying code is available to define these constraints/objectives.

Two software packages have been reviewed and the suitability for the implementation of the optimization problem at hand has been determined.

The software packages that have been reviewed are Hyperworks OptiStruct and Simulia ATOM. This software is based on the material density method but combine it with a boundary method by extracting a smoothed topology from the obtained result. After this a sizing

optimization is done for the final result. The material density method is the most common method used for commercial software.

3-1-1 Hyperworks Optistruct

Hyperworks Optistruct offers, besides the material density method, also optimization by the level-set method as a Beta functionality. This aspect has not been reviewed since it is also not yet developed enough for standard use.

Hyperworks Optistruct allows the user to select from various response types which can be set as either objective or constraint. Multiple responses can be chosen for both. The screenshot in Figure 3-1 shows the response types available.

mass	inertia	static stress	static force	frf strain	weighted freq	psd velocity	rms acceleration
massfrac	compliance	static strain	frf displacement	frf force	compliance index	psd acceleration	rms pressure
volume	static displacement	composite stress	frf velocity	fatigue	beadfrac	psd pressure	temperature
volumefrac	frequency	composite strain	frf acceleration	function	frf pressure	rms displacement	
cog	buckling	composite failure	frf stress	weighted comp	psd displacement	rms velocity	

Figure 3-1: Response types Hyperworks Optistruct

Even though Hyperworks offers the possibility to perform custom mathematical operations and analyses on various data, the input is still restricted to the predetermined responses. Custom responses cannot be designed nor is the optimization process accessible for modification. The only option that remains is using the existing responses and constraints to formulate a work-around that acts as the overhang restriction. Hyperworks Optistruct comes with the possibility to apply the manufacturing constraints shown in Figure 3-2.

Figure 3-2: Manufacturing constraints Hyperworks Optistruct
Member size, stress, fatigue, draw direction, extrusion, symmetry and patterning

Though these options allow a lot of versatility in doing topology optimization, they do not extend to the needs of this research and therefore this software has not been selected for use.

3-1-2 Simulia ATOM

Simulia ATOM works in a similar fashion as Hyperworks Optistruct. Predefined response types can be chosen for the objective function and constraints (Figure 3-3) and some manufacturing constraints are available (Figure 3-4)

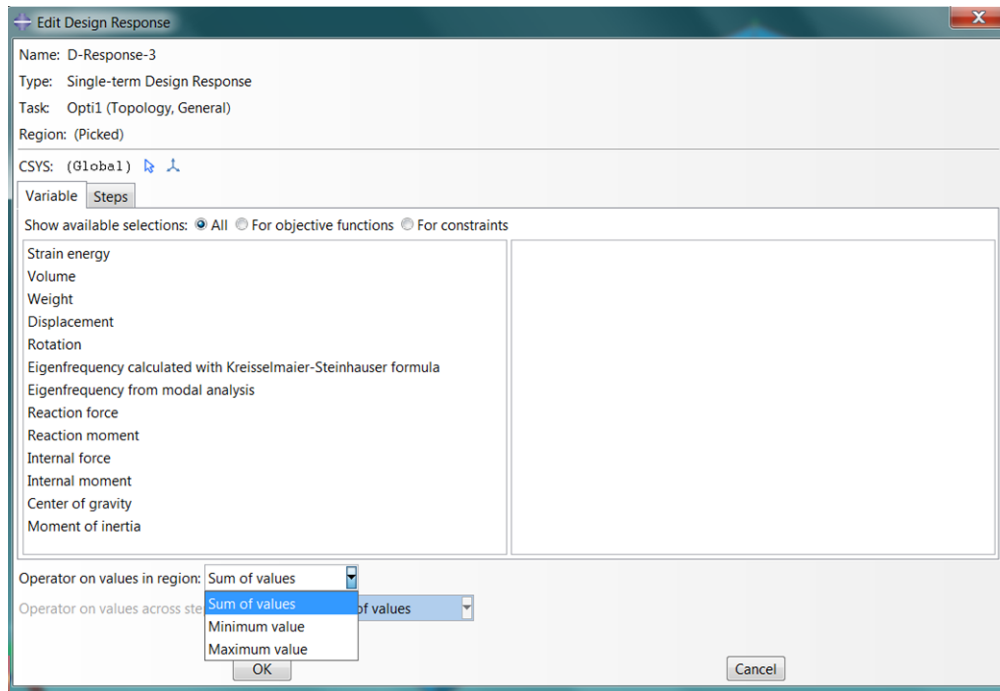


Figure 3-3: Response types Simulia ATOM

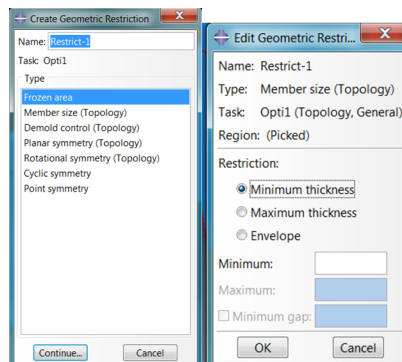


Figure 3-4: Manufacturing constraints Simulia ATOM
Member size, draw direction, symmetry

Simulia ATOM also offers the possibility to use scripting with Python (an open source programming language), which seems promising at first glance. However, this option is meant to incorporate the optimization into a larger process flow and does not grant any access to the optimization code itself.

Simulia ATOM does not offer any advantage over Hyperworks Optistruct for this research and is therefore also not used. It is concluded that commercial software cannot be used for this research and use must be made of tailored code. This will allow an unlimited amount of accessibility and freedom only limited by the programming language itself.

3-2 Description 88-line MATLAB code

To test the concepts developed in this research the formulations of the overhang restriction will be implemented into a publicly available 88-line MATLAB code provided by [7]. This code allows a relatively quick check of the results and makes understanding of the occurring phenomena relatively easy.

In this code the optimization problem solved is a 2D problem that discretizes the design space into square elements forming a structured grid-mesh, see Figure 3-5. New density values are found using the Method of Moving Asymptotes (MMA). MMA is a gradient-based optimization method, which means first-order derivatives of the objective and constraints are used to find an optimum. The derivative of the objective function with respect to the optimization variable is referred to as the sensitivity. The algorithm is coded to terminate when the design change is smaller than or equal to 0.01. The design change is given by the element with the maximum change in density.

This code provides a clear overview of the structure of the optimization, it is efficient and easy to modify. Visual feedback is provided after every iteration, which gives insight into the way the topology evolves. This code allows quick testing of various approaches and most importantly it is easily available. In it's current form this 88-line code is set-up for compliance minimization, which is all that is needed for the simplified problem. The code offers the possibility to choose between two mesh-independency filters; sensitivity-based and density-based. Both filters are controlled by a parameter called the filter radius, which denotes the radius, with respect to the center of an element, over which material is smoothed-out. Use will be made of the density based filter because this is mathematically more consistent. For a more detailed description of the code see [7].

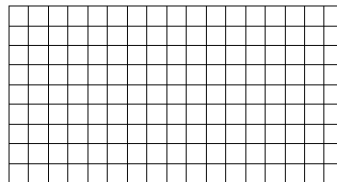


Figure 3-5: Structured grid mesh

3-3 Set-up

It is not the intention to re-evaluate all the aspects of the described code but rather extend the code by including the discussed restrictions.

Using the 88-line code some reference problems are set-up which will act as a control for the implementation of the overhang restriction. These reference models and motivation of choice are explained further in the next section. Three main approaches are presented for the implementation of the 45° overhang restriction. Before implementation the effect of the approaches is validated by applying them to some standard geometry in 2D. The required sensitivities are validated using the finite difference method. The three approaches are implemented in the 88-line code and optimization is run for the 2D reference models. The results and behavior are analyzed based on the evolution of the topology and objective and constraint values.

Based on this a conclusion can be made about the suitability of each approach for further development.

3-4 Reference models

A number of reference models have been set-up to assess the effect of the overhang restriction. In this section these reference models will be introduced and further explained as will the reason for their respective choice.

For the 2D models ran with the 88-line code an elasticity modulus of one is used, for these models the interest is purely conceptual and this value is not of great importance since (in linear analysis) this only has a scaling effect on the compliance. For the same reason applied loads are unit loads. By using these unit values the objective value obtained from the optimization is dimensionless. It does not give the actual compliance of the structure but rather a measure of compliance which can be minimized and that allows comparison between different designs. The Poisson ratio used is 0.3.

All reference models were produced with the following parameters:

Mesh:	30x50 elements
Penalization power:	3
Volume fraction:	≤ 0.5
Filter used:	Density filter
Filter radius:	1.5

3-4-1 Cantilever beams

A classic example used for the illustration of compliance minimization with topology optimization is the so-called cantilever beam. For a 2D rectangular design space the boundary condition imposed is that one side of the design space is fully clamped while on the opposite side a force is applied parallel to the clamped side. The result for this particular problem has been well documented and is therefore easily verified.

Figure 3-6 (left) shows the rectangular design space, clamped on the left side (all degrees of freedom of the nodes here are set to zero), while the red arrow shows the applied load on a single node. In this case the load is applied at mid-height. The result is shown in Figure 3-6 (right). The degree of darkness represents the density of each element in the figure, i.e. white is void, black is fully dense and gray represents intermediate densities. The results were obtained in 121 iterations.

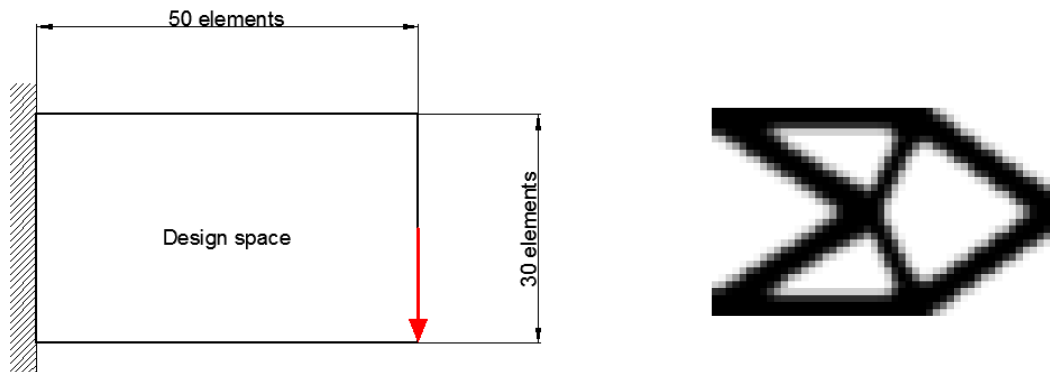


Figure 3-6: (Left) Load case cantilever beam mid-load and (right) the result with: Iterations: 121; Objective value: 57.17; Volume fraction: 0.418

For the same reasons as for the mid-loaded cantilever beam another version of the cantilever beam is used where the load is applied in the bottom right corner. The schematic representation of the load case and the result can be seen in Figure 3-7. The result was obtained in 191 iterations.

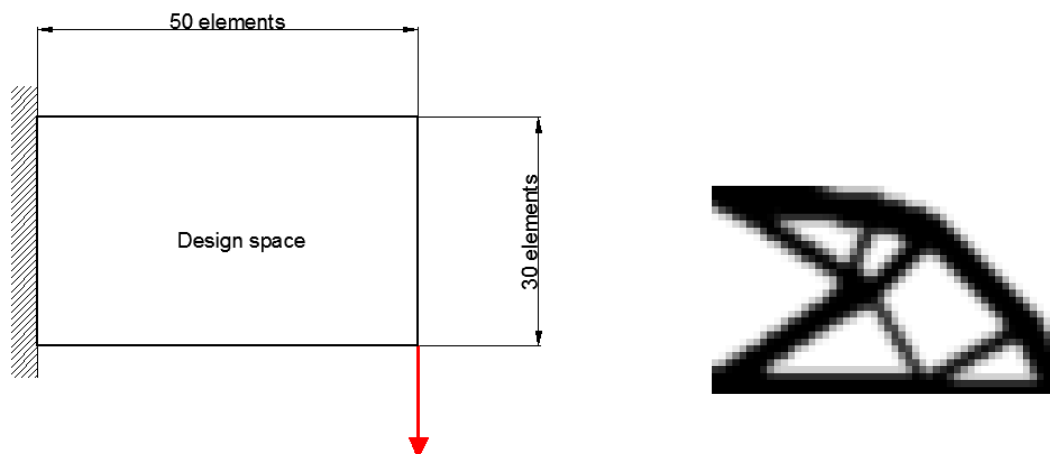


Figure 3-7: (Left) Load case cantilever beam corner-load and (right) the result with: Iterations: 191; Objective value: 64.00; Volume fraction: 0.426

3-4-2 Tension beam

For a final reference model the load is applied, once again, on the opposite side of the clamped condition at mid-height, except now the force is directed perpendicular to the face. This problem is referred to in this text as the tension beam. The load case and result obtained in 1160 iterations are shown in Figure 3-8.

This model has been chosen for two reasons. The first being that the result is easy to predict when no additional restrictions are placed on it. The second is that the solution exists almost exclusively out of overhang which makes for an interesting case once the overhang restriction

is applied. This problem is presumed to exploit any weaknesses of the implementation of the restriction in the simplest way.

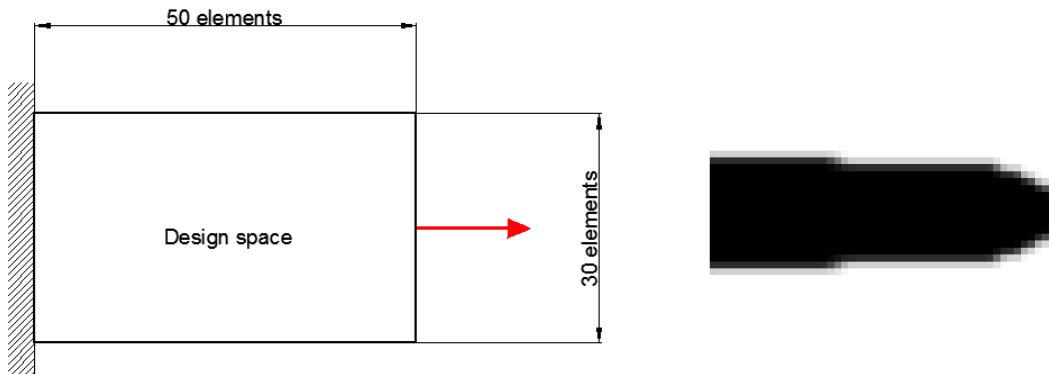


Figure 3-8: (Left) Load case tension beam and (right) the result with:
Iterations: 1160; Objective value: 5.49; Volume fraction: 0.474

Formulation of the overhang restriction

In order to implement a restriction on the geometry of the output of the topology optimization, a method must be found to identify the geometrical property. In this case the geometrical property in question is the presence of supporting material under an angle of at least 45 degrees. The geometrical properties of every (intermediate) solution of the topology optimizer can be addressed in two ways, that is, by assessing the discrete nature of the model or the continuous nature. The discrete nature of the model refers to the finite element discretization of the design space and the continuous nature of the model refers to the density field produced by the various density values of each element. To find out whether material is supported or not a transition from high density material to low density material must be identified, this indicates a border, the angle of this border will have to meet the imposed requirement for the restriction to be implemented successfully.

4-1 Using the continuous nature of TO

Taking a look at the continuous nature of the model it is straightforward that the gradient of the density can be used to find these transition areas, i.e. a high gradient indicates a sharp transition from high to low density. The direction of this gradient vector could then be compared to some reference vector to quantify the angle under which supporting material is present/missing. A restriction could be imposed directly on this angle to control the material distribution such that material is always properly supported. For this approach a value must be defined for which the gradient is deemed to represent a border. This is necessary since the topology optimization (using the SIMP method) always encounters intermediate densities during the optimization process. Figure 4-1 demonstrates this in a section of a result of a 2D topology optimization using the 88-line MATLAB code. In the middle of the image moving toward the top right corner (A) it can be seen that a member can already be identified even

though there is no direct black to white transition, however it becomes increasingly blurred. The bottom right corner (B) also shows such a situation. The bottom left corner (C) shows a situation where a clear distinction is present. A value must thus be defined where the gradient can be regarded as a border and where this is not applicable.

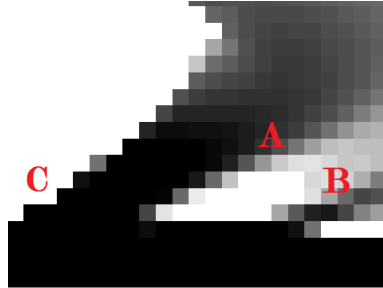


Figure 4-1: Gradient of density field

By choosing a high value for the gradient it is ensured that only true borders are identified, however a consequence of this is that the optimizer may then avoid these gradients in cases where it is very beneficial to have a member under an unallowable angle by using densities just below the specified gradient. Since intermediate densities are undesired this is potentially a big drawback of this method. In other words this restriction competes with the penalization of element densities (introduced to make ‘black and white’ solutions more attractive for the optimizer). A potential solution could be to implement a continuation method, i.e. define the restriction in such a way that it is not active in the initial part of the optimization and as the process progresses so does the restriction become more active. By doing this members will already be partially formed when the restriction becomes active.

Another difficulty that arises in the determining of the boundaries, even in cases where clear black-white structures are generated, is that due to the discrete nature of the mesh the gradient along a boundary is not continuous. Taking the grid mesh as an example, see Figure 4-2, it can be seen that along an inclined boundary a staircase pattern is present, this gives gradients in completely different directions making it difficult to identify the angle of the boundary locally. A solution for this may be found by applying an interpolation over the elements from which the gradient is then determined. This introduces the need for interpretation of the topology, thus introducing an additional step in the optimization process. This step must allow mathematical differentiation in order to determine sensitivities for proper use of the Method of Moving Asymptotes (MMA) optimizer. This additional step is expected to make the new optimization problem overly complex.

4-2 Using the discrete nature of TO

From the point of view of the discrete nature of the optimization process it can be deduced that for an element to be supported in an allowable fashion there must be an adjacent element that is (at least) equally dense and located within the allowable range of a supporting structure. Figure 4-3 shows a section of a grid mesh, the filled element represents an element with some density. The hatched region in the image indicates where support material could be placed to be able to place material in the element in question. For this particular mesh it can be

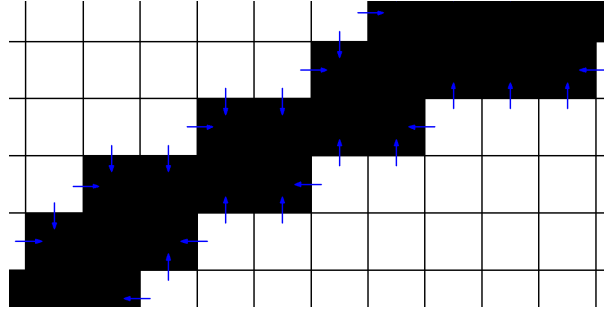


Figure 4-2: Local gradients in black and white topology represented by blue arrows

seen that there are three candidate elements of which at least one would have to have at least the same density of the to-be-supported element. The overhang restriction can be enforced by imposing a relation between the density of elements that fall within the hatched region and the element in question. From the image it can be seen that for the grid type mesh and a 45 degree overhang restriction, there are three main elements (outlined) that can serve as supports. Of these three elements the one with the highest density will determine whether enough support is provided. Hence a maximum value must be determined. To be able to

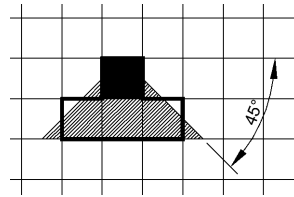


Figure 4-3: Discontinuous aspect of topology optimization showing candidate support elements

make use of this property in the optimization algorithm (in order to determine sensitivities) a mathematical differentiable and continuous description must be formulated to find the maximum value. A way to specify this relation mathematically is to define the P-norm as a function of the densities in the selected elements Eq. (4-1). Taking a finite value of p_n , the output of the P-norm will approximate the highest density value of the selected elements. A condition can then be specified for this value. Imposing this condition on each element should then result in a design that complies with the design rule. The P-norm for k elements numbered from 1 to k is defined as follows:

$$\rho_{max} = \lim_{p_n \rightarrow \infty} \sqrt[p_n]{\sum_{a=1}^k \rho_a^{p_n}} \quad (4-1)$$

Where:

ρ_{max} = the maximum value of the included density values

p_n = a parameter that influences how well the true maximum value is approximated

a = the element number for $a = 1..k$

k = the number of elements being evaluated

ρ_a = the density value of element a

An example of what such an approximation looks like can be seen in Figure 4-4. In this figure two functions have been plotted, one for an inverted parabola (function 1) and one for a parabola (function 2). The P-norm is then plotted in cyan with a (high) value for p_n of 50. Additionally, as a reference, the actual maximum value of each point is plotted (function 3) using a 'max' command.

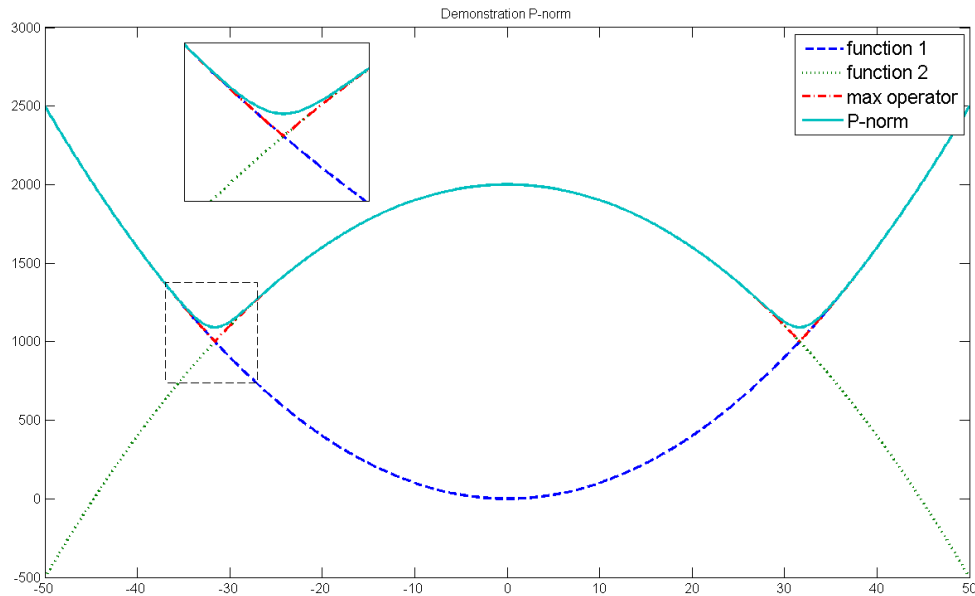


Figure 4-4: Example of P-norm behavior

A drawback of this method is that the selection of elements is highly dependent on the mesh-type used and will thereby influence the structure being created, though this issue might be negligible for elements of small enough size. Furthermore, if this approach is applied to a grid mesh it might promote checkerboarding, i.e. a checkerboard member/structure (of one element thickness) is a sufficient means of support. As an initial indication this is fine, but for a manufacturable and numerically accurate model this would need to be modified by for example a density filter or some other means that imposes a minimum member thickness. It is presumed that the density filter will suffice. This approach is expected to be the most straightforward for implementation and have the best chance of successful implementation, therefore this has been selected as the approach to take for this study.

4-3 Pragmatic approach

As a very first attempt to generate a result that complies with the overhang restriction a pragmatic approach has been examined.

Using the 88-line MATLAB code an extra section of code is added after every optimization iteration.

Each element is evaluated sequentially. Per element the maximum density of the candidate support elements is determined (for this approach the 'max' function in MATLAB is used and

not the P-norm). If this density is equal to or higher than that of the element being evaluated then no action is undertaken. If the opposite is the case, the density of the candidate support element is set equal to that of the element being evaluated. The process in pseudocode is as follows:

1. Determine candidate support elements for element 'i' with density ρ_i
2. Determine maximum density value of candidate support elements ρ_{max}
3. If $\rho_{max} \geq \rho_i$ then do nothing
4. If $\rho_{max} < \rho_i$ then replace ρ_{max} with ρ_i

The algorithm has been executed for the corner-loaded cantilever beam. The result is shown in Figure 4-5.

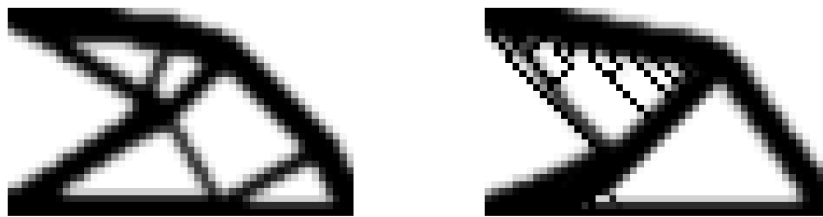


Figure 4-5: (Left) Reference model corner-loaded cantilever beam and (right) result pragmatic approach for: mesh: 30x50; volume fraction: 0.5; filter penalization power: 3; radius: 1.5; Obtained objective after 49 iterations: 67.57; volume fraction: 0.421

In this algorithm the volume fraction constraint is not taken into account. Furthermore the optimizer does not have any way of taking the new behavior of the model into account when generating new values. Despite this, the result in Figure 4-5 shows an altered design with structures that support overhang that can reach an objective value near that of the reference model and only a slight difference in the occupied volume fraction. These results look promising, but when the algorithm is executed for the same problem with a finer mesh a very different result emerges. This approach is extremely mesh-dependent and uncontrollable in terms of optimization.

The supports in Figure 4-6 look quite illogical in certain places (for example on the far left). The stiffness of the support is not taken into account when generating the structure, so the supports do not necessarily improve the stiffness of the structure. Material is simply placed wherever an element is overhanging, the candidate with the highest density is taken as the bias as to where to add this material. Especially in void areas, where the values of the elements are near zero and the densities might even be equal for all candidate support elements, this bias becomes meaningless and the generated support structures look arbitrary in shape.



Figure 4-6: (Left) Reference model corner-loaded cantilever beam for: mesh: 60x100; imposed volume fraction: ≤ 0.5 ; filter penalization power: 3; radius: 1.5; Obtained objective after 270 iterations: 62.69; volume fraction: 0.404 and (right) result pragmatic approach with: Obtained objective after 38 iterations: 67.23; volume fraction: 0.422

4-4 Restriction method

Once a formulation for the quantification of overhang is defined a next step can be made, that is a method for imposing the restriction on the optimization problem can be formulated. Three main approaches have been identified for imposing the overhang restriction: add a constraint to the optimization problem, include an additional term in the objective function that accounts for the restriction (penalty function) or apply a filter over the design that adapts the design so that it complies with the desired restriction.

4-5 Local constraints

With the help of Eq. (4-1) a constraint can be defined for overhanging elements. That is, for each element to be supported the difference between the density of the element under inspection and the candidate support element with the highest density must be zero or negative. In other words the supporting element has a density equal or higher than that of the element under inspection. With this the optimization problem, Eq. (1-1), can now be rewritten as:

$$\begin{aligned}
 \min_{\rho} \quad & c(\rho) = \mathbf{U}^T \mathbf{K} \mathbf{U} = \sum_{e=1}^N (\rho_e)^p \mathbf{u}_e^T \mathbf{k}_e \mathbf{u}_e \\
 \text{subject to} \quad & \mathbf{K} \mathbf{U} = \mathbf{F} \\
 & \frac{V(\rho)}{V_0} = f \\
 & \rho_{\Delta} \leq 0 \\
 & 0 < \rho_{min} \leq \rho \leq 1
 \end{aligned} \tag{4-2}$$

with

$$\rho_{\Delta} = \rho_i - \rho_{max} \tag{4-3}$$

which is the difference, as described earlier, for each element in the design space.

In this description a constraint is assigned to each element in the design space. It is in general desirable to have as little constraints as possible due to the computational cost. A large number of constraints also makes it more difficult for the optimizer to find a solution. By imposing the restriction in this manner as many constraints as elements in the design space are added. In general this is a lot (too many for a well-posed optimization problem). Therefore an alternative approach should be considered.

4-6 Multiple objective and global constraint

4-6-1 Multiple Objective

The overhang can also be viewed as a value which is to be minimized along with the compliance in the objective function of the optimization problem. The mathematical formulation of this, i.e. a multi-objective optimization problem, takes the following form:

$$\begin{aligned}
 \min_{\rho} \quad & \mathbf{U}^T \mathbf{K} \mathbf{U} + \Omega_{fac} \Omega_{tot} = \sum_{e=1}^N (x_e)^p \mathbf{u}_e^T \mathbf{k}_e \mathbf{u}_e + \Omega_{fac} \Omega_{tot} \\
 \text{subject to} \quad & \mathbf{K} \mathbf{U} = \mathbf{F} \\
 & \frac{V(\rho)}{V_0} = f \\
 & \mathbf{0} < \rho_{min} \leq \rho \leq \mathbf{1}
 \end{aligned} \tag{4-4}$$

Where:

Ω_{tot} = A function that defines a value for the level of overhang

Ω_{fac} = A weight factor for the additional overhang term

For the function that represents the total overhang of the geometry (Ω_{tot}) it can be said, based on previous arguments, that the level overhang can be given by the difference between the density of the element being evaluated (ρ_i) and the maximum value of the candidate supporting elements (ρ_{max}). This is given by (ρ_{Δ}). Setting the overhang of an element, Ω , equal to ρ_{Δ} , however, will result in negative values when ρ_{max} is greater than ρ_i . This would mean that the total objective value would be improved (lowered in value) for these cases, which does not represent reality. In fact the level of overhang for these cases should simply be zero. In Figure 4-7 a 3D plot can be seen of ρ_{Δ} for values of ρ_{max} and ρ_i ranging from zero to one. Furthermore, overhang is present for any positive value of ρ_{Δ} and should thus return a positive value for these cases. Once again examining Figure 4-7 it is seen that for cases where ρ_{max} is kept constant (e.g. $\rho_{max} = 0$) and ρ_i is increased, ρ_{Δ} increases linearly. This would imply that overhang is more acceptable when ρ_i has intermediate densities, which is not the case. This would promote intermediate densities because for these values of ρ_i overhang would be perceived as more acceptable. This is not desired. The function for Ω_{tot} should thus not be linear, rather it should give a zero value for any negative ρ_{Δ} and a maximum value for any positive ρ_{Δ} . Taking the maximum value as one, overhang can then be defined as follows:

For an element that is not properly supported, i.e. candidate support elements have a value lower than that of the element under inspection, the overhang has a value of one and when the element *is* supported it has a value zero.

$$\Omega = \begin{cases} 1 & \text{if } \rho_{\Delta} > 0 \\ 0 & \text{if } \rho_{\Delta} \leq 0 \end{cases} \quad (4-5)$$

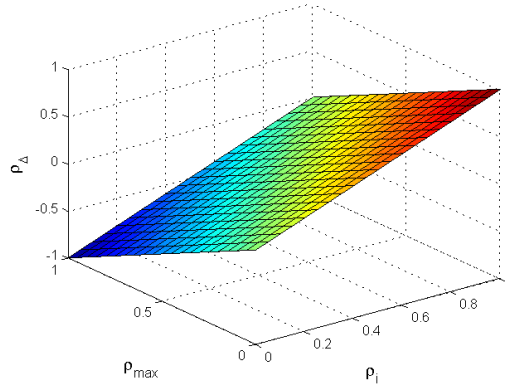


Figure 4-7: Value ρ_{Δ} with respect to ρ_{max} and ρ_i

This response could be achieved by multiplying ρ_{Δ} with a step-function. This approach, however, does not yield a differentiable function. To achieve the desired response for Ω_{tot} use is made of a differentiable approximation of a step-function, the so-called logistic function (see Figure 4-8):

$$f = \frac{1}{1 + e^{-M \cdot x}} \quad (4-6)$$

Where:

M = A parameter that controls the steepness of the curve (i.e. higher values result in a steeper curve)

x = The independent variable in the function

Replacing the independent variable (x) in Eq. (4-6) by ρ_{Δ} the desired response is obtained. It can be seen in Figure 4-8 that for $x = 0$ the function value is 0.5 which is not in agreement with Eq. (4-5), and that the function is still positive for negative values of x . The error of the function for $x < 0$ can be minimized by setting the parameter M higher, however extremely high values of M will result in numerical difficulties due to high gradients in the curve. The error at $x = 0$ will, however, always remain at 0.5 for finite values of M . This error can be reduced by shifting the entire curve to the right, but this comes at a cost. By doing this the value of ρ_{Δ} for which overhang is registered is increased. An extra parameter, δ , is introduced to be able to tweak this property by replacing $x = x - \delta$, see Figure 4-9.

Up till now the function is only applicable to each individual element. A global measure for the amount of overhang in a certain geometry can be formulated using this function, referred to as the overhang coefficient (Ω_{tot}). It is defined by the sum of the overhang of all elements normalized by the number of elements, N , in the design domain.

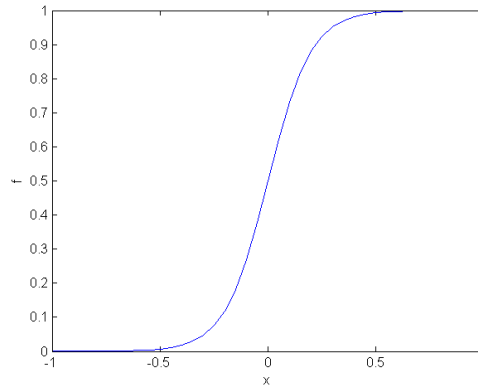


Figure 4-8: Plot of the logistic function with x ranging from -1 to 1

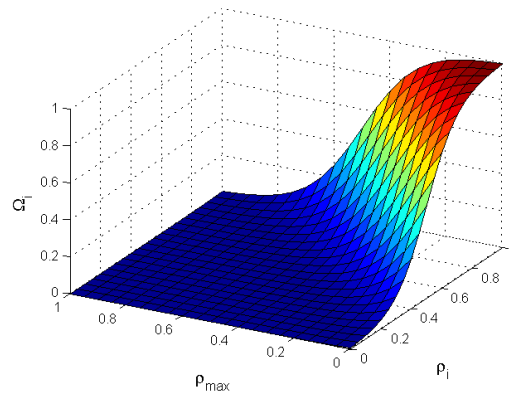


Figure 4-9: Overhang with $M = 10$ and $\delta = 0,5$

$$\Omega_{tot} = \sum_{i=1}^N \Omega_i \frac{1}{N} \quad (4-7)$$

now with:

$$\Omega_i = \frac{1}{1 + e^{-M(\rho_{\Delta} - \delta)}} \quad (4-8)$$

Alternatively this can be formulated as:

$$\Omega_{tot} = \sum_{i=1}^N \Omega_i^* \quad (4-9)$$

with:

$$\Omega_i^* = \frac{1}{1 + e^{-M(\rho_{\Delta} - \delta)}} \frac{1}{N} \quad (4-10)$$

Where Ω_i and Ω_i^* are the overhang and normalized overhang of an individual element i respectively.

Now a global measure of overhang for any geometry is available with a value between zero and one which can now be minimized.

4-6-2 Multiple objective function sensitivities

Since the new objective function is the sum of the original (compliance) term and the new overhang term ($\Omega_{fac}\Omega_{tot}$) the total sensitivities ($\frac{df}{d\rho}$) will also be a sum of the derivatives of each term:

$$\frac{df}{d\rho} = \frac{\partial c}{\partial \rho} + \Omega_{fac} \frac{\partial \Omega_{tot}}{\partial \rho} \quad (4-11)$$

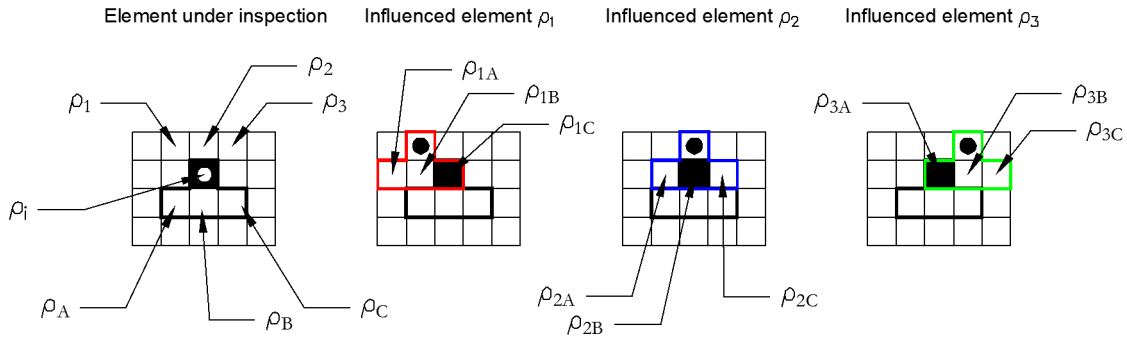


Figure 4-10: Influenced elements for sensitivities

The derivatives of the original term, $\frac{\partial c}{\partial \rho}$, remain unchanged. An array is generated with the derivative of Ω_{tot} with respect to each element and ordered accordingly. To calculate the sensitivity of Ω_{tot} with respect to an arbitrary element, ρ_i , the effect on the overhang of surrounding elements should also be taken into account. Figure 4-10 shows an element ρ_i (black) and its surrounding elements. Varying the density of ρ_i will affect the overhang of the element itself and elements ρ_1 , ρ_2 and ρ_3 as is indicated in the figure. The elements ρ_1 , ρ_2 and ρ_3 are referred to as the influenced elements. Elements ρ_A , ρ_B and ρ_C denote the candidate support elements. The overhang of the rest of the elements in the design space will not be affected by this density change and thus the contributions of these elements to the total derivative is zero. With this the sensitivity $\frac{d\Omega_{tot}}{d\rho_i}$ becomes:

$$\frac{d\Omega_{tot}}{d\rho_i} = \frac{d}{d\rho_i} \sum_{i=1}^N \Omega_i^* \quad (4-12)$$

$$= \left(\frac{\partial \Omega_i^*}{\partial \rho_i} + \frac{\partial \Omega_1^*}{\partial \rho_i} + \frac{\partial \Omega_2^*}{\partial \rho_i} + \frac{\partial \Omega_3^*}{\partial \rho_i} \right) \quad (4-13)$$

with

$$\Omega_i^* = \frac{1}{1 + e^{-M(\rho_\Delta - \delta)}} \frac{1}{N} \quad (4-14)$$

$$\rho_\Delta = \rho_i - \sqrt[p_n]{\rho_A^{p_n} + \rho_B^{p_n} + \rho_C^{p_n}}$$

To evaluate the partial derivatives in Eq. (4-13) the chain rule of differentiation is applied:

$$\frac{d\Omega_i^*}{d\rho_i} = \frac{\partial\Omega_i^*}{\partial\rho_\Delta} \frac{\partial\rho_\Delta}{\partial\rho_i} \quad (4-15)$$

$$\frac{d\Omega_i^*}{d\rho_1} = \frac{\partial\Omega_i^*}{\partial\rho_{1\Delta}} \frac{\partial\rho_{1\Delta}}{\partial\rho_1} \quad (4-16)$$

$$\frac{d\Omega_i^*}{d\rho_2} = \frac{\partial\Omega_i^*}{\partial\rho_{2\Delta}} \frac{\partial\rho_{2\Delta}}{\partial\rho_2} \quad (4-17)$$

$$\frac{d\Omega_i^*}{d\rho_3} = \frac{\partial\Omega_i^*}{\partial\rho_{3\Delta}} \frac{\partial\rho_{3\Delta}}{\partial\rho_3} \quad (4-18)$$

Working this out then gives the following terms:

$$\frac{d\Omega_i^*}{d\rho_i} = \frac{1}{N} \left(-\frac{(-M)e^{-M(\rho_\Delta-\delta)}}{(1+e^{-M(\rho_\Delta-\delta)})^2} \right) \quad (4-19)$$

$$\frac{d\Omega_i^*}{d\rho_{1C}} = \frac{1}{N} \left(-\frac{e^{-M(\rho_{1\Delta}-\delta)} \cdot (\rho_{1A}^{p_n} + \rho_{1B}^{p_n} + \rho_{1C}^{p_n})^{\frac{1}{p_n}} \cdot \rho_{1C}^{p_n-1}}{(1+e^{-M(\rho_{1\Delta}-\delta)})^2} \right) \quad (4-20)$$

$$\frac{d\Omega_i^*}{d\rho_{2B}} = \frac{1}{N} \left(-\frac{e^{-M(\rho_{2\Delta}-\delta)} \cdot (\rho_{2A}^{p_n} + \rho_{2B}^{p_n} + \rho_{2C}^{p_n})^{\frac{1}{p_n}} \cdot \rho_{2B}^{p_n-1}}{(1+e^{-M(\rho_{2\Delta}-\delta)})^2} \right) \quad (4-21)$$

$$\frac{d\Omega_i^*}{d\rho_{3A}} = \frac{1}{N} \left(-\frac{e^{-M(\rho_{3\Delta}-\delta)} \cdot (\rho_{3A}^{p_n} + \rho_{3B}^{p_n} + \rho_{3C}^{p_n})^{\frac{1}{p_n}} \cdot \rho_{3A}^{p_n-1}}{(1+e^{-M(\rho_{3\Delta}-\delta)})^2} \right) \quad (4-22)$$

Where

$$\rho_{1\Delta} = \rho_1 - \sqrt[p_n]{\rho_{1A}^{p_n} + \rho_{1B}^{p_n} + \rho_{1C}^{p_n}} \quad (4-23)$$

$$\rho_{2\Delta} = \rho_2 - \sqrt[p_n]{\rho_{2A}^{p_n} + \rho_{2B}^{p_n} + \rho_{2C}^{p_n}} \quad (4-24)$$

$$\rho_{3\Delta} = \rho_3 - \sqrt[p_n]{\rho_{3A}^{p_n} + \rho_{3B}^{p_n} + \rho_{3C}^{p_n}} \quad (4-25)$$

$$\rho_{1B} = \rho_{2A} \quad (4-26)$$

$$\rho_{2C} = \rho_{3B} \quad (4-27)$$

$$\rho_{1C} = \rho_{2B} = \rho_{3A} = \rho_i \quad (4-28)$$

Substituting these terms back into Eq. (4-13) yields the sensitivity of Ω_{tot} with respect to element ρ_i .

Once all Ω_{tot} derivatives have been calculated the two arrays of derivatives (compliance and overhang multiplied by the weight factor) can be summed elementwise to obtain an array with the total derivatives of each element; the sensitivities.

4-6-3 Global constraint

The formulation derived in the previous section can also directly be used for a global constraint. In this case an equality constraint is introduced that requires that $\Omega_{fac}\Omega_{tot} = 0$. With this the new optimization problem becomes:

$$\begin{aligned}
\min_{\boldsymbol{\rho}} \quad & c(\boldsymbol{\rho}) = \mathbf{U}^T \mathbf{K} \mathbf{U} = \sum_{e=1}^N (\rho_e)^p \mathbf{u}_e^T \mathbf{k}_e \mathbf{u}_e \\
\text{subject to} \quad & \mathbf{K} \mathbf{U} = \mathbf{F} \\
& \frac{V(\boldsymbol{\rho})}{V_0} = f \\
& \Omega_{fac} \Omega_{tot} = 0 \\
& \mathbf{0} < \boldsymbol{\rho}_{min} \leq \boldsymbol{\rho} \leq \mathbf{1}
\end{aligned} \tag{4-29}$$

4-7 Filter

An alternative method to impose a geometrical restriction to the design is by applying a filter. A (density-based) filter modifies the densities of the elements to meet the imposed requirements after which Finite Element Analysis (FEA) and calculation of the sensitivities are performed with the new, modified, densities. This is done after the optimizer update. That is the density matrix $\boldsymbol{\rho}$ becomes $\tilde{\boldsymbol{\rho}}$ by:

$$\tilde{\boldsymbol{\rho}} = \mathbf{F} * \boldsymbol{\rho} \tag{4-30}$$

Where \mathbf{F} is a convolution matrix representing the filter.

The sensitivities of the elements must then be calculated by the chain rule:

$$\frac{dc}{d\boldsymbol{\rho}} = \frac{\partial c}{\partial \tilde{\boldsymbol{\rho}}} \frac{\partial \tilde{\boldsymbol{\rho}}}{\partial \boldsymbol{\rho}} \tag{4-31}$$

Using a filtering approach can be thought of as using a virtual fabrication process where $\boldsymbol{\rho}$ represents the fabrication plan and $\tilde{\boldsymbol{\rho}}$ the result. For the specific problem at hand, restricting overhang, two approaches have been identified for the design of the filter. Overhang can be eliminated by either removing material from an unsupported element or by adding material to (at least one of) the candidate support elements to achieve a supported element. The latter, however, may present an ambiguity problem in the case where all candidate support elements have an equal value. A choice must be made by the filter to which of the elements material will be added. During construction of the filter there is no information available to motivate which element should then be selected, thus making this choice ambiguous (this would be a

lot like the pragmatic approach presented earlier). For this reason the approach that removes material is chosen to be developed further.

4-7-1 Modification by sequential scanning

For this approach the maximum value of the candidate supporting elements is again checked using the P-norm. The maximum density value is then compared with the density of the element being analyzed, if the maximum density is larger than or equal to the analyzed element (no overhang) no action is undertaken and the density remains unchanged. If the maximum density of the candidate support elements is lower (overhang is present) the density of the element under inspection is set equal to that of the maximum density of the candidate support element, thereby eliminating overhang. The mathematical formulation of this for an element ρ_i can be stated as follows:

$$\tilde{\rho}_i = \begin{cases} \rho_i & \text{if } \rho_i \leq \rho_{max} \\ \rho_{max} & \text{if } \rho_i > \rho_{max} \end{cases} \quad (4-32)$$

or equivalently:

$$\tilde{\rho}_i = \min(\rho_i, \rho_{max}) = 1 - \max(1 - \rho_i, 1 - \rho_{max}) \quad (4-33)$$

Now, once again, the maximum value can be determined by using the P-norm. This yields the following differentiable equation for the modified densities ($\tilde{\rho}$):

$$\tilde{\rho}_i = 1 - \sqrt[p_n]{(1 - \rho_i)^{p_n} + (1 - \rho_{max})^{p_n}} \quad (4-34)$$

Applying this sequentially to each element from the bottom to the top of the design space will eliminate any overhanging elements. Since the bottom row of elements is always supported these densities do not need to be modified. Therefore the scanning of the elements is started one row higher.

Filter sensitivities

Recalling Eq. (4-31) the sensitivity with respect to an element ρ_j is then found to be:

$$\frac{dc}{d\rho_j} = \sum_{i=1}^N \frac{\partial c}{\partial \tilde{\rho}_i} \frac{\partial \tilde{\rho}_i}{\partial \rho_j} \quad (4-35)$$

Using the chain rule of differentiation and Eq. (4-34) gives:

$$\frac{\partial \tilde{\rho}_i}{\partial \rho_j} = ((1 - \rho_i)^{p_n} + (1 - \rho_{max})^{p_n})^{\frac{1}{p_n} - 1} \cdot \left((1 - \rho_{max})^{p_n - 1} \frac{\partial \rho_{max}}{\partial \rho_j} + (1 - \rho_i)^{p_n - 1} \frac{\partial \rho_i}{\partial \rho_j} \right) \quad (4-36)$$

with

$$\begin{aligned} \left(\frac{\partial \rho_{max}}{\partial \rho_j} \right)_{i \neq j} &= (\tilde{\rho}_A^{p_n} + \tilde{\rho}_B^{p_n} + \tilde{\rho}_C^{p_n})^{\frac{1}{p_n} - 1} \cdot \left(\tilde{\rho}_A^{p_n} \frac{\partial \tilde{\rho}_A}{\partial \rho_j} + \tilde{\rho}_B^{p_n} \frac{\partial \tilde{\rho}_B}{\partial \rho_j} + \tilde{\rho}_C^{p_n} \frac{\partial \tilde{\rho}_C}{\partial \rho_j} \right) \\ \left(\frac{\partial \rho_{max}}{\partial \rho_j} \right)_{i=j} &= 0 \end{aligned} \quad (4-37)$$

and

$$\frac{\partial \rho_i}{\partial \rho_j} = \delta_{ij} \quad (4-38)$$

Where δ_{ij} is the Kronecker delta. In Eq. (4-37) $\frac{\partial \tilde{\rho}_A}{\partial \rho_j}$, $\frac{\partial \tilde{\rho}_B}{\partial \rho_j}$ and $\frac{\partial \tilde{\rho}_C}{\partial \rho_j}$ should have been previously determined by calculating the sensitivities of each element from the bottom of the design space to the top. For the bottom row of elements the sensitivities are:

$$\left(\frac{\partial \tilde{\rho}_i}{\partial \rho_j} \right)_{\text{Bottom row}} = \delta_{ij} \quad (4-39)$$

These elements have the same value after filtering as before filtering, a change in the unfiltered density will translate to the same change in the filtered density. Density values of all other elements have no influence.

Validation

In order to verify the expressions formulated for the overhang in Chapter 4 some standard test geometry has been set-up in MATLAB, i.e. a portal, a ring and a gradient. This has been done by defining an array with dimensions that correspond to that of a desired mesh, the elements in the array represent material elements that may assume a value between zero and one. The value represents the density of the element. Initially all values in this array have a value of zero. A value of one is assigned to selected elements such that when displayed in a colormap the desired geometry is obtained. To generate a gradient the value of the element is made dependent on the index values. The resulting (grayscale) colormaps are shown in Figure 5-1. This method corresponds to the way the problem is set-up in the 88-line code from [7]. The test geometry used has been created in a 50x50 element mesh.

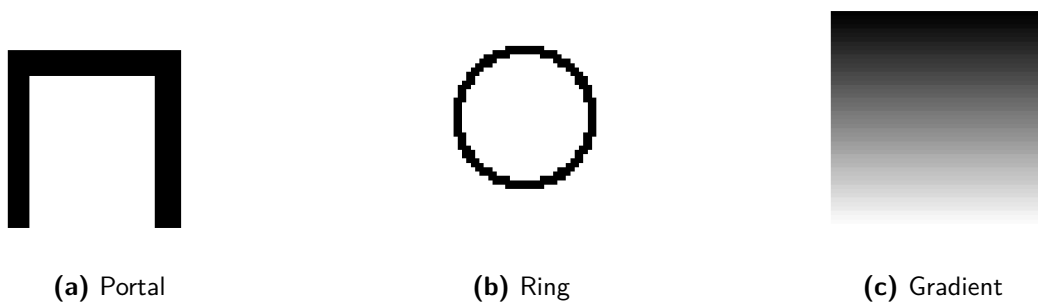


Figure 5-1: Standard geometry for verification

5-1 Validation of the multiple objective and global constraint

Using a function set-up in MATLAB to calculate the overhang according to the formulation described in section 4-6, a matrix is generated with the values of Ω^* for each element and Ω_{tot} . Plotting this matrix in a colormap reveals which elements have been registered as overhanging as can be seen in Figure 5-3.

For reference a function is defined in MATLAB in which no use is made of the formulation described in Section 4-6. Rather use is made of the ‘max’ command and an *if* statement to determine the maximum value of the candidate support elements and register the overhang of an element (as 0 or 1) respectively. Ω^* is then $\frac{1}{N}$ for an overhanging element and 0 for a supported element. A matrix is constructed in which all these values are stored. Summing Ω^* of all elements will then give the exact value for Ω_{tot} . Plotting the constructed matrix in a colormap will then show exactly which elements are overhanging, see Figure 5-2 where the overhanging elements are depicted in red.

Comparing the results of the exact determination and the formulated approximation of the overhang and Ω_{tot} , it is seen that for the portal and ring a satisfactory result is obtained. The gradient, however, is not approximated well at all. In the following section it will be explained that this is due to the choice of the parameters.

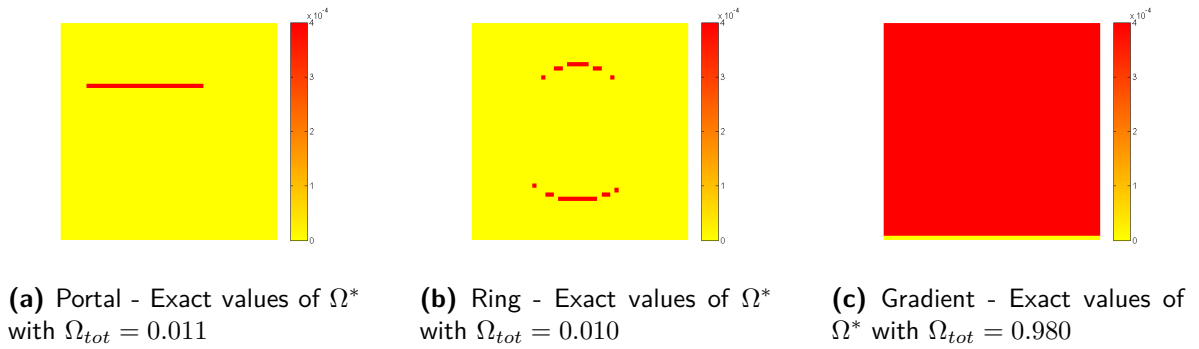


Figure 5-2: Exact OH detection in standard geometry

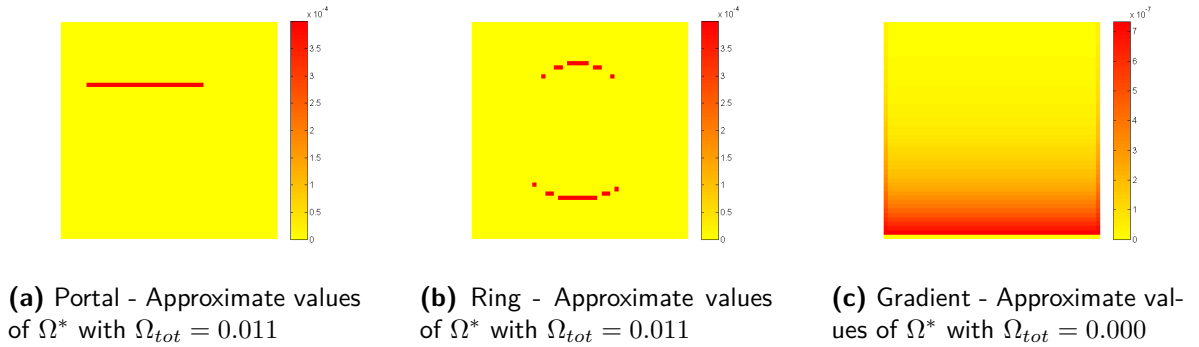


Figure 5-3: Approximate OH detection in standard geometry, with $M = 35$, $p_n = 8$ and $\delta = 0.2$

5-1-1 Parameters M , δ and p_n

Next the effects of the parameters M , p_n and δ are investigated. Each parameter is varied for each of the three test geometries.

Recalling the logistic function used to approximate a step function, the effect of the parameters on the overhang detection is deduced. The parameter M controls the steepness of the function, for higher values of M a better approximation of the step function is obtained. This can be

seen in Figure 5-4. Choosing M too high, however, makes it more difficult for the optimizer to find a solution due to the abrupt transitions in the curve. For low values of M , it can be seen in Figure 5-4, that Ω_i will take on higher positive values for negative values of ρ_Δ while all these values should actually return a Ω_i of zero. This will result in an Ω_{tot} that is higher than it should be. In Figure 5-5 the effect on Ω_{tot} of varying M is plotted for the three geometries. M is varied from 10 to 100 keeping $p_n = 8$ and $\delta = 0.2$. In these figures it can be seen that the Ω_{tot} converges at about $M = 50$. For the portal and the ring the value to which Ω_{tot} converges is in accordance with the exact values obtained in the previous section. The gradient geometry converges to zero, which is far from the exact value, this has to do with the δ parameter and the error introduced by the P-norm approximation. This is discussed in the following sections.

Returning to the logistic function in Figure 5-4 it is shown that the δ parameter shifts the center of the curve along the horizontal. This has a similar effect as M in terms of Ω_i at $\rho_\Delta = 0$. Increasing δ will lower Ω_i , in return the value for which Ω_i reaches one is also shifted. In effect this means that overhang is detected for higher values of ρ_Δ . This parameter should be kept as close as possible to zero and negative values should be avoided. For negative values of δ , negative values of ρ_Δ are identified as overhang, which in general is undesirable. The lower the value of M the more important it is to increase δ .

For the gradient in Figure 5-1c ρ is increased from 0 to 1 over 50 elements (50x50 mesh), and thus the difference in ρ between each row is only 0.02. This means that for any δ value larger than 0.02 overhang will not or barely be detected in this case. Setting $\delta = 0$ results in a higher Ω_{tot} for the gradient geometry, but the value is still not in correspondence with the calculated exact value, a plot of Ω^* for this case is shown in Figure 5-7. Figure 5-6 shows the effect of varying δ on Ω_{tot} for the three respective test geometry cases. Figure 5-6c shows that the correct value for Ω_{tot} is found when δ is negative, implying that the detected ρ_Δ is negative. This is due to the error introduced by the P-norm approximation.

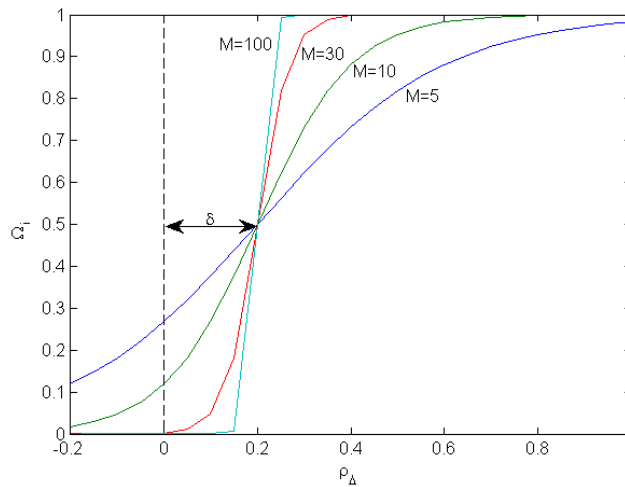
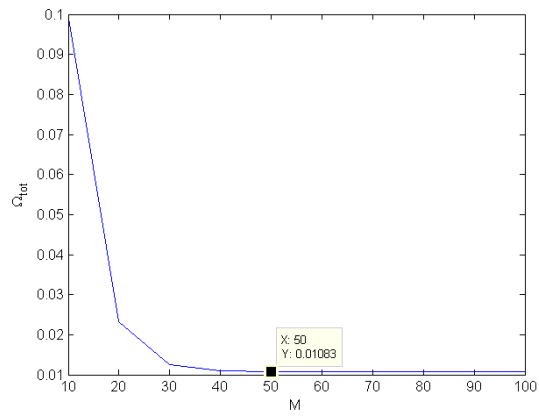
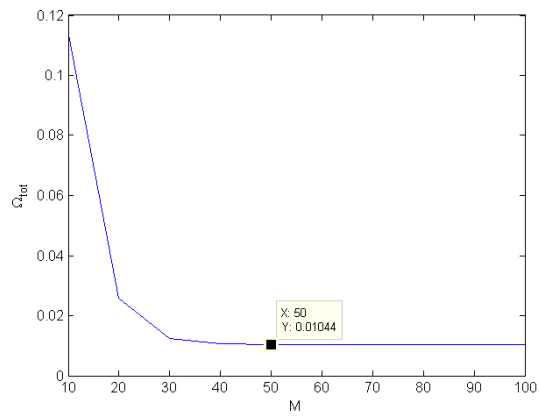


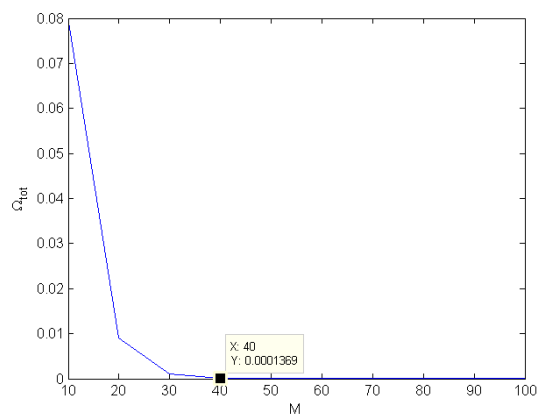
Figure 5-4: Logistic function for varying values of M



(a) Portal

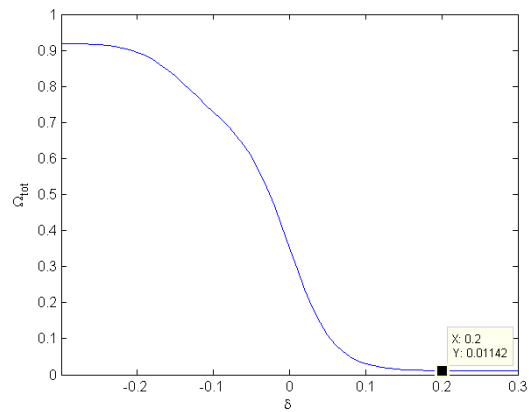


(b) Ring

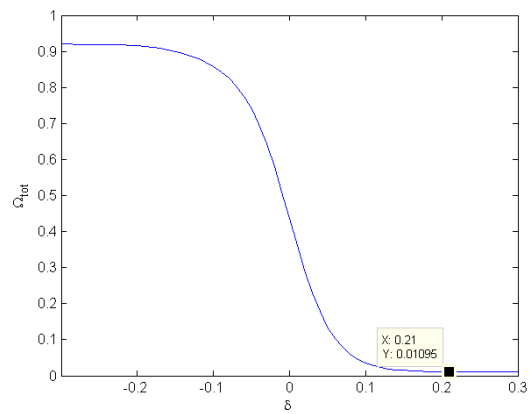


(c) Gradient

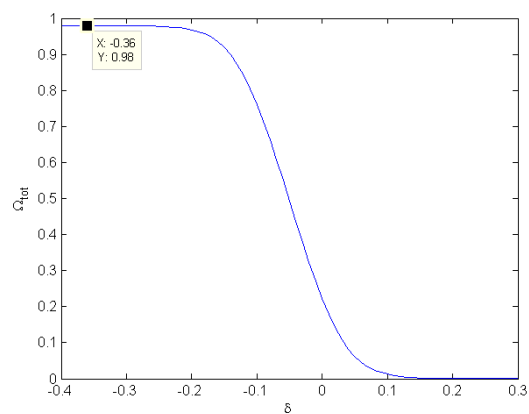
Figure 5-5: Ω_{tot} for parameter M from 10-100



(a) Portal



(b) Ring



(c) Gradient

Figure 5-6: Ω_{tot} for varying parameter δ

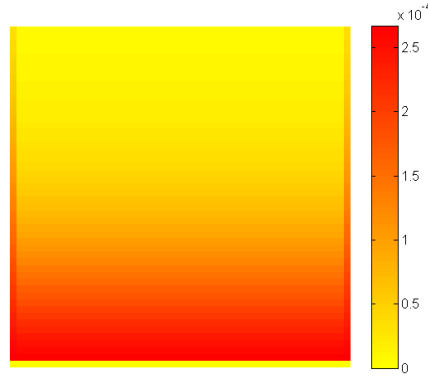


Figure 5-7: Ω^* for gradient geometry with $\delta = 0$ giving $\Omega_{tot} = 0.223$

The error introduced by the P-norm can be shown to increase linearly with the density of the candidate support elements. Recalling the P-norm and taking ρ to be the actual maximum value of the candidate support elements, the approximated maximum value ρ_{max} can be written as:

$$\rho_{max} = \sqrt[p_n]{\rho^{p_n} + (\alpha\rho)^{p_n} + (\beta\rho)^{p_n}} \quad (5-1)$$

$$= \rho \sqrt[p_n]{1 + \alpha^{p_n} + \beta^{p_n}} \quad (5-2)$$

with:

$$0 \leq \alpha \leq 1 \quad (5-3)$$

$$0 \leq \beta \leq 1 \quad (5-4)$$

The error is then found to be:

$$err = \rho_{max} - \rho = \rho(\sqrt[p_n]{1 + \alpha^{p_n} + \beta^{p_n}} - 1) \quad (5-5)$$

showing that the error is linearly dependent on ρ . This explains why, in Figure 5-7, a gradient is seen for the detected overhang. A minimum error is found for $\alpha = \beta = 0$ while a maximum error is found for $\alpha = \beta = 1$, which is the case for the gradient.

Figure 5-8 illustrates how the calculated maximum value ρ_{max} deviates from the actual maximum value ρ increasingly for higher values of ρ with $\alpha = \beta = 1$.

This error can be minimized by increasing p_n since:

$$\lim_{p_n \rightarrow \infty} err = 0 \quad (5-6)$$

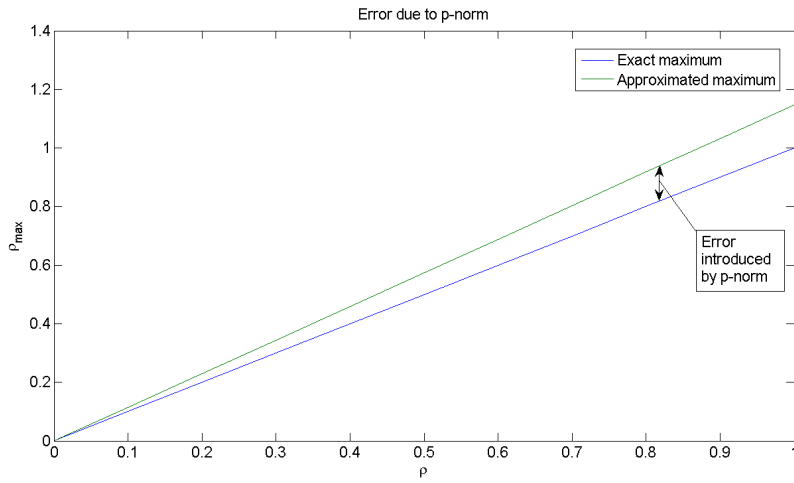


Figure 5-8: Error due to P-norm

Now it is proven that for the gradient geometry a negative value of ρ_{Δ} is detected as a result of the P-norm error. With $\alpha = \beta = 1$, for an arbitrary element ρ_i , the actual difference in density between each row 0.02 and $p_n = 8$ the following is found:

$$\rho_{max} = \rho \sqrt[8]{3} \quad (5-7)$$

with $\sqrt[8]{3} \approx 1.15$ and

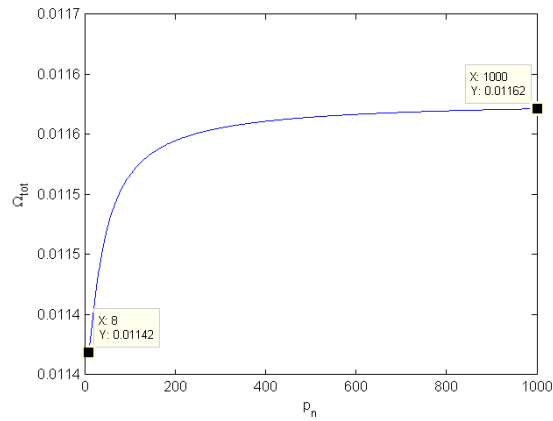
$$\rho_i = \rho + 0.02 \quad (5-8)$$

then for $\rho = 1$:

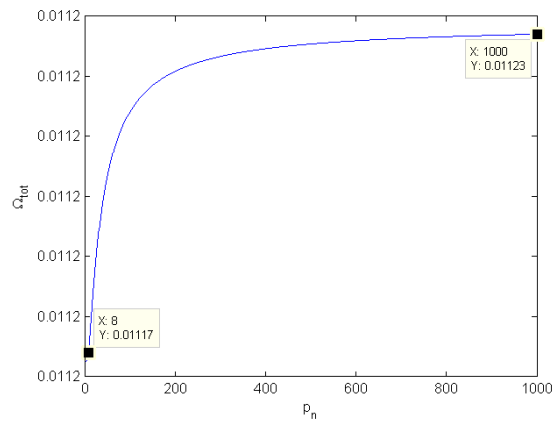
$$\rho_{\Delta} = \rho + 0.02 - 1.15\rho \quad (5-9)$$

$$= -\rho \cdot 0.15 + 0.02 = -0.13 \quad (5-10)$$

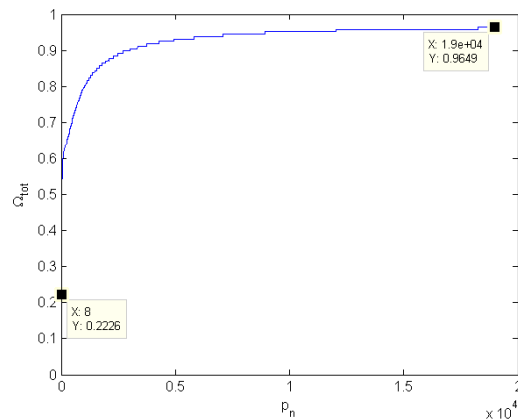
Thus the detected ρ_{Δ} is negative at the top of the gradient geometry. In Figure 5-9 the effect of an increasing P-norm power on Ω_{tot} is shown for the three test geometries.



(a) Portal - varying p_n from 1 to 1000 with $\delta = 0.2$ and $M = 35$



(b) Ring - varying p_n from 1 to 1000 with $\delta = 0.2$ and $M = 35$



(c) Gradient - varying p_n from 1 to 19000 with $\delta = 0$ and $M = 35$

Figure 5-9: Ω_{tot} for varying P-norm power p_n

As expected the values converge for extremely high p_n , though the portal and the ring already are very close to the limit value for very low p_n . This is due to the black-white nature of the geometry. The gradient needs extremely high values of p_n which is due to the small difference in ρ between each row. It can be calculated that for $p_n = 8$, $\delta = 0.2$ and $M = 35$ and the assumption that overhang is registered for $\Omega = 0.8$ the minimum difference in density to be registered as overhanging is:

$$\frac{1}{1 + e^{-35(\rho_{\Delta} - 0.2)}} = 0.8 \quad (5-11)$$

$$\Rightarrow \rho_{\Delta} \approx 0.24 \quad (5-12)$$

Taking into account the maximum error introduced by the P-norm with $\rho = 1$ the difference for which overhang starts to register is:

$$0.24 + \rho(1 - \sqrt[8]{3}) = 0.39 \quad (5-13)$$

This is assumed to be sufficient for further investigations.

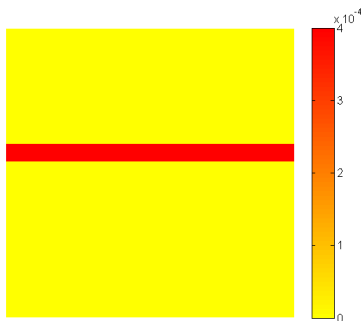
Figure 5-10 shows a density plot with the exact overhang and the approximated overhang calculations. The density plot shows a small section of gradient that increases the density in the following manner: $\rho = 0 > \rho = 0.2 > \rho = 0.6 > \rho = 1$ from bottom to top. The transition from $\rho = 0$ to $\rho = 0.2$ is not detected as well as the others since this is below the previously calculated minimum difference. This accounts for the deviation in the approximate and exact values of Ω_{tot} , 0.05 and 0.06 respectively.

5-1-2 Sensitivity check

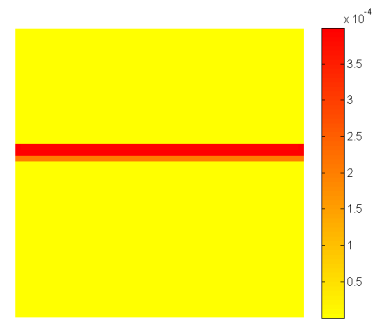
To check the sensitivities of the overhang term in the multiple objective use is made of the finite difference method. To do this an arbitrary element is selected in the test geometries and the density of this element is incrementally increased to eventually produce a dot. Figure 5-11 shows this for the ring, with the dot in the center of the ring. For every value of this dot Ω_{tot} and the sensitivity of Ω_{tot} with respect to the density of the dot is calculated using the equation for the sensitivity derived in Subsection 4-6-2. These calculated sensitivities are plotted in Figure 5-12a. Using the Ω_{tot} value calculated for every density of the dot and the increment of density change (here set to 0.01) the finite difference approximation can be computed, this result is shown in Figure 5-12b. As can be seen in these plots the calculated values and the finite difference values agree, indicating that the sensitivities are correct. This was also seen for the other test geometries.



(a) Geometry with small section of gradient with $\rho = 0$; $\rho = 0.2$; $\rho = 0.6$; $\rho = 1$ from bottom to top, all other elements have $\rho = 1$



(b) Exact Ω^* with $\Omega_{tot} = 0.060$



(c) Approximate Ω^* with $\Omega_{tot} = 0.050$

Figure 5-10: Minimum detectable ρ difference

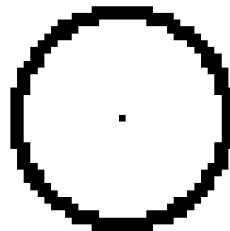
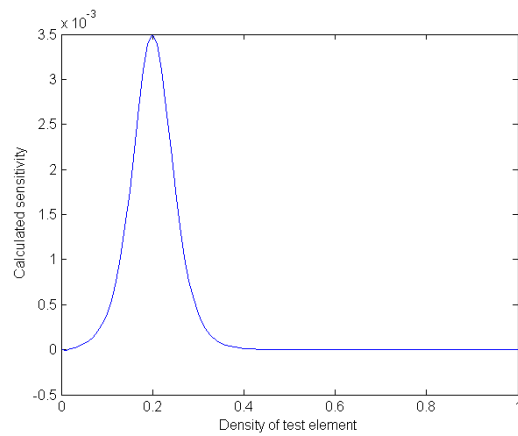
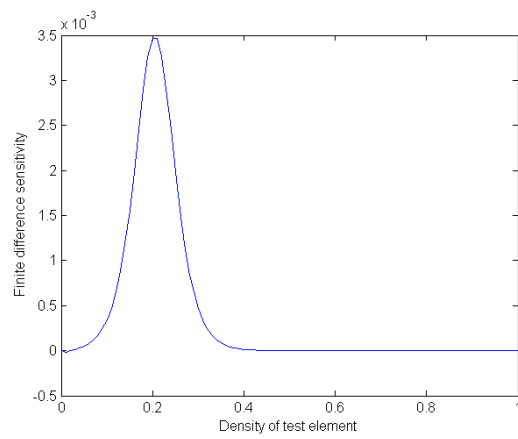
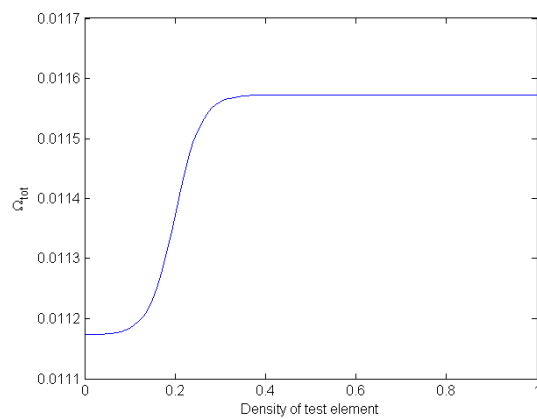


Figure 5-11: Density of arbitrary element (in the center of the ring) is incrementally increased from 0 to 1

**(a)** Calculated sensitivity**(b)** Finite difference sensitivity**(c)** Ω_{tot} for the density of dot**Figure 5-12:** Comparison of the calculated and the finite difference sensitivity

5-2 Verification of filter formulation

In this section the filter and its sensitivities are checked. The filter is applied to the portal geometry. Ω_{tot} is determined for the portal before and after filtering using the exact method and the density distribution is visually inspected. To more easily identify the density gradients the colormaps have been set to vary from dark red indicating low density to dark blue indicating high density.

To verify the derived sensitivities for the filter a coarse version of the portal geometry is used due to the long computation time. The portal is now constructed in a 15x15 element mesh. The sensitivity of a single element with respect to another arbitrarily selected element is determined, i.e. $\frac{\partial \tilde{\rho}_i}{\partial \rho_j}$. The element with respect to which the sensitivity is being determined, ρ_j , is varied from zero to one. For each value of ρ_j the value $\tilde{\rho}_i$ is determined and stored, using this information the finite difference approximation can be determined over the entire domain of ρ_j from one to zero. This is then compared to the calculated values. The elements chosen to be inspected are shown in Figure 5-13.

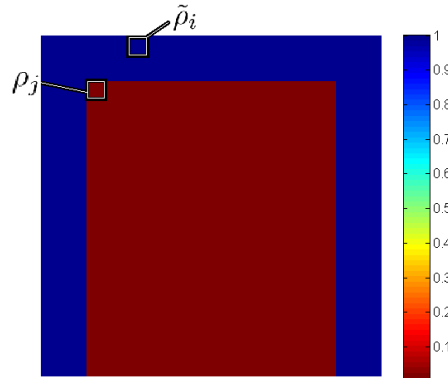


Figure 5-13: Element to be varied and element of which the sensitivity is determined

5-2-1 Modification by sequential scanning

The results for the sequential filtering method are shown in Figure 5-14. The first image shows the original geometry while the two others show the filtered geometry using $p_n = 8$ and $p_n = 1000$ respectively. The overall result is as desired; the mid-section of the overhanging part has been removed under a 45° angle. On the other hand some unexpected gradients are seen, but for the very high value of 1000 for p_n this disappears. Closer inspection shows that this result also shows the same alternating pattern in densities except the differences between density in each row are so small that they are not visible.

Looking at the calculated (exact) Ω_{tot} it is found that the overhang coefficient has increased after filtering. For the result with $p_n = 1000$ the overhang too is not zero. This is directly linked to the alternating density pattern. Every other row contributes positively to the overhang coefficient since these elements are not supported properly.

These deviations from the desired result can be explained again by the error introduced by the P-norm:

The elements in the bottom row have the correct values (ones and zeros), the values in the

second to bottom row are slightly lower than they should be. Taking the middle element of one of the pillars as a representative point, it is clear that ρ_i and ρ_{max} in Eq. (4-34) in reality are both one resulting in $\tilde{\rho} = 1$. Nevertheless in calculating ρ_{max} an error is introduced as described in Subsection 5-1-1. Since all candidate support elements are of density one the error is at its maximum, i.e. $\sqrt[p_n]{3}$ which for $p_n = 8$ is about 1.15. Plugging this in to Eq. (4-34) gives $\tilde{\rho} = 0.85$, which corresponds to the value produced by MATLAB. Note that since p_n is an even number the term $(1 - \rho_{max})^{p_n}$ is positive, if an uneven power is chosen complex values will be registered in MATLAB.

Moving on to the void section on the same row, taking the same approach $\rho_i = 0$ and $\rho_{max} = 0$. Unlike for the situation with the solid elements, for elements with a value of zero ρ_{max} returns zero, with no error. This time Eq. (4-34) becomes $\tilde{\rho} = 1 - \sqrt[p_n]{2}$ which for $p_n = 8$ gives $\tilde{\rho} = -0.09$. Doing this experiment for subsequent rows confirms the alternating pattern seen in Figure 5-14b.

It is clear that these errors are of the same type but originate from a different source. Needless to say increasing p_n reduces these errors, but they are not completely eliminated which has already been demonstrated by setting $p_n = 1000$. For this value for the P-norm power an Ω_{tot} is found near that of the unfiltered geometry. This is because the error produces a distinct border of elements with a value slightly above zero where the overhanging structure used to be under which elements of negative value are present (how this value varies with respect to p_n is shown in Figure 5-15). The (exact) overhang calculator registers this as overhang (ρ_Δ is smaller but still present) explaining the near unfiltered value of Ω_{tot} . This border is not seen in Figure 5-14c but it is present albeit for very low values of ρ_Δ .

Applying the filter to the corner loaded cantilever beam gives an indication of the effect the filter will have, see Figure 5-16.

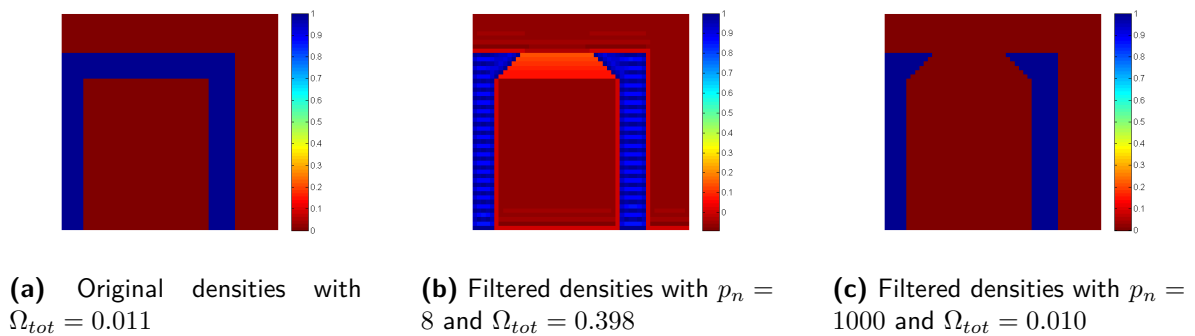


Figure 5-14: Filtering the densities by sequential scanning of the elements

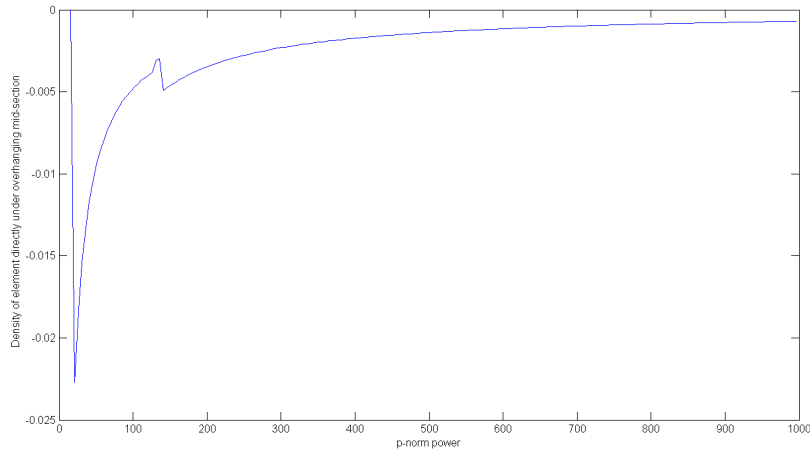


Figure 5-15: Effect of P-norm power on element density directly below overhang

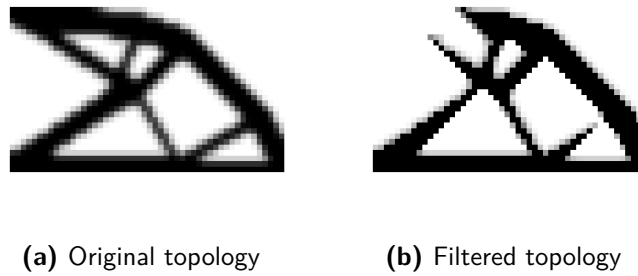


Figure 5-16: Filtering the corner loaded cantilever beam by sequential scanning of the elements

Sensitivity check

Varying the density of an element ρ_j in the portal produced the results shown in Figure 5-18 for the value and sensitivity of an element $\tilde{\rho}_i$. The element being varied, ρ_j (annotated in Figure 5-13) provides indirect support to element $\tilde{\rho}_i$. For $\rho_j = 0$ element $\tilde{\rho}_i$ is unsupported and thus the density is zero after filtering. As the density of ρ_j increases elements along the diagonal path leading to $\tilde{\rho}_i$, which were previously unsupported, become supported. Hence $\tilde{\rho}_i$ is increasingly supported allowing the density of this element to remain after filtering in an increasing quantity. Figure 5-17 shows the unfiltered and filtered densities of the portal for ρ_j equal to zero and one. Comparing Figure 5-17b and Figure 5-17d the additional strip of elements can be identified.

From this it can be deduced that the value of $\tilde{\rho}_i$ should be approximately proportional to ρ_j .

As is seen in Figure 5-18a the value of $\tilde{\rho}_i$ is indeed roughly proportional to ρ_j . Comparing the calculated and finite difference sensitivities in Figure 5-18b and Figure 5-18c respectively, it is seen that the sensitivity has been properly determined. Doing the same experiment for other element pairs also produced agreeing results.

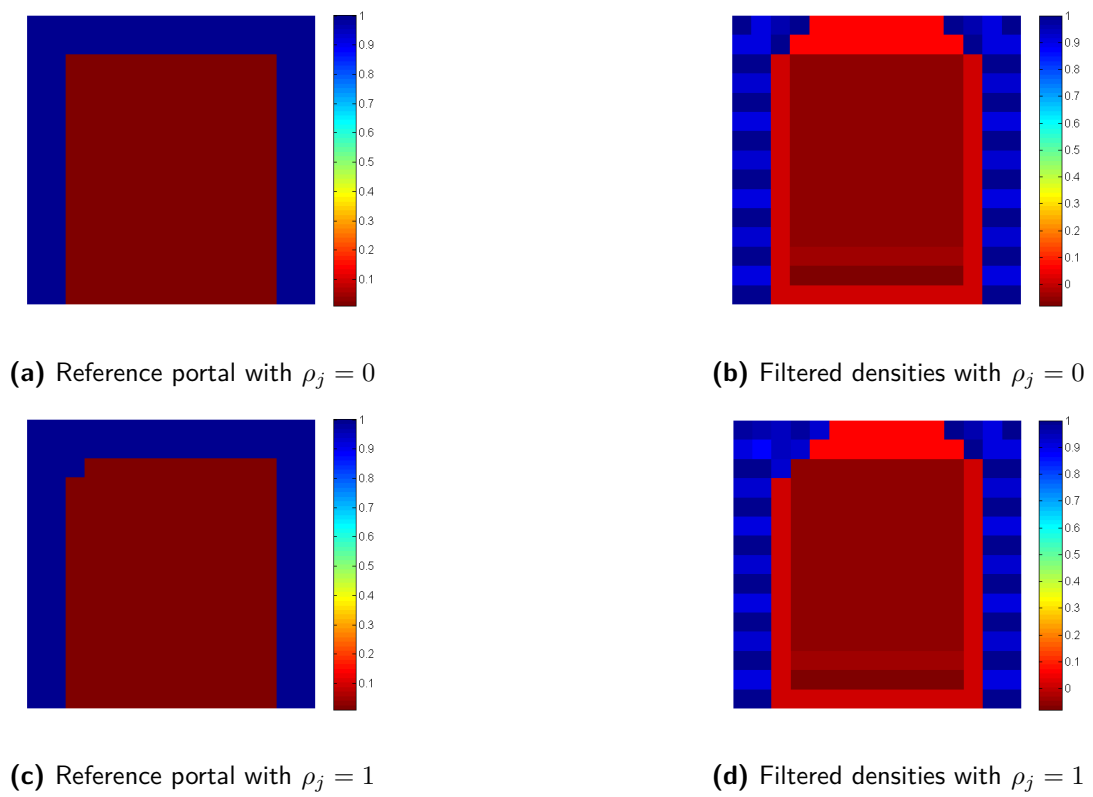
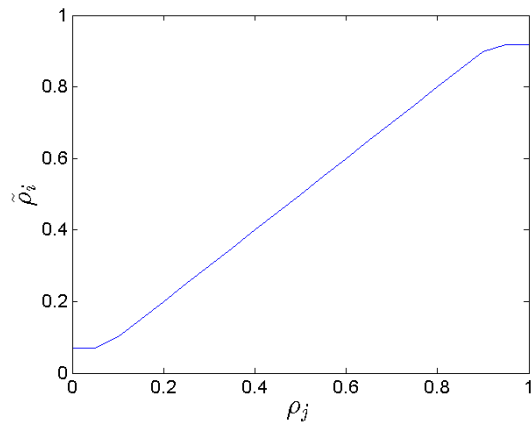
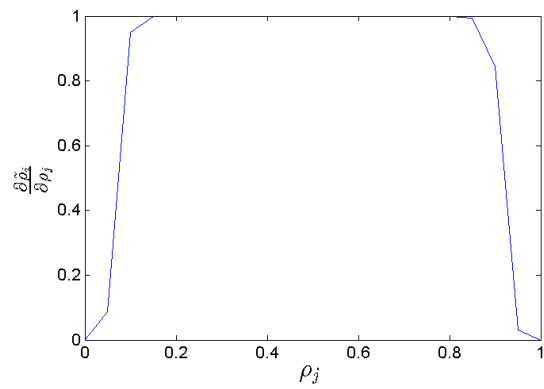


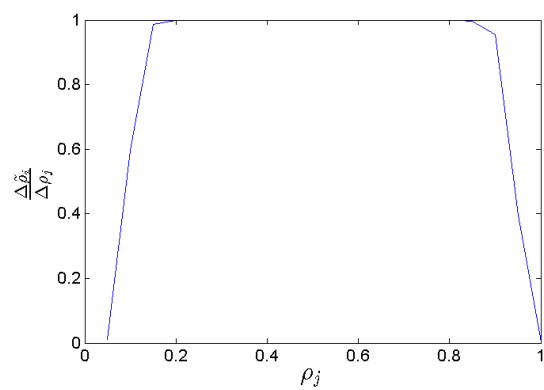
Figure 5-17: Filtered densities for varying density of test element



(a) Value of $\tilde{\rho}_i$ vs. ρ_j



(b) Calculated sensitivity



(c) Finite difference sensitivity

Figure 5-18: Comparison of calculated and finite difference sensitivity

Notes on implementation

In this chapter some issues encountered in the implementation of the previously described restriction methods into the 88-line topology optimization MATLAB code are discussed.

6-1 Element selection

All three restriction methods require the identification of candidate support elements. The multiple objective and global constraint approach also require the additional influenced elements to be identified for the calculation of the sensitivities. For this study a mask has been used to properly select the correct elements. That is, indices of the candidate support elements and influenced elements were predetermined with respect to the indices of the element under inspection. In the mesh used element rows are numbered from top to bottom and columns from left to right. Recalling Figure 6-1, for an element under inspection with row index i and column index j the candidate support elements (in the case of 45° overhang) are located one row lower, i.e. with row index $i + 1$. The column index of the candidate support elements are then $j - 1$, j and $j + 1$ from left to right.

A next step would be to introduce an element-selector which automatically selects the correct candidate support elements and influenced elements depending on the desired orientation and build angle. This would allow a more general formulation that could be applied to unstructured meshes and also allow inclusion of the build orientation into the optimization problem.

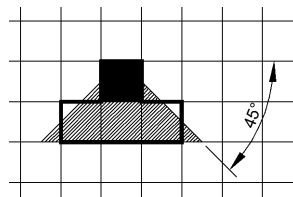


Figure 6-1: Candidate support elements for an element under inspection

6-2 Ghost-layers

In determining the overhang with the previously described mask, an issue arises when doing so for the elements along the boundaries of the design space. At these locations the mask will require elements that fall outside the design space, which do not exist. To account for these missing elements an extra layer of ‘ghost’ elements is added around the design space. This is done by embedding the density field into a larger matrix. The surrounding elements are given a value of zero, which corresponds to the inability to support any other elements, see Figure 6-2. The bottom layer of elements must be perceived as supported, but instead of setting the ghost layer of elements at this boundary to one, the bottom layer elements are simply not included in the operation. That is element scanning starts one layer higher. In determining the overhang coefficient as well as when filtering the densities, skipping the bottom row of elements results in no contribution to the overhang constraint and no changes due to filtering respectively. This corresponds to the elements being supported. To include the influenced elements needed when determining the sensitivities another ghost layer is needed. Thus two ghost layers have been added; $GL=2$ elements.

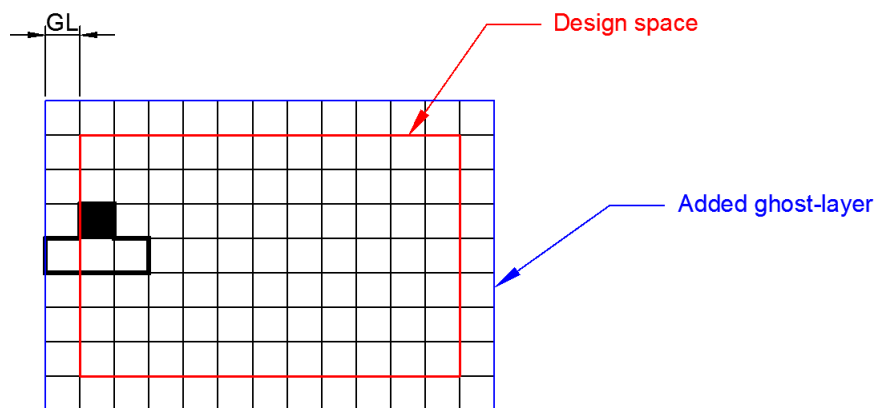


Figure 6-2: Ghost-layer

6-3 Invalid values

In calculating the sensitivities cases occur where density values of zero are raised to a negative power (e.g. $0^{\frac{1}{p_n}-1}$), for this MATLAB will return ‘Inf’ (infinity) as a solution. In all the cases where this happens the value is also multiplied by zero resulting in an undefined numerical result, in MATLAB this gives a ‘NaN’ value which stands for Not-a-Number. These values have been replaced by zero for the calculations to make sense.

6-4 Constraint in MMA

The Method of Moving Asymptotes (MMA) function used for the optimization (for a detailed description see [8]) is designed for optimization problems in which constraint functions are

of the form: $f_{constraint} \leq 0$. This means that the equality constraint presented in Subsection 4-6-3 cannot be implemented as such. Instead this becomes $\Omega_{fac}\Omega_{tot} \leq 0$, which still gives the optimizer the incentive to set the overhang to zero even though negative values are not possible.

Chapter 7

Final results

In this chapter the results of the implementation of the formulated restriction methods, i.e. multiple objective, global constraint and filter, applied to the load cases described in Chapter 3 are summarized. The obtained results are compared to the reference models and differences are identified. The complete set of results can be found in Appendix C.

7-1 Multiple Objective

Various runs were executed for all three load cases for several values of Ω_{fac} . The chosen Ω_{fac} values differ by an order of magnitude.

In all three load cases the topology changes for a sufficiently high Ω_{fac} . In the cases of the corner-loaded and mid-loaded cantilever beam struts in the design are reoriented. All topologies obtained with the multiple objective remained with overhanging sections where stalactite-like formations appeared. This is particularly visible for the tension beam. For increasing Ω_{fac} the volume fraction decreases. The overhang coefficient shows erratic behavior for Ω_{fac} values of 10^2 and up for the corner-loaded and mid-loaded cantilever beams. For the tension beam this is already the case for $\Omega_{fac} = 10$. The objective and compliance value also start to show erratic behavior for Ω_{fac} values of 10^3 and up.

None of the results converge nicely. Taking the results obtained for the same amount of iterations as was necessary to obtain the reference model still allows comparison of designs. In the following subsections these results are presented for each load case along with a more detailed description of the overall results.

7-1-1 Cantilever beam corner-load

Using a weight factor of 10 for the corner-loaded cantilever beam has no noticeable effect on the topology. The obtained compliance is almost identical to that of the reference model. Slight changes in topology start to appear when the weight factor is increased to 10^2 . The compliance is increased and the overhang coefficient has been decreased significantly. For

a weight factor of 10^3 much more drastic changes can be seen in the design. The volume fraction is pushed down further and the compliance is increased to about 159. The optimizer ends up cycling around this point after about 500 iterations. Design changes throughout the process are small though, the optimization can be terminated earlier while keeping the same general topology. The trend in the objective value during the optimization process is erratic showing many sharp peaks. This behavior is encountered in both terms that make up the objective, the compliance and overhang term. The topology obtained after 191 iterations Figure 7-1c shows the elimination of many of the struts encountered in the reference design. Instead a triangular structure is formed with two struts under 45 degree angles with another overhanging strut connecting the tip of the triangle to the constrained side of the design space. Some vague stalactite formation can be recognized on this overhanging strut. Looking at the plot of Ω^* in Figure 7-2c it is indeed seen that this overhanging strut is the major contributor to overhang in this design. For a weight factor of 10^4 a similar design as for a weight factor of 10^3 is found. The volume fraction continues to decrease as the compliance of the structure increases. Stalactite formations are present around the same area. The same general behavior is found for the objective value, namely an erratic distribution of values and cycling which occurs after about 650 iterations. The overhang coefficient has been reduced and is lower than any of the other results, but so is the volume fraction. Increasing the weight factor to 10^5 results in incoherent patches of material appearing and disappearing in the design space with no structural characteristics. The optimizer fails to find a topology that can provide a reasonable value of compliance, values are of the order 10^6 . Cycling is observed after about 70 iterations. The volume fraction has reduced to a value around a mere 0.047 and the overhang coefficient has become meaningless.

The results for the multiple objective approach for the corner-loaded cantilever beam are shown in Figure 7-1. The reference model is shown along with the result for a weight factor Ω_{fac} of 10^2 and 10^3 respectively.

The Ω^* values along with their respective overhang coefficients for these results are shown in Figure 7-2. An improvement in Ω_{tot} can be seen, which corresponds with a less overhanging elements.

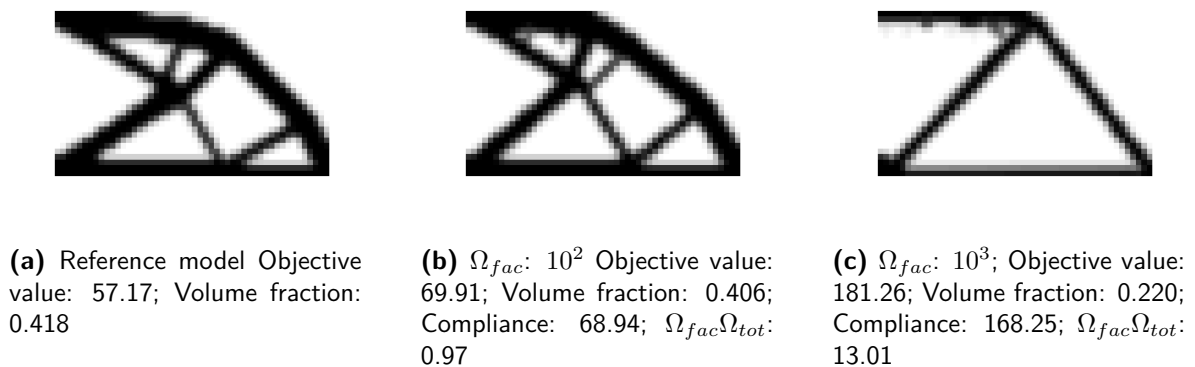


Figure 7-1: Results multiple objective for cantilever corner-load obtained in 191 iterations



(a) Ω^* for the reference model with $\Omega_{tot}=0.0274$

(b) Ω^* for $\Omega_{fac}=10^2$ with $\Omega_{tot}=0.0114$

(c) Ω^* for $\Omega_{fac}=10^3$ with $\Omega_{tot}=0.0165$

Figure 7-2: Ω^* multiple objective for cantilever corner-load; Using the following parameter values:
 $M = 35$; $\delta = 0.2$; $p_n = 8$

7-1-2 Cantilever beam mid-load

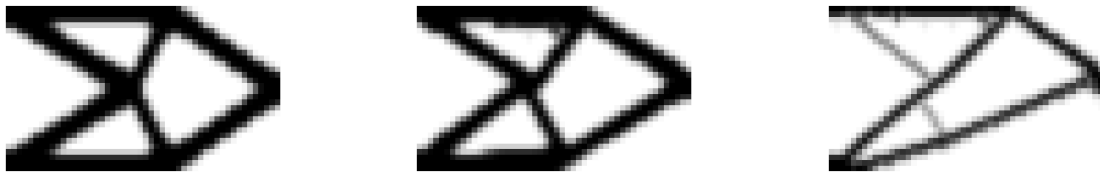
As with the corner-loaded cantilever beam a weight factor of 10 has no noticeable effect on the design of the mid-loaded cantilever beam. For a weight factor of 10^2 struts start to rearrange, but the overhang coefficient actually becomes higher. The onset of some stalactite formations can be recognized. The bottom section of the design starts to raise resulting in an overhanging strut. The compliance increases and the volume fraction decreases. The trend in overhang coefficient is not smooth. Setting the weight factor to 10^3 results in a design in which stalactite formations are more evident and the struts have been drastically rearranged. The overhang coefficient has increased further and the volume fraction has become lower. The compliance and objective value have increased and their behavior is erratic. Further increasing the weight factor to 10^4 , the volume fraction is reduced till about 30 iterations at which point the volume fraction becomes too low to form a coherent structure of reasonable compliance.

The results for the mid-loaded cantilever beam for Ω_{fac} equal to 10^2 and 10^3 obtained with a multiple objective are shown in Figure 7-3. The results shown here were obtained in 121 iterations.

The topology for the multiple objective becomes asymmetric and Figure 7-4 reveals that, even though one of the struts has been angled at 45° , a large portion of the structure (front/lower strut) has been angled at a smaller angle. The upper overhanging strut is extended introducing more overhanging elements.

7-1-3 Tension beam

For a weight factor of 10 stalactite formations are seen along the overhanging underside of the structure. A decrease in volume fraction is seen and the objective function and its compliance term shows an increase. The overhang coefficient has been reduced. A strongly decreased volume fraction is seen for a weight factor of 10^2 and stalactite formation has become more evident. The compliance and objective function have increased. The overhang coefficient has also increased slightly with respect to the result for a weight factor of 10. For a weight factor of 10^3 , the volume fraction is further reduced. The remaining topology shows many stalactite formations and a reduced overhang coefficient. The objective value and compliance have increased further. Setting the weight factor to 10^4 results in incoherent patches of material

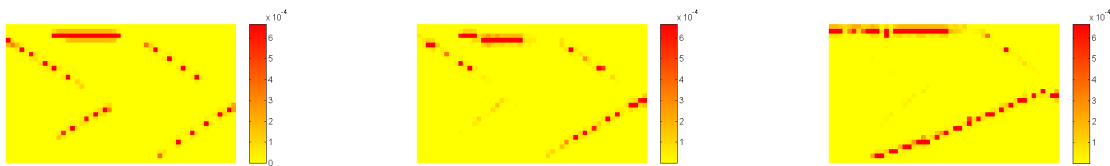


(a) Reference model Objective value: 64.00; Volume fraction: 0.426

(b) Ω_{fac} : 10^2 ; Objective value: 67.57; Volume fraction: 0.387; Compliance: 64.93; $\Omega_{fac}\Omega_{tot}$: 2.64

(c) Ω_{fac} : 10^3 ; Objective value: 256.6159; Volume fraction: 0.201; Compliance: 218.034; $\Omega_{fac}\Omega_{tot}$: 38.582

Figure 7-3: Results multiple objective for cantilever mid-load obtained in 121 iterations



(a) Ω^* for the reference model with $\Omega_{tot}=0.0352$

(b) Ω^* for $\Omega_{fac}=10^2$ with $\Omega_{tot}=0.0294$

(c) Ω^* for $\Omega_{fac}=10^3$ with $\Omega_{tot}=0.0452$

Figure 7-4: Ω^* global constraint for cantilever mid-load; Using the following parameter values: $M = 35$; $\delta = 0.2$; $p_n = 8$

appearing and disappearing throughout the design space.

In the reference model the tension beam load case needed 1160 iterations to meet the original termination criteria set in the 88-line MATLAB code. When running the optimization algorithm for the multiple objective the output showed cycling behavior around 80 iterations. Therefore this was set as the new termination criteria.

The results for the multiple objective problem are shown in Figure 7-5 and Figure 7-6. These figures show that the volume fraction occupied is drastically reduced for an increasing weight factor which increases the compliance. The overhang coefficient is slightly improved.

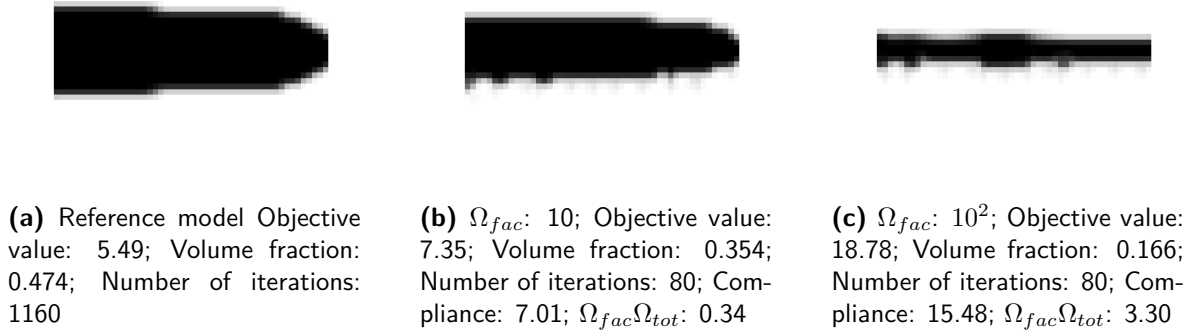


Figure 7-5: Results multiple objective for tension beam

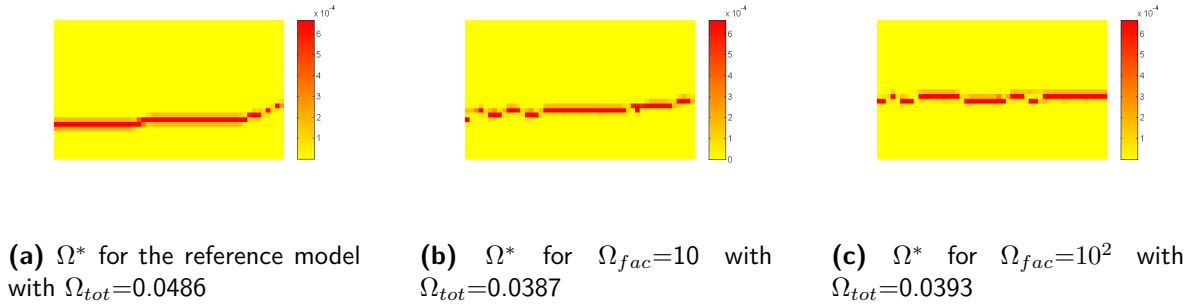


Figure 7-6: Ω^* multiple objective for tension beam; Using the following parameter values: $M = 35$; $\delta = 0.2$; $p_n = 8$

7-2 Global constraint

In general the designs obtained by the global constraint approach have comparable features to those obtained by the multiple objective approach. Reorientation of struts and stalactite formation can be found in all the designs. The lowering of volume fraction is also a recurring trait. Various values of Ω_{fac} do not affect the results very much. For the cantilever beams a value of 10^5 does lead to instability in the form of light patches of material appearing and disappearing in the design space. Since Ω_{fac} has little influence on the result comparison will only be made with results obtained with $\Omega_{fac} = 10$.

The erratic behavior described for the multiple objective is also present with the global constraint. In this case the erratic behavior is already present for $\Omega_{fac} = 10$.

7-2-1 Cantilever beam corner-load

Figure 7-7 shows the topology results results for the corner-loaded cantilever beam terminated after 191 iterations.

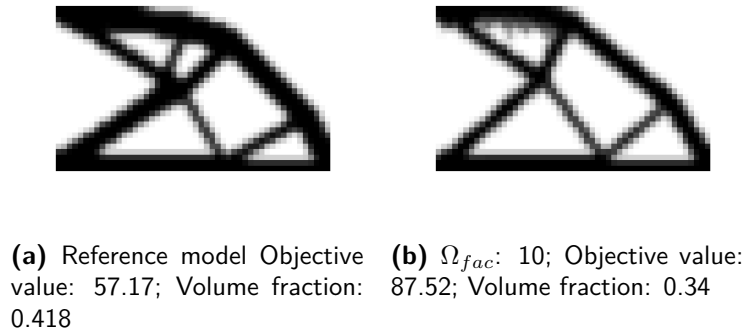


Figure 7-7: Results global constraint for cantilever corner-load obtained in 191 iterations

The Ω^* values along with their respective overhang coefficients for these results are shown in Figure 7-8. A significant improvement in Ω_{tot} is seen. The objective value is significantly increased for the added constraint and the volume fraction has decreased. As with the multiple objective, struts have been angled at 45° and more pronounced stalactite formations appear at the top of the design.

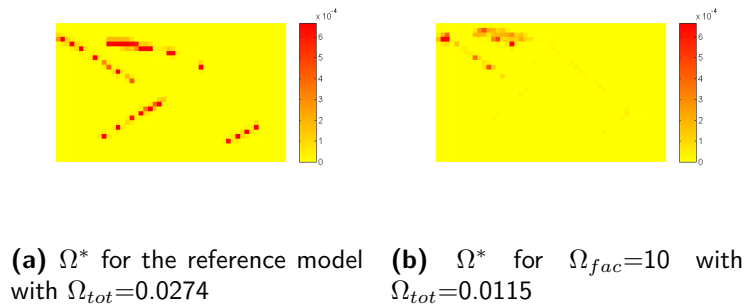
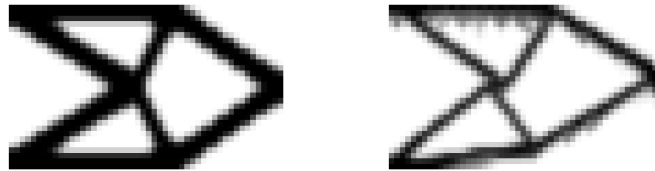


Figure 7-8: Ω^* global constraint for cantilever corner-load; Using the following parameter values: $M = 35$; $\delta = 0.2$; $p_n = 8$

7-2-2 Cantilever beam mid-load

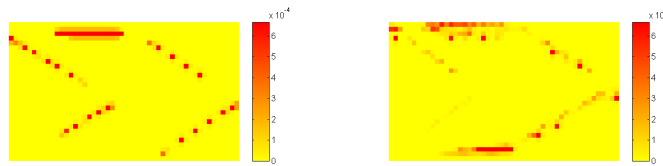
Running the optimization for the mid-loaded cantilever beam gives the results shown in Figure 7-9. Just as with the corner-loaded cantilever beam the effects are now much more pronounced than for the multiple objective. Formation of stalactites and a very low volume

fraction are observed. An increase of about 147% in objective value is seen accompanied by a slight decrease in overhang coefficient. The structure has become asymmetric, which is an unexpected result. Other struts have been altered such that these are under a smaller angle than the prescribed constraint this can be deduced from Figure 7-10.



(a) Reference model Objective value: 64.00; Volume fraction: 0.426
 (b) Ω_{fac} : 10; Objective value: 158.31; Volume fraction: 0.25

Figure 7-9: Results cantilever mid-load obtained in 121 iterations



(a) Ω^* for the reference model with $\Omega_{tot}=0.0352$
 (b) Ω^* for $\Omega_{fac}=10$ with $\Omega_{tot}=0.0333$

Figure 7-10: Ω^* global constraint for cantilever mid-load; Using the following parameter values: $M = 35$; $\delta = 0.2$; $p_n = 8$

7-2-3 Tension beam

Just as with the multiple objective the tension beam showed cycling, therefore the comparison model is terminated for a fewer amount of iterations than the reference model. In this case 250 iterations.

As seen in Figure 7-11 and Figure 7-12 the results for the tension beam show the same trends but again much more pronounced. An extremely low volume fraction results in higher compliance and stalactite formation is present. The overhang coefficient is generally much lower.

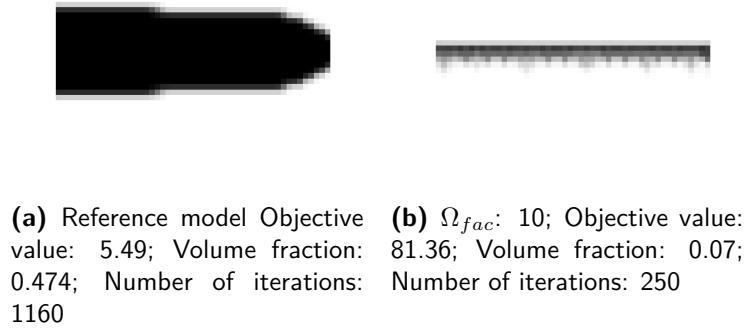


Figure 7-11: Results tension beam obtained

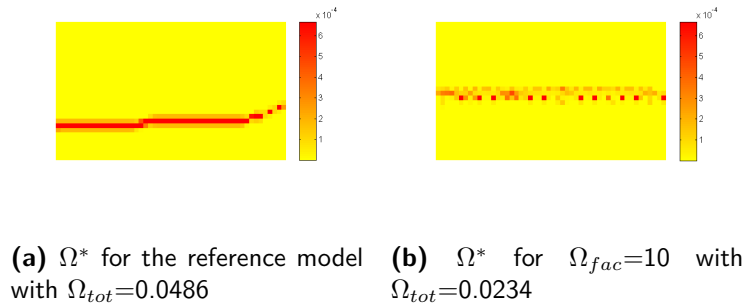


Figure 7-12: Ω^* global constraint for tension beam; Using the following parameter values: $M = 35$; $\delta = 0.2$; $p_n = 8$

7-3 Filter

As was the case in validating the sensitivities, computation time for the topology optimization with filter is extremely long. For reasonable computing times the mesh sizes for the test models have been reduced, maintaining the aspect ratio of the design space, to 25×15 elements.

None of the optimization runs with the filtering method converge. As the optimization progresses the topology becomes more pronounced but also lowered in volume fraction. This continues till at some point errors occur in the Method of Moving Asymptotes (MMA) optimizer. The objective and volume fraction values leading to this point do not show a smooth distribution, though there are not as many peaks and sharp transitions as in the results obtained for the multiple objective and global constraint approach.

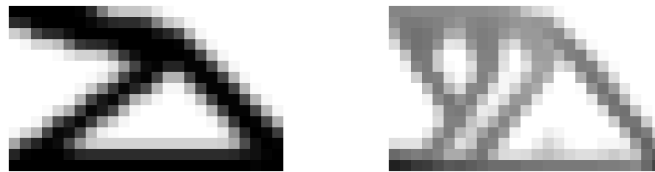
The topologies shown in this section have been obtained by terminating the algorithm near error introduction, but as pronounced as possible. In these topologies elements were encountered with negative valued densities.

Overhang of these results has not been calculated due to the alternating density nature of the topology for this filter (also seen in section 5-2). This makes the calculated overhang values meaningless.

Cantilever beam corner-load

The topology found for the corner-loaded cantilever beam by the filtering method has a very low volume fraction. The objective/compliance is very high. Nevertheless by visual inspection it can be deduced that this design has no overhang whatsoever.

The structure has been modified in a similar fashion as with the multiple objective and global constraint, except in this case internal supporting structures have been added to eliminate the remaining overhang.

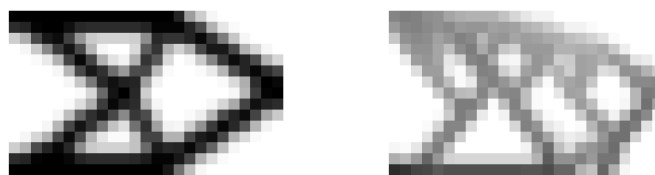


(a) Reference model Objective value: 63.60; Volume fraction: 0.46
(b) Objective value: 583.93; Volume fraction: 0.24 ; Number of iterations: 35

Figure 7-13: Results filter for cantilever corner-load

Cantilever beam mid-load

Similar to the corner-loaded cantilever beam, the mid-loaded beam has a low volume fraction a high objective/compliance value and no overhang. The design has again been slightly altered in general shape and augmented by internal supporting structures..



(a) Reference model Objective value: 63.41; Volume fraction: 0.45; Number of iterations: 75
(b) Objective value: 474.55; Volume fraction: 0.24; Number of iterations: 98

Figure 7-14: Results filter for cantilever mid-load

Tension beam

Once again the obtained structure is low in volume fraction and high in objective/compliance but without overhanging elements.



(a) Reference model Objective value: 5.36; Volume fraction: 0.48; Number of iterations: 304

(b) Objective value: 115.11; Volume fraction: 0.15; Number of iterations: 35

Figure 7-15: Results filter for tension beam

Chapter 8

Discussion

The results of the multiple objective and the global constraint approach show three main behaviors in the topology when introducing the overhang restriction. These are: slight modifications in strut orientation, stalactite formation, and the lowering of the volume fraction. In general the behavior is seen to be the same for both methods but more exaggerated for the global constraint. Which could be expected since the global constraint is a strict condition for which the optimizer must find a solution, while in the case of a multiple objective formulation the solution is allowed to be a compromise between the two objective terms. The fact that overhang is still present in the global constraint approach is due to the inner workings of the optimizer itself, Method of Moving Asymptotes (MMA). In cases where no solution can be found that complies with the imposed constraint the optimizer presents a non-feasible solution instead.

Additionally both these restriction methods show erratic behavior of the objective, compliance and Ω_{tot} value at some point.

The filter succeeded in creating structures that were fully supported by a combination of reorienting struts and introducing support structures.

In the following sections the observed behaviors will be discussed in further detail.

8-1 Modification of strut orientation

The fact that all three methods show reorientation of struts to meet the 45 degree overhang restriction indicates potential for all methods. The multiple objective and global constraint also altered struts such that these introduced more overhang. This may be due to the large contribution of these elements to the compliance of the structure. Another explanation for this can be that due to the lowered volume fraction and other alterations in the design the optimizer cannot find any other solution that provides a lower compliance value.

The filtering method demonstrated the ability to create support structures in the cases in the cases where elements had a large contribution to the compliance. The multiple objective and

global constraint resort to the formation of stalactites. The tension beam illustrates this very well since the only way to comply with the added restriction is to add support structures and the results for this load case showed a lot of stalactite formation.

8-2 Stalactites in multiple objective method and global constraint method

Formation of stalactite-like structures appear where elements need support. This phenomenon can be explained by taking a closer look at what the implications are of such a surface for the additional overhang term. A representation of these stalactites is shown in Figure 8-1. The contribution to the overhang term (marked in red) is decreased by reducing the number of unsupported elements to a single element. This way instead of having multiple unsupported elements, only one unsupported element remains. Such a structure does indeed present a good solution to the problem of reducing overhang, however it is impractical and not of any use in the fabrication process of Selective Laser Melting (SLM). For this it is necessary that the structure is fully supported and not simply reduced to a single point.

Since these stalactites form where radical changes in topology are necessary it can also be interpreted as a suggestion for the location of placement of support structures. The question remains why these stalactites are not extended to form fully developed support structures. This must be attributed to the nature of the way the overhang is formulated. The overhang behaves like a step function and as mentioned before the M-parameter determines how steep the curve is. If the value is too high the gradients in the function become extremely high and optimization is difficult. It seems that the chosen value for M of 35 is still too high and that this obstructs the optimizer from finding solutions with support structures. Setting this value to $M = 8$ gives a result for the corner-loaded cantilever beam in which support structures do form, see Figure 8-2.

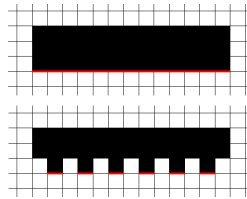


Figure 8-1: Stalactite formation

8-3 Erratic objective values, instability and Ω_{fac}

The effect of the step step function also explains the erratic behavior observed for the objective, compliance and overhang values. The steep transition in overhang coefficient causes these values to vary drastically for every iteration. For lower values of M this behavior will be smoother.

Since the filter does not make use of the overhang coefficient formulation the sharp transitions here originate from a different source. In this case the design may still experience drastic



Figure 8-2: Cantilever beam corner-load with parameters $\delta = 0.2$, $M = 8$, $p_n = 8$ and $\Omega_{fac} = 10^3$

changes due to lack of support, but these changes are the result of the sensitivity behavior. One may recall that the filtering method is also based on the approximation of a discrete valued concept. Namely that an element under inspection takes on the value of a candidate support element if support is not sufficient, otherwise nothing happens. The sharpness of this transition is determined by the value of the P-norm. A lower P-norm value will result in a worse approximation of the value to be assigned to the element under inspection which will diminish the quality of the filter. In Section 5-2 it was shown that the P-norm power is also responsible for negative values in the filtered design. The optimizer does not succeed in avoiding these negative values which at some point leads to instability in the algorithm. The Finite Element Analysis (FEA) in the algorithm cannot handle these negative values and ‘NaN’ values are produced. Consequently these ‘NaN’ values become the input for the MMA algorithm which results in an error. This is an important aspect of the filter that must be dealt with in further development. Another filtering method has also been formulated in the process of this research but not further developed due to time constraints. This method can be found in Appendix B. In this method densities are never negative but do take on values far greater than one, which is the drawback of this method.

The multiple objective and global constraint also show some instability. This occurs when Ω_{fac} is chosen to be very high. When this is done the volume fraction is lowered to such a point that not enough material is available to produce a coherent structure. Elements take on strongly varying density values but the optimizer is unable to find a solution anymore.

Increasing the value of Ω_{fac} allows the overhang term to become more important in finding the optimal solution. As Ω_{fac} is increased the overhang coefficient is seen to decrease as would be expected. Along with this the volume fraction of the topology is lowered which leads to the unstable behavior. The global constraint is less dependent on the weight factor. This is because for the MMA optimizer the value of the constraint is aimed to be set to zero or lower regardless of its magnitude. Setting Ω_{fac} sufficiently high though will still cause instability for the same reasons as the multiple objective. This is related to the way the optimization problem is solved in the MMA algorithm.

8-4 Lowered volume fraction and high compliance

The lowering volume fraction is presumed to be the result of behavior of the sensitivities. The sensitivities of the three methods (see Figure 5-12 and Figure 5-18) show that a zero value is obtained for low density values. In other words a minimum is found for a density of

zero. In minimizing the overhang coefficient this is, numerically, an acceptable method. This manifests as a lowering of the volume fraction of the topology.

Naturally, decreasing the volume fraction will result in increasing compliance values. The high compliance of the designs should not be a reason to render the obtained results worthless. The produced topology still shows useful structures. Taking the result obtained by the filter for the mid-loaded cantilever beam as an example the potential can be shown. Elements with a value lower than 0.3 have been set to zero and all other element densities have been increased to one. The resulting black-white topology shown in Figure 8-3 has a volume fraction of 0.5 and no overhanging elements. An FEA has been performed on this structure and a compliance of 53.88 is the result. This value is lower than that of the reference model (which was 63.41). Though the reference model has not been post-processed to be fully black and white this result indicates the potential of the topology.

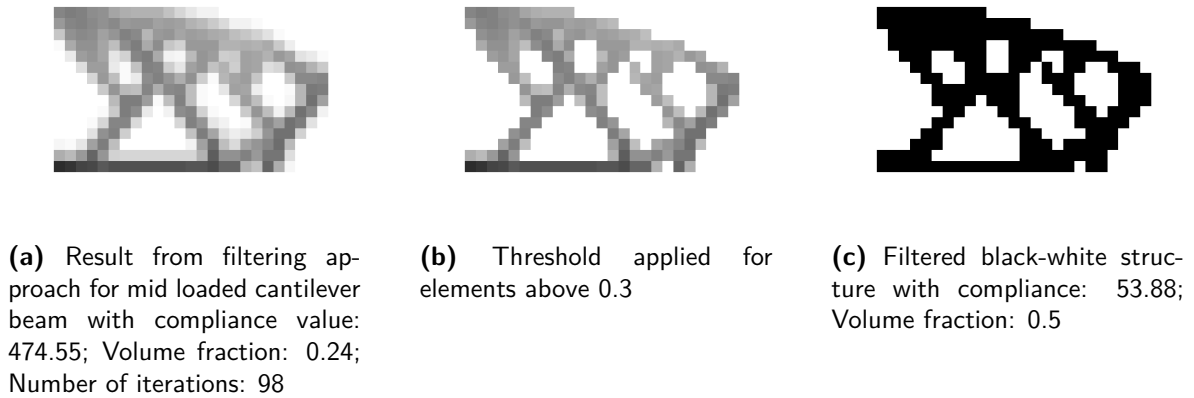


Figure 8-3: Extracting a black-white topology from the filter result

8-5 Additional considerations

Up till now the filter has shown the best results in terms of topology but the computation time is a major drawback. The main factor for this is the calculation of the sensitivities. For each element the sensitivity must be calculated with respect to all other elements in the design domain. This data is then stored for calculation of the sensitivities of the subsequent elements. A total of $N \cdot N$ calculations must be done (N is the number of elements in the design domain). For the implementation for this research memory pre-allocation has already been applied but a solution might be found in vectorization of operations. The nature of the filter might make this difficult since for every calculation the results of previous elements are needed (the sequential nature of the filter). The number of elements in the design domain for a 2D problem is

$$N = n_x \cdot n_y \quad (8-1)$$

where n_x and n_y are the number of elements along the horizontal (x-axis) and vertical (y-axis) of the design domain respectively. Making the number of calculations needed $n_x^2 \cdot n_y^2$. Extending this to 3D would mean the number of calculations needed would increase by a factor n_z^2 where n_z is the number of elements along the z-axis. Unless the method can be

implemented in a more efficient way practical application of this method may be ill-fated. Besides this extension to 3D also introduces a further increase in error when calculating ρ_{max} . In this case there are nine candidate support elements which need to be taken into account. Analogous to Eq. (5-5) the maximum introduced error is then found to be $\sqrt[3]{9} - 1$. This applies to all approaches

One must not lose sight of the big picture in developing these restriction methods. Eventually it is the goal to also take part orientation into account. It could very well be that by arranging the part to be built in a different orientation, i.e. changing the build direction, that modifications are not necessary. The tension beam is an example of this. If the entire beam were to be oriented to be built at a 45 degree angle the optimal design could be built without modification. It is therefore necessary to extend these restriction methods so this can be taken into account. In Section 6-1 element selection was discussed. If successfully applied the automated element selector can serve as a way to indicate the build direction. By defining this as a variable the optimization algorithm can be extended to include part orientation. A nested optimization could be a possible approach.

Chapter 9

Conclusion

The goal of this research has been to include the 45° overhang manufacturing constraint for Selective Laser Melting (SLM) into a topology optimization algorithm. Three methods to do this have been proposed, these are:

- By replacing the objective function by a multiple objective
- By adding a global constraint
- By applying a density filter

For the multiple objective and the global constraint a global measure for overhang in a design has been formulated. A filtering scheme has been formulated for the density filter which modifies the densities such that no overhanging elements remain.

The three methods have been implemented in a 2D topology optimization algorithm written in MATLAB. Tests have been carried out on three predictable reference models. All three methods produced results that showed promising behavior, but only the results obtained by the filtering method fully met the manufacturing constraint. The filter method generated results that were modified versions of the reference models augmented by supporting structures. Even the most extreme case where the reference design consisted of purely overhanging elements, a topology has been found where support structures have formed.

The other two methods should not be immediately discarded though. It has been found that a detailed investigation of parameter choice for these methods may yield parameters that lead to useful results.

The results revealed that the filter also needs further development due to instabilities in the optimization process. The instabilities have been presumed to be the repercussion of densities taking on negative values. Moreover the implementation of the filter as used in this research proved to be slow and convergence has not been achieved. Nonetheless the concept of a filtering method has been demonstrated to be a candidate for inclusion of the 45° overhang manufacturing constraint. The multiple objective and global constraint still show potential but have not been proven to generate the desired result.

The formulated restriction methods form a first step into obtaining a manufacturable design for SLM directly from topology optimization. The methods proposed form a basis for further research and provide a proof of concept.

Chapter 10

Recommendations

The approaches presented and investigated in this research have shown promising results, but it is clear that further development is needed. There are various aspects of the proposed approaches which can be developed. A list of some topics for future work and ideas for further investigation follows.

- The influence of the parameters associated with the overhang coefficient on the results of the topology optimization must be further investigated. Due to time constraint this could not be properly done in this research, though an indication of its potential was given in Chapter 8.
- The behaviour of the three methods may be influenced by other parameters in the optimization as well. These have not been investigated. The settings for the Method of Moving Asymptotes (MMA) algorithm are some of these parameters. Other parameters are the volume fraction, penalization power and filter radius of the mesh-independency filter.
- The filtering scheme presented in this thesis results in instabilities. This needs to be resolved. The filter concept presented in the appendix may provide a solution for this.
- The filtering method should be further improved so that computation time is reduced. A possible direction could be the vectorization of certain operations.
- Various implementation methods might also be possible. Applying a continuation method to the multiple objective or global constraint may be beneficial. Some suggestions could be:
 - Make the weight factor dependent on the iteration
 - Reset the optimization to start from an initial design which has already been optimized for compliance only

-
- Allowing a varying amount of overhang in the constrained approach instead of the strict rule that overhang must be at most zero.
 - To further advance in the direction of an SLM-ready topology optimized result, inclusion of orientation is necessary. This can be done by writing an element selecting algorithm. By including build direction in this selector the optimization problem can be extended to treat this as a variable.
 - Other methods of including the restriction could also be considered. For example a damage approach where overhanging elements are present but do not contribute to the stiffness of the structure.
 - In this research the choice has been made to focus on the discrete nature of the topology optimization process. Making use of the continuous nature of topology optimization remains another path which can be taken to incorporate restrictions.
 - It might also be of interest to consider other topology optimization methods than the Solid Isotropic Material Penalization (SIMP) method. The level-set method may prove to be a favorable alternative due to the well defined boundaries.

Appendix A

A-ADS hinge-bracket

In this chapter a description is given of how the topology optimization has been done for the A-ADS hinge-bracket.

First the design driving requirements are determined. Next two sub problems are set up to prepare the topology optimization. Finally the set-up for the topology optimization of the hinge-bracket is presented.

A-1 Design requirements

A list of requirements has been made that drive the design. These requirements follow from the operational requirements. The system is a precision pointing system and therefore stiffness (and eigenfrequency) play a large role. Based on the allowable eigenfrequency, dimensions and material properties of the booms a required rotational stiffness of $30^{kNm}/rad$ for the hinge-bracket around the y- and z-axis has been determined, see Figure A-1. In general, however, stiffer is better.

Besides the stiffness requirement it is desirable to minimize the mass of the hinge-bracket since this translates to cost in the sense of rocket fuel needed to transport the system into space. Additionally this also reduces material cost when manufacturing with Additive Manufacturing (AM).

The hinge-bracket will be of metallic material but will have to interface with the Carbon Fiber Reinforced Polymer (CFRP) booms. The lay-up of the booms will be designed such that the Thermo-elastic deformation (TED) is minimized to minimize disturbances in pointing. This will result in a mismatch of coefficient of thermal expansion (CTE) at the interface between boom and hinge-bracket. The final design should be able to cope with this. The TED of the total hinge assembly (hinge-bracket including synchro pulley-system, spring and lock mechanism) is also restricted and must be smaller than 0.005° in the operational temperature range, which is $-150^\circ C$ to $90^\circ C$.

These main design requirements for the hinge-bracket are summarized below.

- Rotational stiffness of at least $30^kNm/rad$ around y- and z-axis (derived from allowable system eigenfrequency)
- Mass of hinge assembly (incl. brackets, hinge unit, synchro-pulleys) < 2.6 kg
- Interface to CFRP boom with inner diameter $100\text{ mm} \pm 0.5\text{ mm}$ and $CTE = -0.2^{micron}/m \cdot K$
- Design for minimum mass, compatible with strength, stiffness and TED requirement
- TED of the hinge assembly $< 0.005^\circ$ in operational temp. range
- Operational temp. $-150^\circ C$ to $90^\circ C$

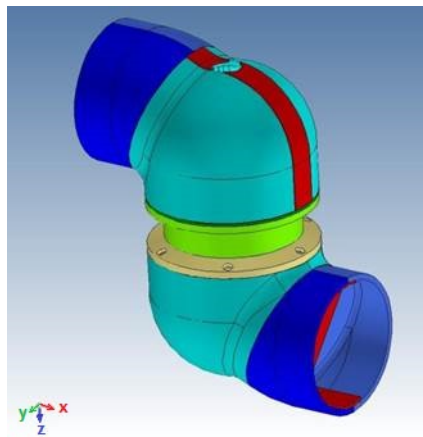


Figure A-1: Schematic representation of the hinge-bracket

For this thesis the problem has been greatly simplified by excluding the thermal mismatch of the assembly. For a functional design it is crucial that this is taken into account. Hence the following results are purely demonstrative for the topology optimization process. This leaves the main design requirements of stiffness and mass. This has been interpreted as a compliance minimization problem of which the expected result is a conceptual design which gives insight in how material can be best distributed.

The problem can be split up into two main load cases; loading around the z-axis and loading around the y-axis. Loading around the z-axis is an in-plane torque, while loading around the y-axis is an out-of-plane torque. These load cases have first been set-up independently in two sub problems.

An experimental topology optimization code provided by the TU Delft has been used to obtain the results in this chapter. The finite elements in this algorithm are solid isotropic and do not support rotations. The mesh generated is a 3D grid mesh. The optimizer is based on Method of Moving Asymptotes (MMA). The results presented in this chapter were obtained with the following parameters:

Penalization power: 3
 Filter radius: 1.8
 Volume fraction: 0.5

A-2 Circular in-plane torque

The first 3D model, presented here, is that with a circular load case of in-plane torque. The design space is cuboid with dimensions 50x50x100 elements. One of the square faces is fully clamped and the torque is applied over a ring of nodes. Such a load case is a common one in practice and the results can be compared with the many practical applications and can be expected to be tubular.

Figure A-2 shows the schematic representation of the problem. The red arrows indicate the clamped degrees of freedom applied to all nodes on the respective side, while the green arrow shows the applied load on the group of nodes that fall within the green box. The clamped condition is applied to the pink face and the green ring indicates the volume over which the torque is applied. The finite elements of the optimizer do not allow simple application of a torque. Instead, to emulate a torque, the ring has been divided into subsections on which a force is applied tangent to the ring. Doing this over the entire ring will effectively result in torque. The saw-tooth appearance of the ring is due to all the force vectors on the subsections.

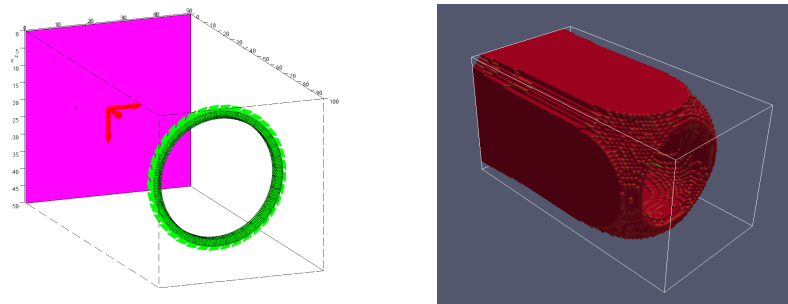


Figure A-2: Load case circular in-plane torque (left) and result (right)

A-3 Circular out-of-plane torque

The second load case is the out-of-plane torque applied over a ring. As in the in-plane torque, one face is fully clamped and a ring divided into subsections is used to impose a torque. In this case the force vectors are applied perpendicular to the ring and the magnitude of the force varies sinusoidally with its angular location on the ring. The design space dimensions are kept the same as for the circular in-plane torque case.

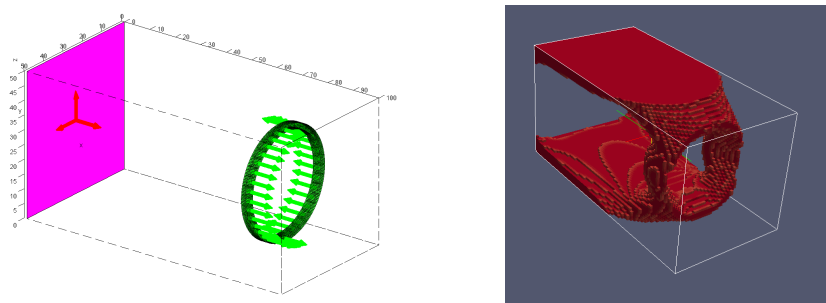


Figure A-3: Load case circular out-of-plane torque (left) and result (right)

A-4 Hinge-bracket

For the hinge-bracket the design space is a 150x150x250 element cuboid in which one of the square faces is fully clamped. Attached to this face is a tube that represents the CFRP tube to which the hinge-bracket will connect. This plays an important role in a later stage of design in the modeling of the thermal mismatch between the tube and the bracket. This section is also of importance to be able to take the effect of the adhesive connection into account. Due to the limitations of the code being used the CFRP tube can only be modeled as an isotropic material, therefore some replacement values must be determined to get the proper response. Since the thermal mismatch is the main reason for the inclusion of the tube, the critical stiffness for this situation is chosen for the bulk value of the tube. The most important stiffness in this case is that tangential to the tube, the tube will be manufactured such that this will be 89 GPa.

The inner diameter of the tube is 100mm and the wall thickness will be 2mm. The length of the modeled tube is set at 60mm. To make sure the optimizer sees the tube as potential connection surface and not the clamped face, a rectangular void is imposed against the entire (clamped) face. A remainder of tube is left protruding the void space, this protrusion will serve as adhesive surface. The length of this surface has been chosen to be 25mm since this is the maximum length commonly used for adhesive surfaces. A cylindrical void is imposed where a spring and latching system will be inserted, the diameter of the cylinder is 47mm and the height is set to 64.2mm. Forces will be applied at the (base) connection point of this spring and latching system. The connection is ring-shaped and therefore so will be the forces. The two load cases presented earlier (circular in-plane torque and circular out-of-plane torque) will be applied. The torques will both be of unit magnitude.

Figure A-4 shows a schematic representation of the boundary conditions and loads, pink represents the fully clamped surface (with the arrows indicating the clamped DOFs), yellow indicates void space and the forces are shown in green.

The results for this configuration are shown in Figure A-5.

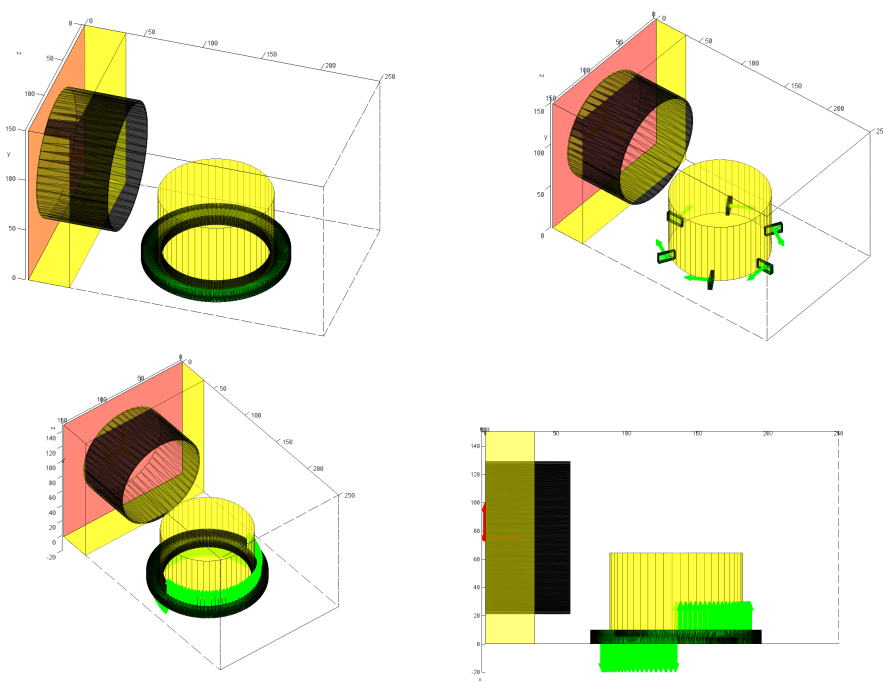


Figure A-4: Load case of the hinge-bracket

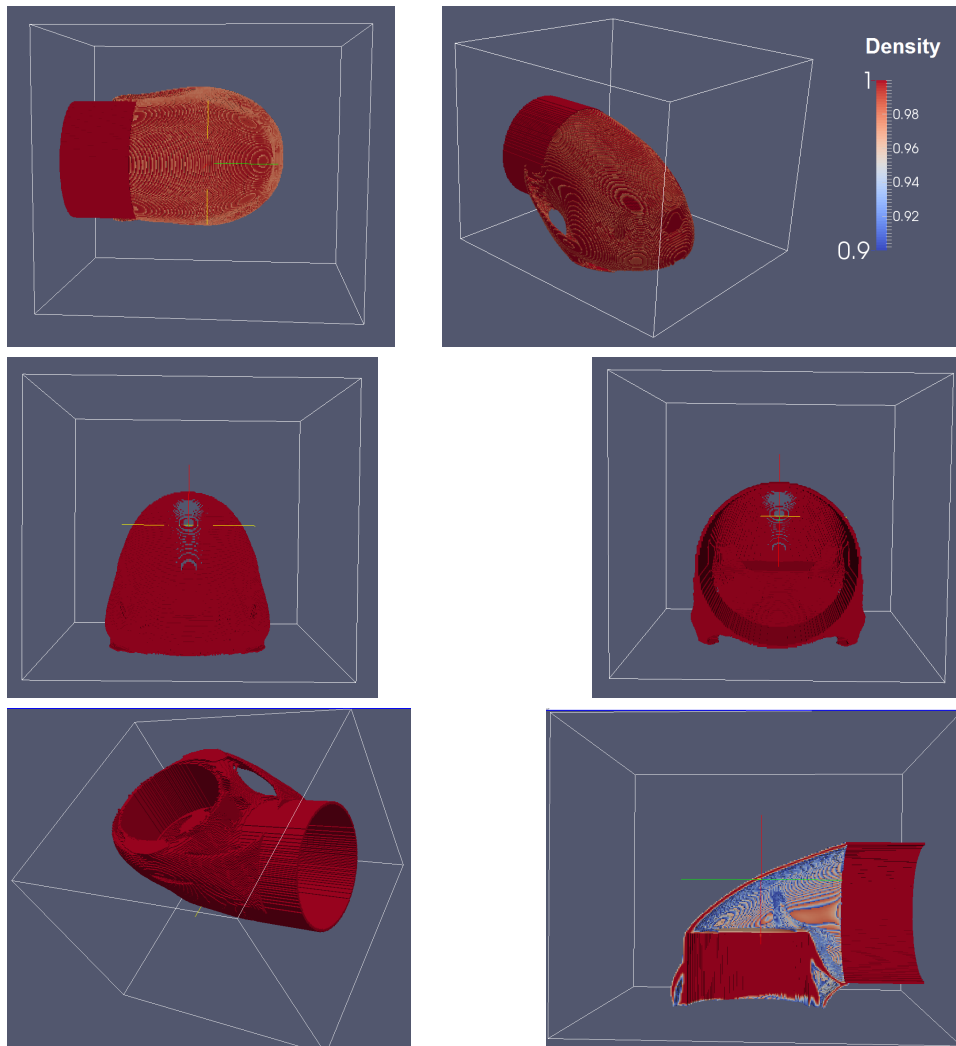


Figure A-5: Result of the hinge-bracket

Appendix B

Another filter approach

B-1 Formulation of the filter - Modification by supportivity matrix

In this chapter another filtering approach is presented. The idea behind this filter is to modify the element densities by scaling these with a measure that accounts for the amount of support available.

To achieve this, first a new definition is introduced, the so-called supportivity of an element. The supportivity is a value between zero and one assigned to an element that quantifies to what extent an element is supported, i.e. a maximally supported element has a supportivity of one while an absolutely unsupported element has a value of zero. One must note however that the supportivity of one element is dependent on the supportivity of the elements below it. An element that is not supported, in turn, cannot support any other element, thereby influencing the supportivity of an element above it.

For ease of implementation the supportivity of each element is stored in a matrix, the supportivity matrix, so that these values can be called for the calculation of supportivity of elements above. By executing an element-wise multiplication (denoted by \circ) with the supportivity matrix and density matrix, a modified density matrix is obtained in which the densities of all unsupported elements have been scaled such that they are supported and all other densities are modified accordingly. By this the desired effect of the filter has been achieved. The key difference in this filter is that the densities are scaled with a value between zero and one and can thus never take on negative values.

The supportivity has been defined as:

$$S_i = S_{max_i} \cdot \rho_{max_i} \quad (\text{B-1})$$

Where:

S_i = The supportivity of element i

S_{max_i} = The maximum value of the supportivity of the candidate support elements for element i

ρ_{max_i} = The maximum density of the candidate support elements for element i

In Eq. (B-1) S_{max_i} accounts for the dependence on all elements below element i . All these elements must be supported as should these elements be supported by the elements below them and so on. This is thus a global term. S_{max_i} is approximated by again using the P-norm. The supportivity is then scaled with the maximum density value of the candidate support elements by multiplying with ρ_{max_i} , since an element can only support as much material as it is supported by. ρ_{max_i} is a local term.

A matrix is constructed containing the supportivity of each element, the supportivity matrix. In this matrix all the values of the bottom row will always have a value of one. This accounts for the support of the base-plate on which the design would be built.

The new element densities now become:

$$\tilde{\rho} = S_{max} \circ \rho_{max} \circ \rho \quad (\text{B-2})$$

or for an arbitrary element ρ_i :

$$\tilde{\rho}_i = S_{max_i} \cdot \rho_{max_i} \cdot \rho_i \quad (\text{B-3})$$

Per example the calculation of the modified density is demonstrated for an element ρ_0 as displayed in Figure B-1. The numbering denotes the element numbers, note that this numbering does *not* correspond to the numbering of the elements in the code. The element under inspection is at the top, ρ_0 , elements 1-3 are the first line of support, these are supported by elements 4-8 and these are then in turn supported by elements 9-15. For the modified density of ρ_0 we have:

$$\rho_{max_0} = \sqrt[p_n]{\rho_1^{p_n} + \rho_2^{p_n} + \rho_3^{p_n}} \quad (\text{B-4})$$

$$S_{max_0} = \sqrt[p_n]{S_1^{p_n} + S_2^{p_n} + S_3^{p_n}} \quad (\text{B-5})$$

			0			
		1	2	3		
	4	5	6	7	8	
9	10	11	12	13	14	15

Figure B-1: Involved elements in determining the supportivity of an element ρ_0 .
Numbers denote element numbers (not corresponding to actual numbering in the MATLAB code).

Where:

$$S_1 = S_{max_1} \cdot \rho_{max_1} \quad (B-6)$$

$$\text{with:} \quad (B-7)$$

$$S_{max_1} = \sqrt[p_n]{S_4^{p_n} + S_5^{p_n} + S_6^{p_n}} \quad (B-8)$$

$$\rho_{max_1} = \sqrt[p_n]{\rho_4^{p_n} + \rho_5^{p_n} + \rho_6^{p_n}} \quad (B-9)$$

$$\text{and} \quad (B-10)$$

$$S_4 = S_{max_4} \cdot \rho_{max_4} \quad (B-11)$$

$$S_5 = S_{max_5} \cdot \rho_{max_5} \quad (B-12)$$

$$S_6 = S_{max_6} \cdot \rho_{max_6} \quad (B-13)$$

$$\text{with:} \quad (B-14)$$

$$S_{max_4} = \sqrt[p_n]{S_9^{p_n} + S_{10}^{p_n} + S_{11}^{p_n}} \quad (B-15)$$

$$\rho_{max_4} = \sqrt[p_n]{\rho_9^{p_n} + \rho_{10}^{p_n} + \rho_{11}^{p_n}} \quad (B-16)$$

$$S_{max_5} = \sqrt[p_n]{S_{10}^{p_n} + S_{11}^{p_n} + S_{12}^{p_n}} \quad (B-17)$$

$$\rho_{max_5} = \sqrt[p_n]{\rho_{10}^{p_n} + \rho_{11}^{p_n} + \rho_{12}^{p_n}} \quad (B-18)$$

$$S_{max_6} = \sqrt[p_n]{S_{11}^{p_n} + S_{12}^{p_n} + S_{13}^{p_n}} \quad (B-19)$$

$$\rho_{max_6} = \sqrt[p_n]{\rho_{11}^{p_n} + \rho_{12}^{p_n} + \rho_{13}^{p_n}} \quad (B-20)$$

$$(B-21)$$

Since the supportivity of all the elements on the bottom row, elements 9-15, are one (supported by the base-plate), S_{max_4} , S_{max_5} and S_{max_6} are each equal to $\sqrt[p_n]{3}$, this is also the case for S_{max_7} and S_{max_8} . This will approximate one for large values of p_n , the deviation from one is an error that is introduced by the use of the P-norm. With this we now get:

$$S_4 = \sqrt[p_n]{3} \cdot \rho_{max_4} \quad (B-22)$$

$$S_5 = \sqrt[p_n]{3} \cdot \rho_{max_5} \quad (B-23)$$

$$S_6 = \sqrt[p_n]{3} \cdot \rho_{max_6} \quad (B-24)$$

$$(B-25)$$

substituting and rewriting then gives:

$$S_1 = \sqrt[p_n]{3} \sqrt[p_n]{\rho_9^{p_n} + \rho_{10}^{p_n} + \rho_{11}^{p_n} + \rho_{10}^{p_n} + \rho_{11}^{p_n} + \rho_{12}^{p_n} + \rho_{11}^{p_n} + \rho_{12}^{p_n} + \rho_{13}^{p_n}} \cdot \sqrt[p_n]{\rho_4^{p_n} + \rho_5^{p_n} + \rho_6^{p_n}} \quad (\text{B-26})$$

$$= \sqrt[p_n]{3} \cdot \sqrt[p_n]{\sum_{i=9}^{13} \rho_i^{p_n} \cdot \sum_{i=4}^6 \rho_i^{p_n}} \quad (\text{B-27})$$

Analogously S_2 and S_3 can be found to be:

$$S_2 = S_{max_2} \cdot \rho_{max_2} \quad (\text{B-28})$$

$$= \sqrt[p_n]{3} \cdot \sqrt[p_n]{\sum_{i=10}^{14} \rho_i^{p_n} \cdot \sum_{i=5}^7 \rho_i^{p_n}} \quad (\text{B-29})$$

$$S_3 = S_{max_3} \cdot \rho_{max_3} \quad (\text{B-30})$$

$$= \sqrt[p_n]{3} \cdot \sqrt[p_n]{\sum_{i=11}^{15} \rho_i^{p_n} \cdot \sum_{i=6}^8 \rho_i^{p_n}} \quad (\text{B-31})$$

By substituting all this into Eq. (B-3) the modified density is found to be:

$$\rho_{Phys_0} = \left(\sqrt[p_n]{3} \cdot \sqrt[p_n]{\sum_{i=9}^{13} \rho_i^{p_n} \cdot \sum_{i=4}^6 \rho_i^{p_n} + \sum_{i=10}^{14} \rho_i^{p_n} \cdot \sum_{i=5}^7 \rho_i^{p_n} + \sum_{i=11}^{15} \rho_i^{p_n} \cdot \sum_{i=6}^8 \rho_i^{p_n}} \right) \cdot \sqrt[p_n]{\sum_{i=1}^3 \rho_i^{p_n} \cdot \rho_0} \quad (\text{B-32})$$

It can be seen from this example that all elements that could possibly contribute to the support of element ρ_0 all the way down to the base of the design space are involved in this method.

B-2 Validation - Modification by supportivity matrix

For verification the filter is applied to the portal geometry, Ω_{tot} is determined for the portal before and after filtering using the exact method and the density distribution is visually inspected. To more easily identify the density gradients the colormaps have been set to vary from dark red indicating low density to dark blue indicating high density.

Figure B-2 shows the results for the filter using the supportivity matrix. In this case all elements that were originally void ($\rho = 0$) are still void after filtering, i.e. no negative values. For values above zero, as with the sequential filter, the bottom row of elements all have the correct values (ones or zeros), but every sequential row has a value that deviates from what

it should be. In this case a relatively smooth gradient is seen (as opposed to the alternating pattern in the sequential filter). The element densities increase as they near the top of the geometry. This divergence from the correct value can again be attributed to the P-norm approximation. In this case the error is introduced in two ways, first of all by the ρ_{max_i} term and secondly by the S_{max_i} term in Eq. (B-3). The error introduced by the S_{max_i} term increases for every row since it includes the ρ_{max_i} and S_{max_i} values of the elements below it. Thus the error accumulates further towards the top of the geometry. For $p_n = 8$ the top element of the geometry has a value of 30620, which is an absolutely unacceptable value considering ρ may only vary from one to zero. Increasing p_n to 1000 this value reduces to 1,086 (this behavior is shown in Figure B-3).

Besides the introduced error the general behavior of the filter is as desired. The overhanging mid-section of the portal has been properly removed, leaving 45 degree angles at the edges. The overhang coefficient found for the filtered geometry is not zero, this is due to the gradient in the geometry which registers as overhang.

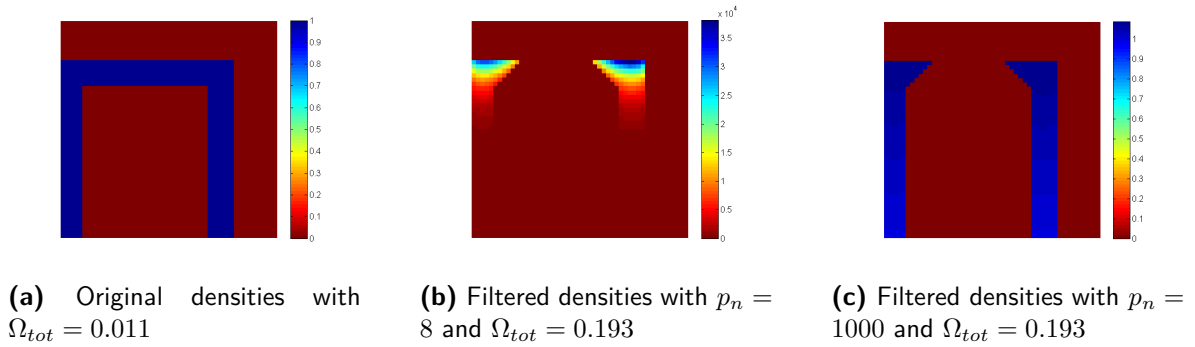


Figure B-2: Filtering the densities using the supportivity matrix

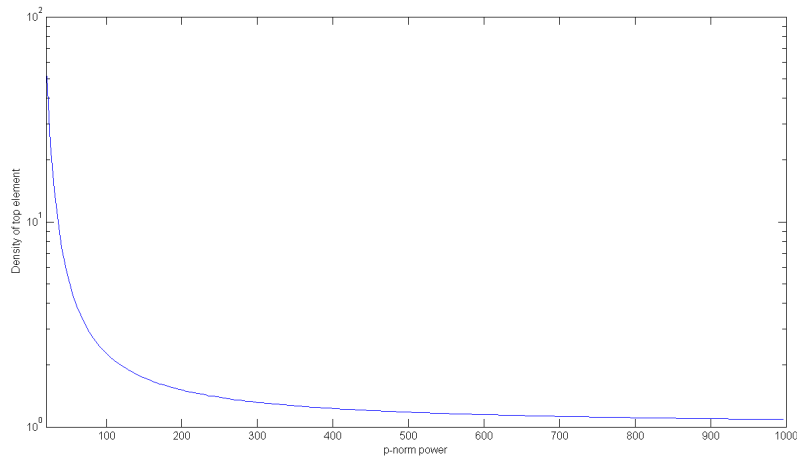


Figure B-3: Effect of P-norm power on the density of a element at the top of the structure

Applying the filter to the corner loaded cantilever beam gives an indication of the effect the filter will have, see Figure B-4.

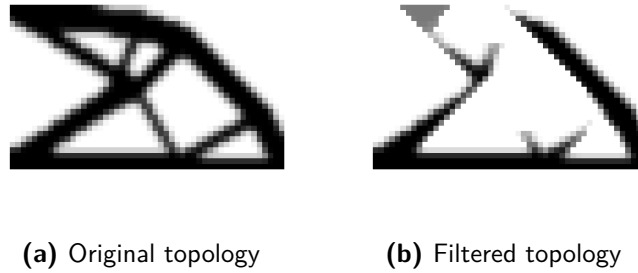


Figure B-4: Filtering the corner loaded cantilever beam using the supportivity matrix

The need for extremely high values of P-norm power is a large drawback of this filter and will most-likely cause difficulties in implementation in the topology optimization. The accumulating error makes the quality of the filter mesh-dependent, the error is increasingly large for larger meshes. Extending this approach to 3D will increase the accumulative error even further making implementation even more challenging. Nevertheless the concept may provide a more numerically stable alternative to the sequential filter introduced in Section 4-7, though much development is needed. Due to time constraints this approach has not been developed any further.

Appendix C

Results

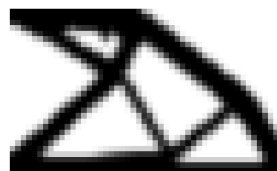
In this chapter the results for the three overhang restriction methods are presented. Each method has been applied to the corner-loaded and mid-loaded cantilever beam and the tension beam. Graphs of the objective, volume fraction and where applicable the overhang coefficient and compliance values for each iteration are given. The obtained topology and where applicable Ω^* are given for the final iteration unless stated otherwise in the caption.

C-1 Multiple objective

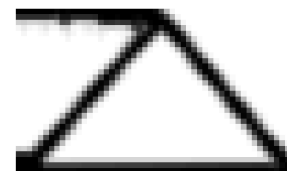
C-1-1 Corner-loaded cantilever beam



(a) $\Omega_{fac} = 10$



(b) $\Omega_{fac} = 10^2$



(c) $\Omega_{fac} = 10^3$

Figure C-1: Topology

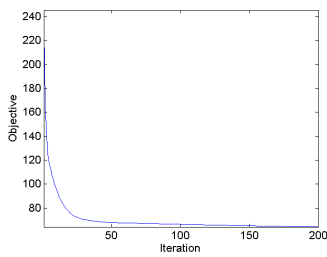


(a) $\Omega_{fac} = 10$

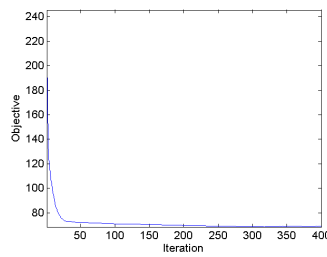
(b) $\Omega_{fac} = 10^2$

(c) $\Omega_{fac} = 10^3$

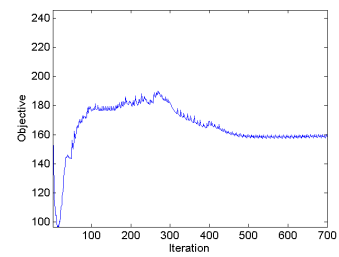
Figure C-2: Ω^*



(a) $\Omega_{fac} = 10$

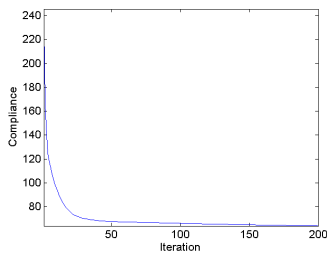


(b) $\Omega_{fac} = 10^2$

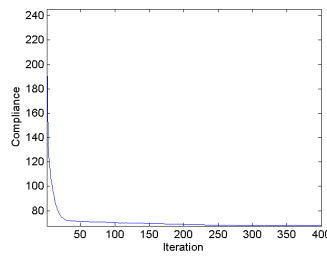


(c) $\Omega_{fac} = 10^3$

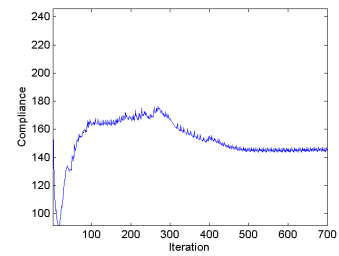
Figure C-3: Objective value



(a) $\Omega_{fac} = 10$

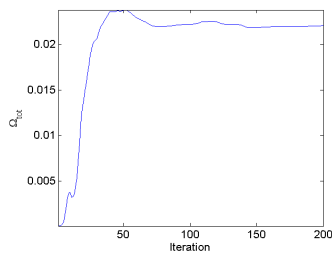


(b) $\Omega_{fac} = 10^2$

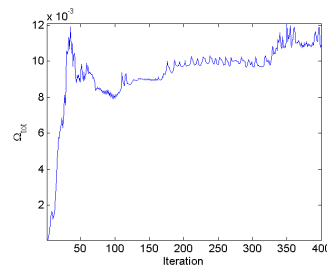


(c) $\Omega_{fac} = 10^3$

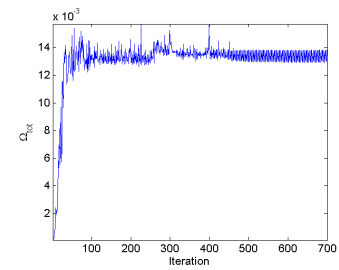
Figure C-4: Compliance value



(a) $\Omega_{fac} = 10$



(b) $\Omega_{fac} = 10^2$



(c) $\Omega_{fac} = 10^3$

Figure C-5: Overhang coefficient value

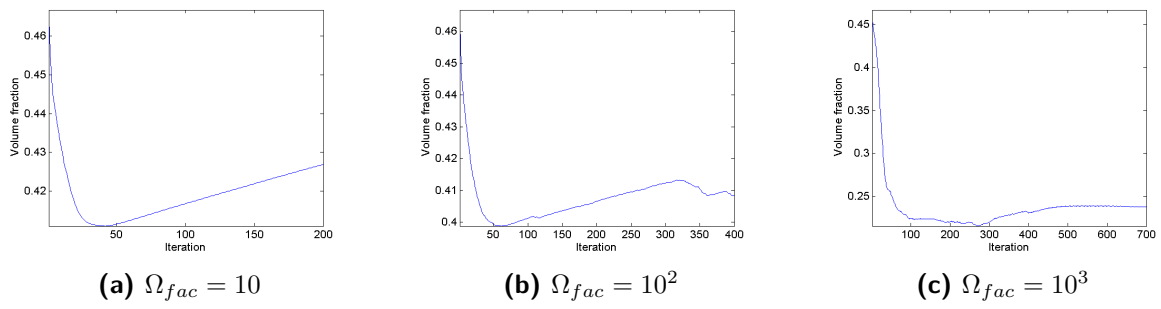


Figure C-6: Volume fraction

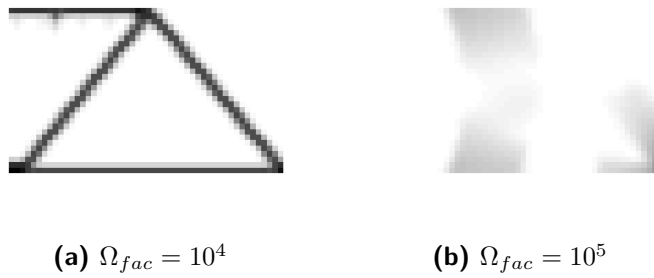


Figure C-7: Topology

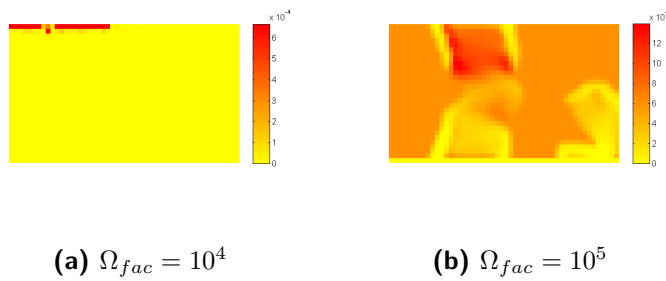


Figure C-8: Ω^*

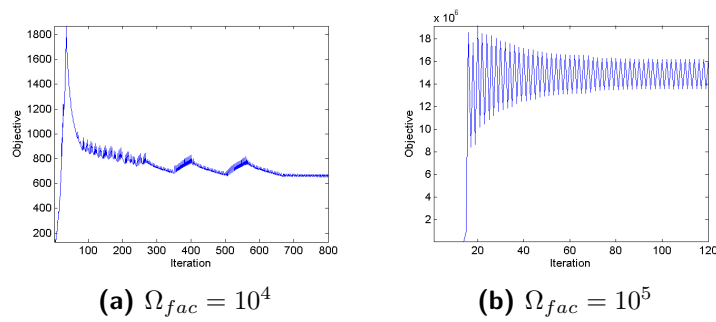


Figure C-9: Objective value

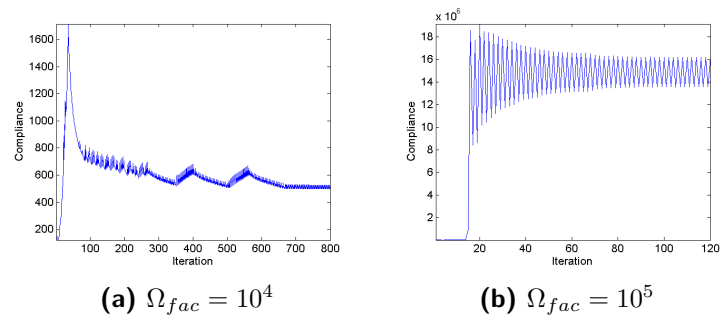


Figure C-10: Compliance value

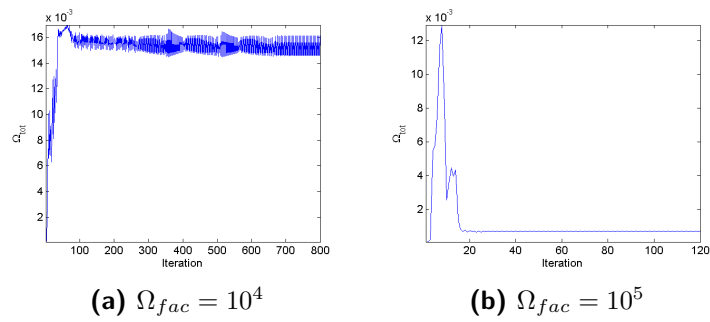


Figure C-11: Overhang coefficient value

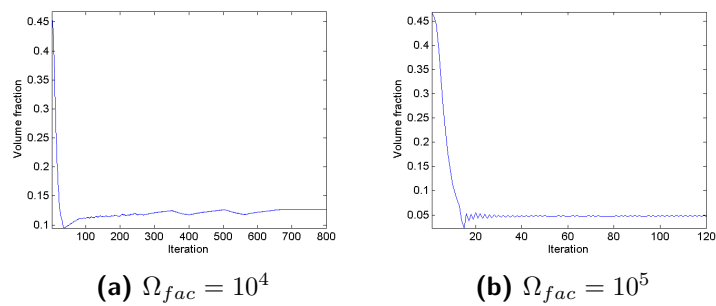


Figure C-12: Volume fraction

C-1-2 Mid-loaded cantilever beam

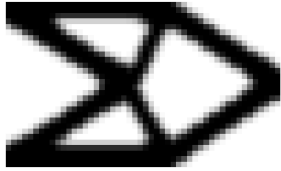
(a) $\Omega_{fac} = 10$ (b) $\Omega_{fac} = 10^2$ (c) $\Omega_{fac} = 10^3$

Figure C-13: Topology

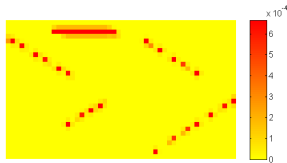
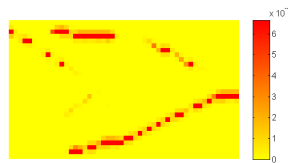
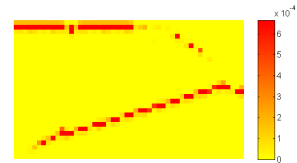
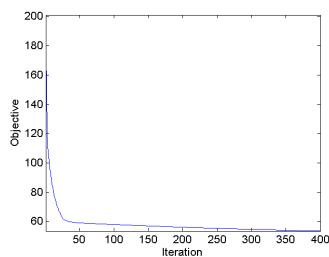
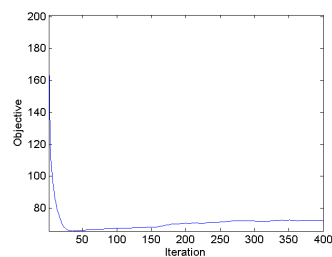
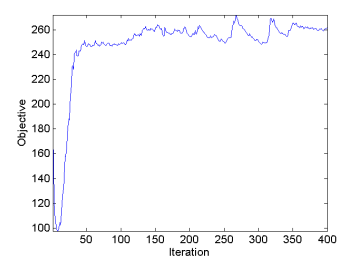
(a) $\Omega_{fac} = 10$ (b) $\Omega_{fac} = 10^2$ (c) $\Omega_{fac} = 10^3$ Figure C-14: Ω^* (a) $\Omega_{fac} = 10$ (b) $\Omega_{fac} = 10^2$ (c) $\Omega_{fac} = 10^3$

Figure C-15: Objective value

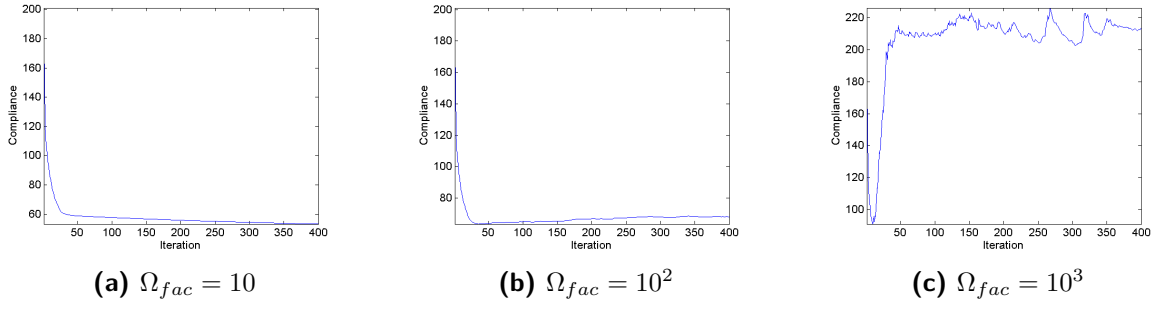


Figure C-16: Compliance value

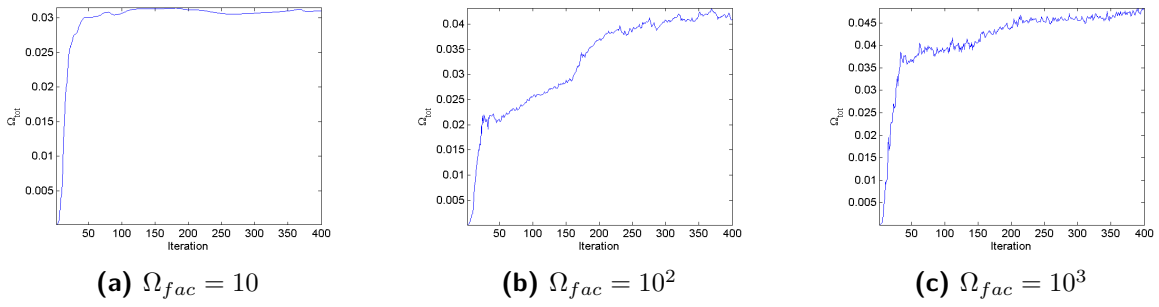


Figure C-17: Overhang coefficient value

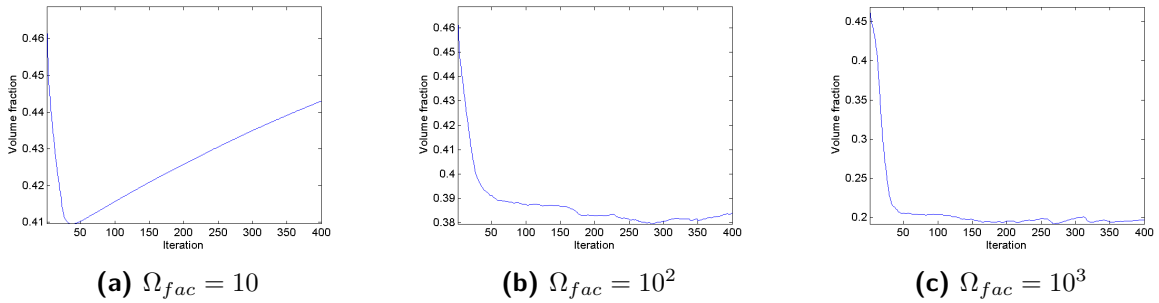
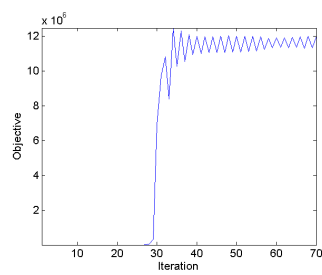
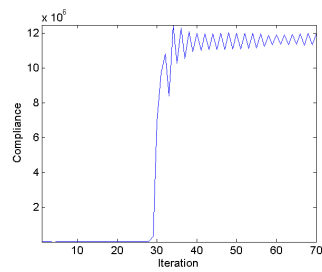
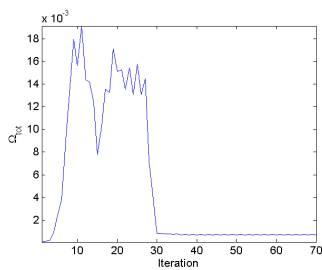


Figure C-18: Volume fraction



(a) $\Omega_{fac} = 10^4$

Figure C-19: Topology

(a) $\Omega_{fac} = 10^4$ **Figure C-20: Ω^*** (a) $\Omega_{fac} = 10^4$ **Figure C-21: Objective value**(a) $\Omega_{fac} = 10^4$ **Figure C-22: Compliance value**(a) $\Omega_{fac} = 10^4$ **Figure C-23: Overhang coefficient value**

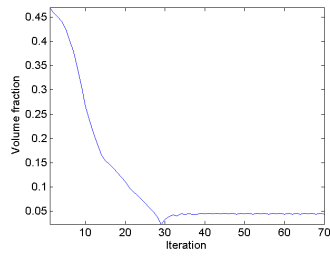
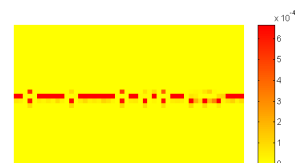
(a) $\Omega_{fac} = 10^4$

Figure C-24: Volume fraction

C-1-3 Tension beam

(a) $\Omega_{fac} = 10$ (b) $\Omega_{fac} = 10^2$ (c) $\Omega_{fac} = 10^3$

Figure C-25: Topology

(a) $\Omega_{fac} = 10$ (b) $\Omega_{fac} = 10^2$ (c) $\Omega_{fac} = 10^3$ Figure C-26: Ω^*

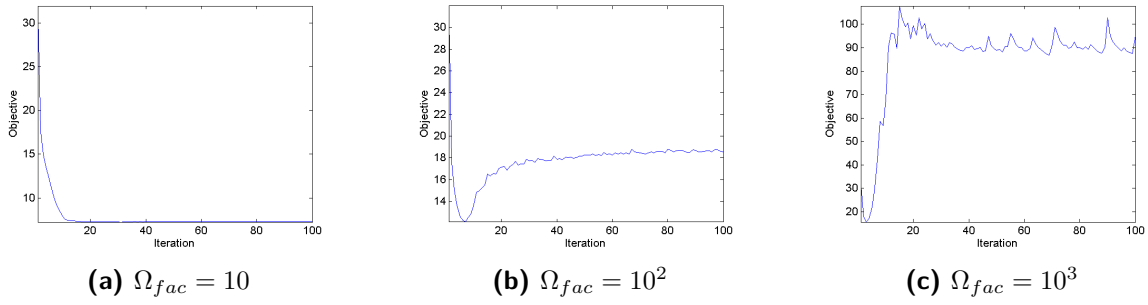


Figure C-27: Objective value

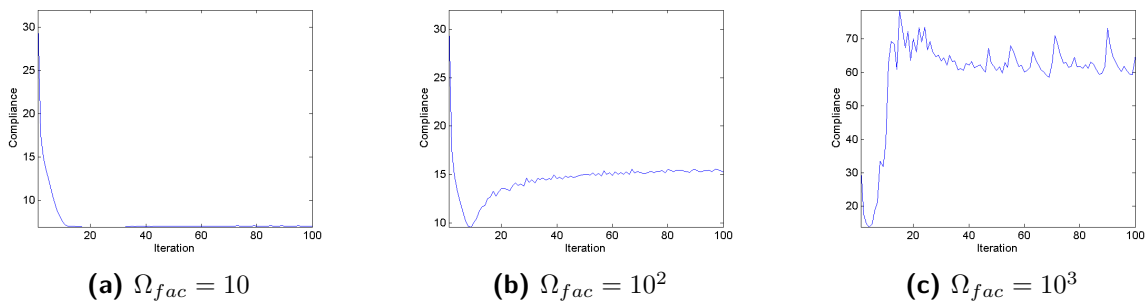


Figure C-28: Compliance value

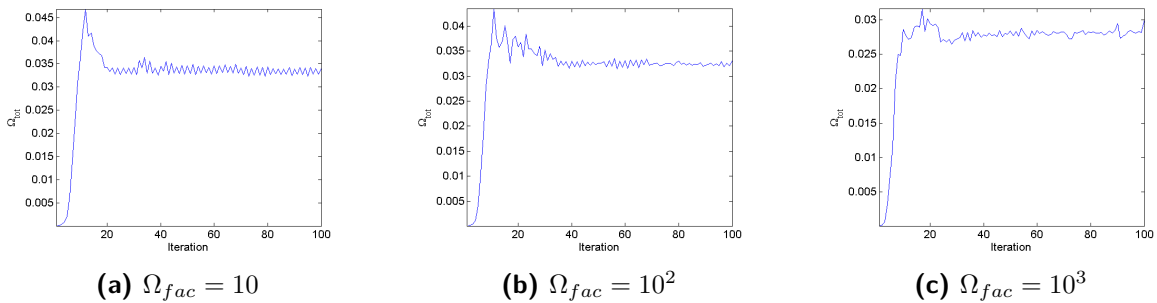


Figure C-29: Overhang coefficient value

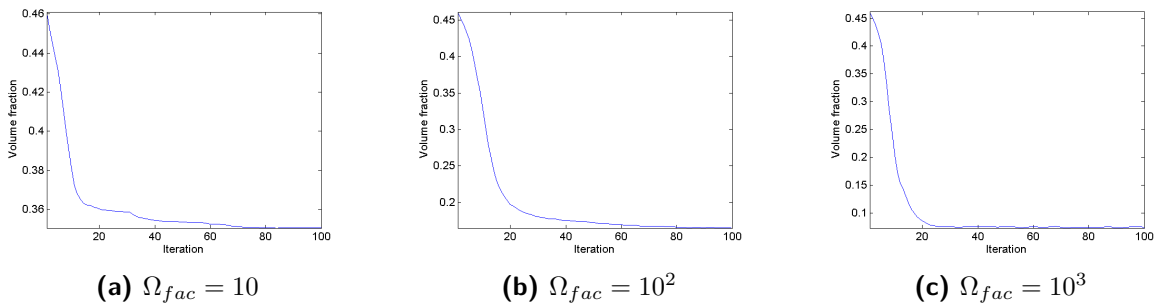


Figure C-30: Volume fraction

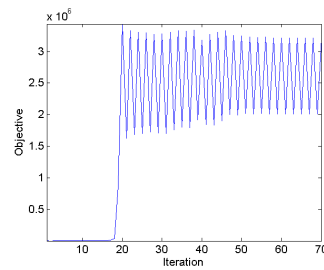
(a) $\Omega_{fac} = 10^4$

Figure C-31: Topology



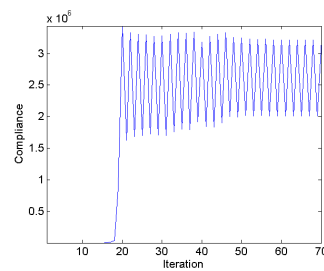
(a) $\Omega_{fac} = 10^4$

Figure C-32: Ω^*

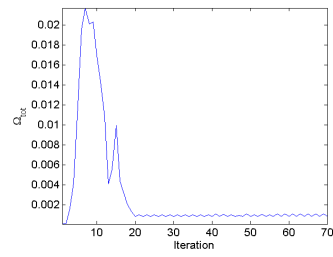


(a) $\Omega_{fac} = 10^4$

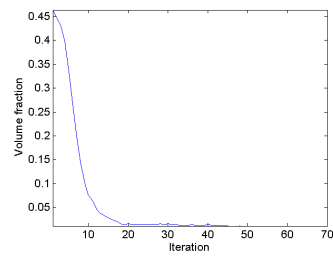
Figure C-33: Objective value



(a) $\Omega_{fac} = 10^4$



(b) $\Omega_{fac} = 10^4$

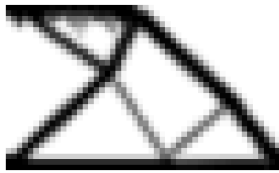


(c) $\Omega_{fac} = 10^4$

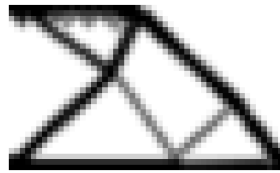
Figure C-34: Volume fraction

C-2 Global constraint

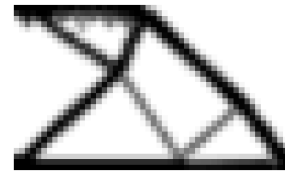
C-2-1 Corner-loaded cantilever beam



(a) $\Omega_{fac} = 10$



(b) $\Omega_{fac} = 10^2$



(c) $\Omega_{fac} = 10^3$

Figure C-35: Topology



(a) $\Omega_{fac} = 10$

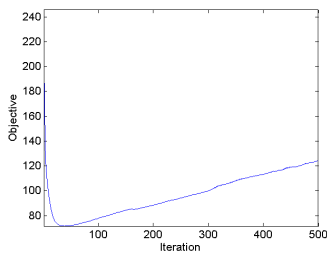


(b) $\Omega_{fac} = 10^2$

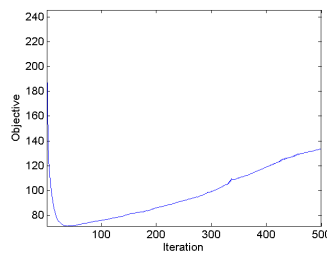


(c) $\Omega_{fac} = 10^3$

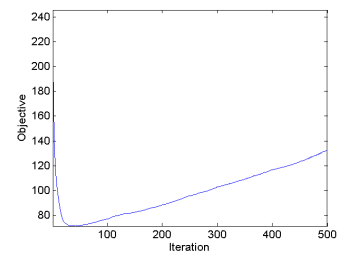
Figure C-36: Ω^*



(a) $\Omega_{fac} = 10$



(b) $\Omega_{fac} = 10^2$



(c) $\Omega_{fac} = 10^3$

Figure C-37: Objective value

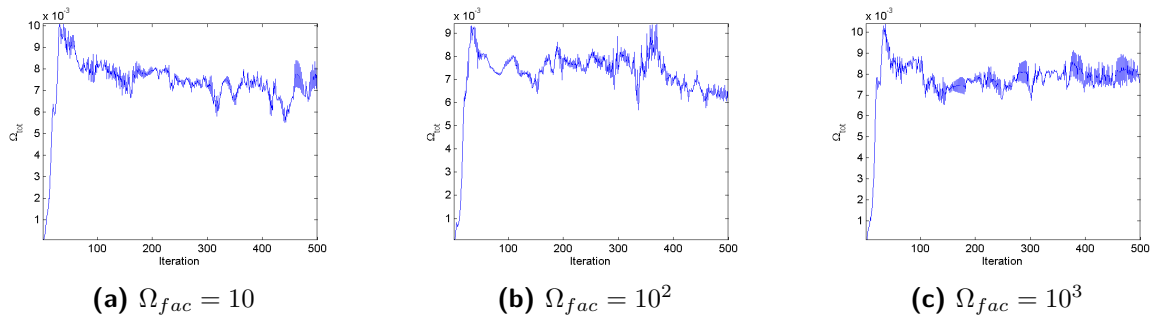


Figure C-38: Overhang coefficient value

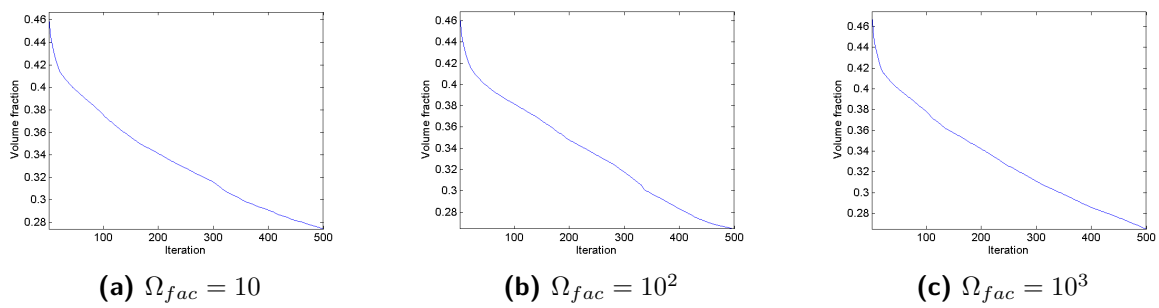


Figure C-39: Volume fraction

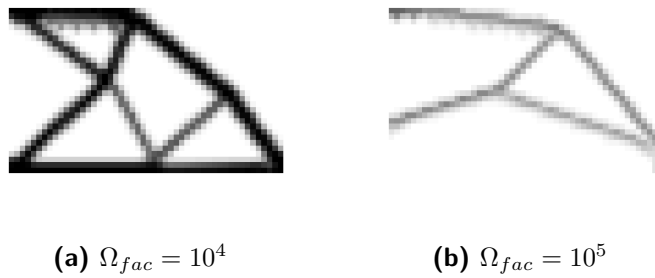


Figure C-40: Topology

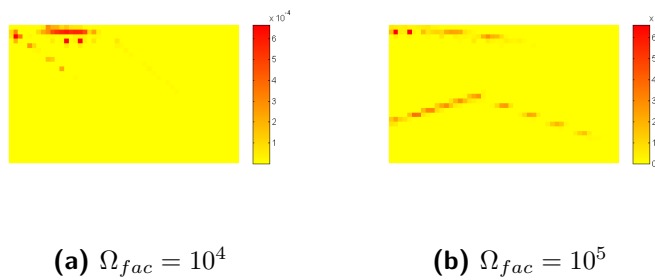


Figure C-41: Ω^*

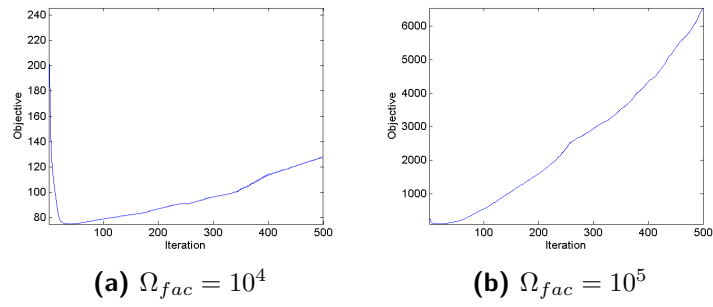


Figure C-42: Objective value

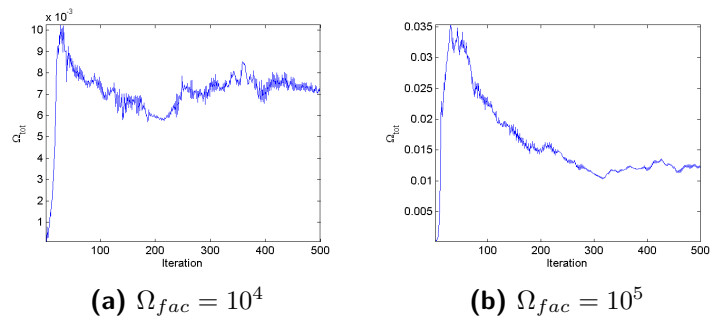


Figure C-43: Overhang coefficient value

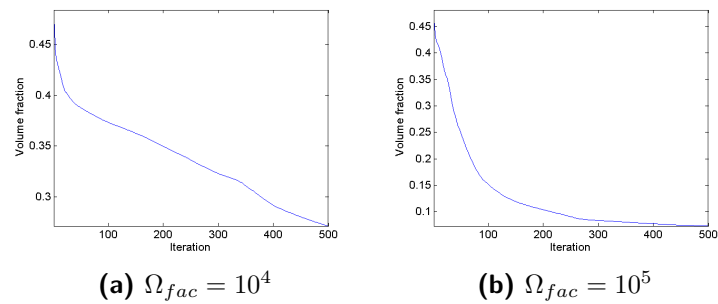


Figure C-44: Volume fraction

C-2-2 Mid-loaded cantilever beam

(a) $\Omega_{fac} = 10$ (b) $\Omega_{fac} = 10^2$ (c) $\Omega_{fac} = 10^3$

Figure C-45: Topology

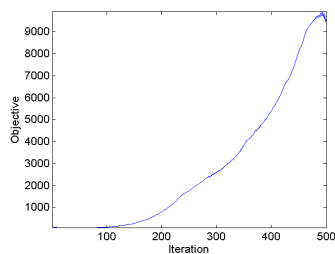
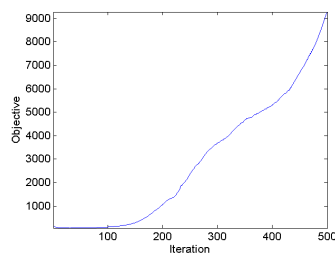
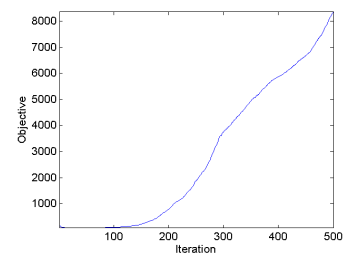
(a) $\Omega_{fac} = 10$ (b) $\Omega_{fac} = 10^2$ (c) $\Omega_{fac} = 10^3$ Figure C-46: Ω^* (a) $\Omega_{fac} = 10$ (b) $\Omega_{fac} = 10^2$ (c) $\Omega_{fac} = 10^3$

Figure C-47: Objective value

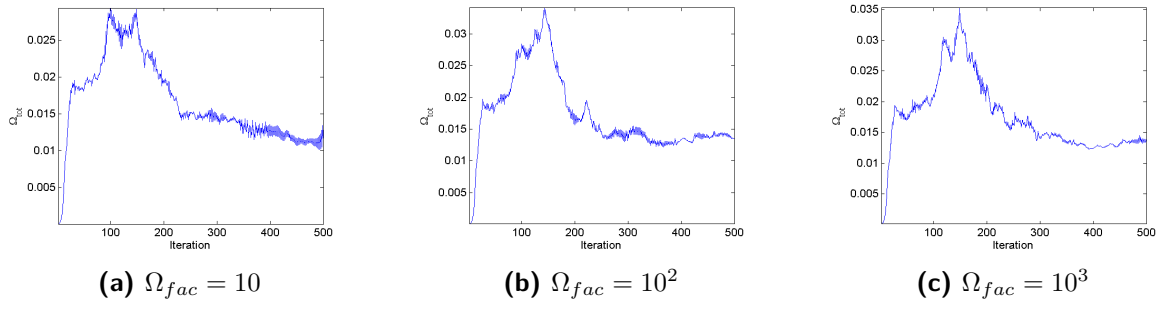


Figure C-48: Overhang coefficient value

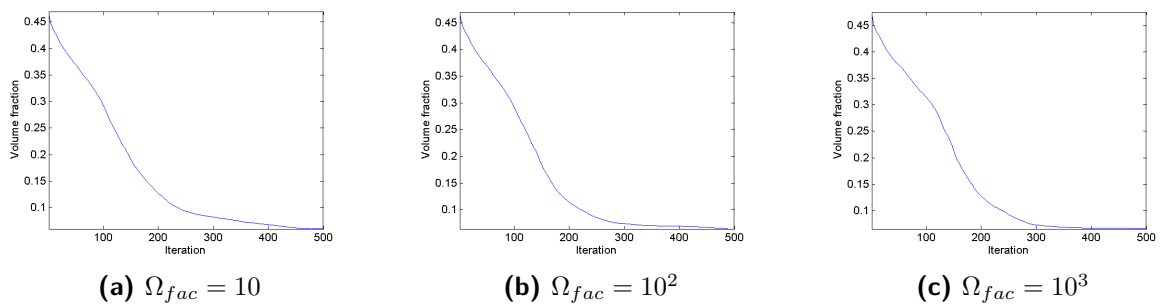


Figure C-49: Volume fraction

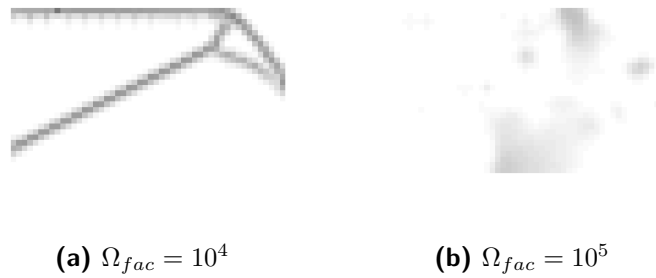


Figure C-50: Topology

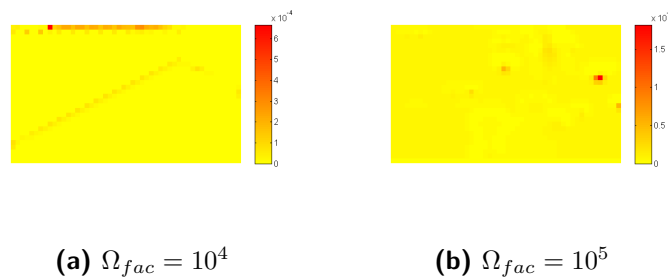


Figure C-51: Ω^*

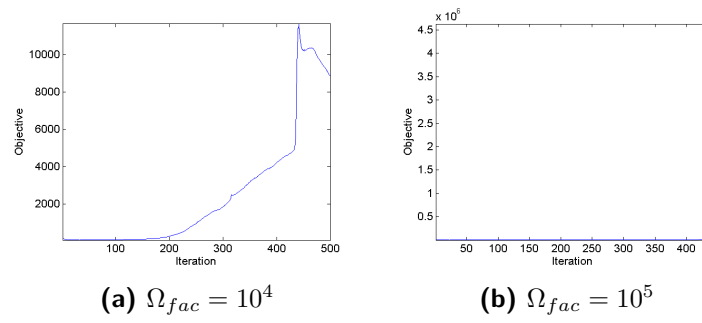


Figure C-52: Objective value

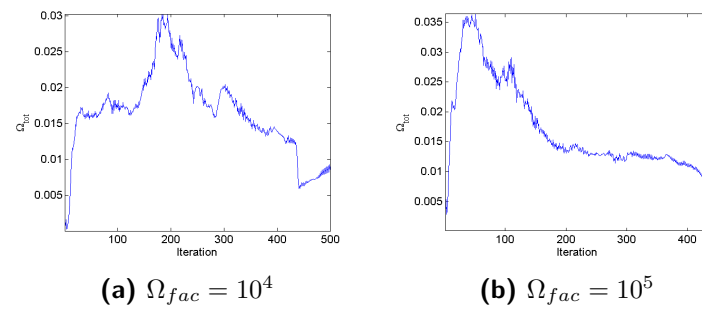


Figure C-53: Overhang coefficient value

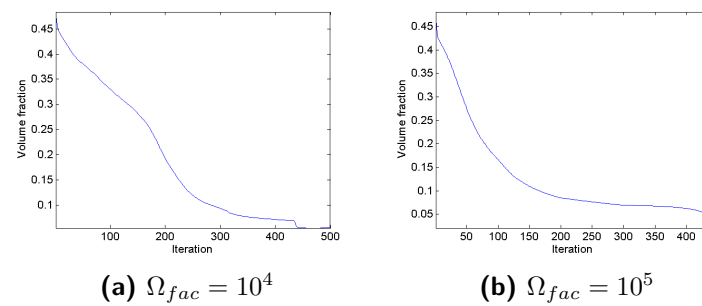


Figure C-54: Volume fraction

C-2-3 Tension beam



(a) $\Omega_{fac} = 10$

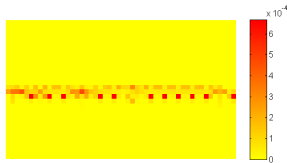


(b) $\Omega_{fac} = 10^2$



(c) $\Omega_{fac} = 10^3$

Figure C-55: Topology



(a) $\Omega_{fac} = 10$

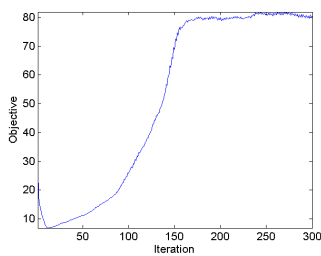


(b) $\Omega_{fac} = 10^2$

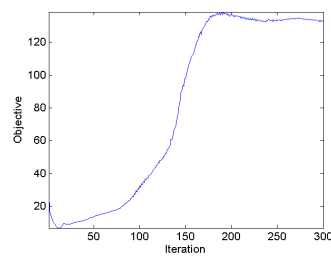


(c) $\Omega_{fac} = 10^3$

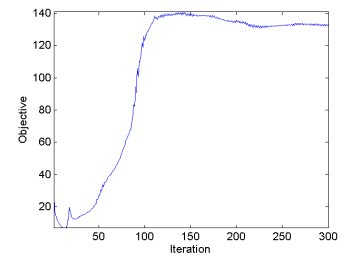
Figure C-56: Ω^*



(a) $\Omega_{fac} = 10$



(b) $\Omega_{fac} = 10^2$



(c) $\Omega_{fac} = 10^3$

Figure C-57: Objective value

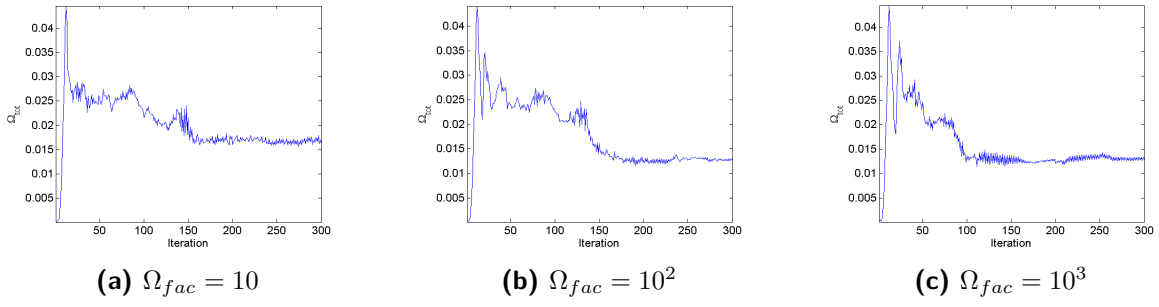


Figure C-58: Overhang coefficient value

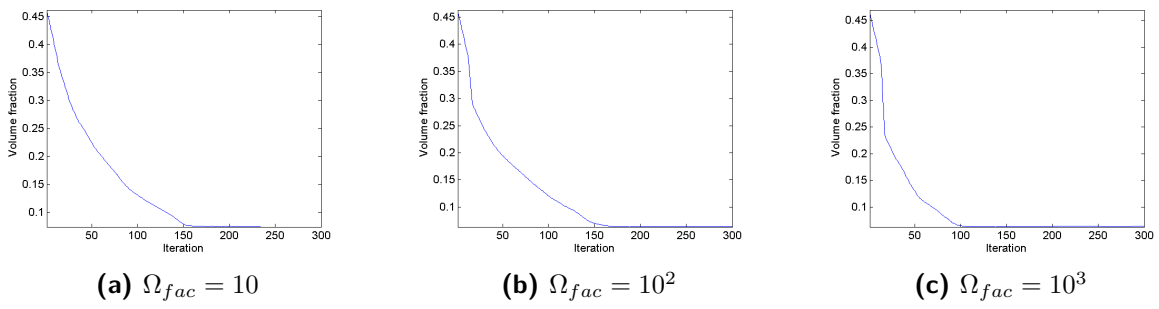


Figure C-59: Volume fraction



Figure C-60: Topology

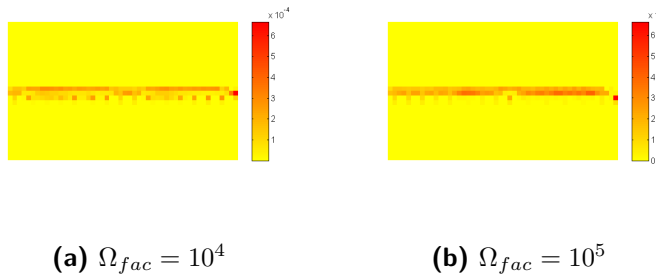


Figure C-61: Ω^*

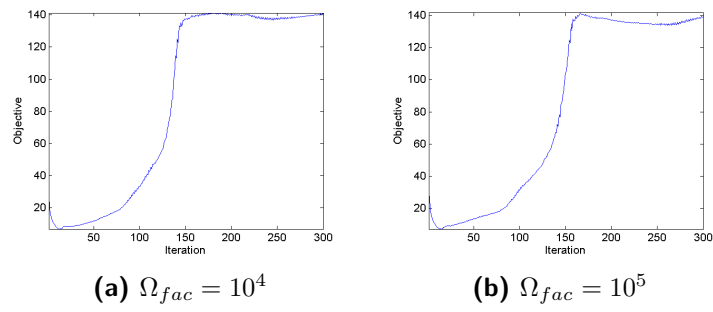


Figure C-62: Objective value

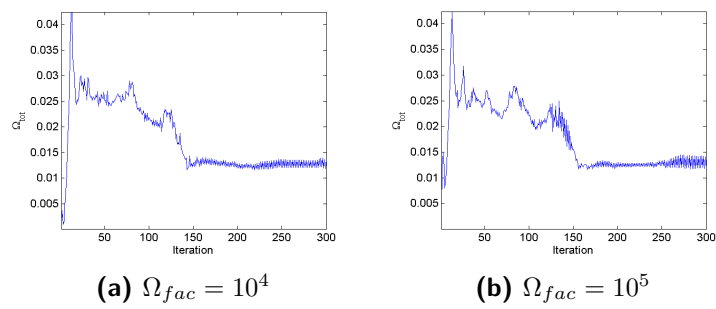


Figure C-63: Overhang coefficient value

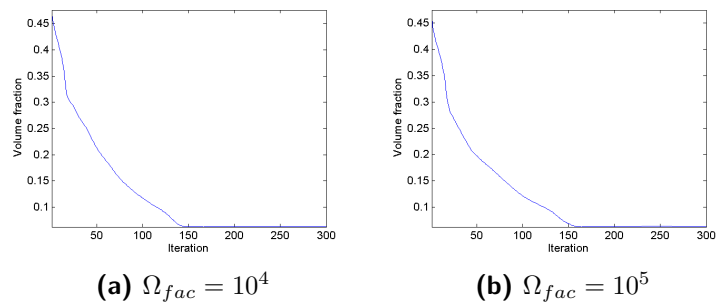


Figure C-64: Volume fraction

C-3 Filter

C-3-1 Corner-loaded cantilever beam

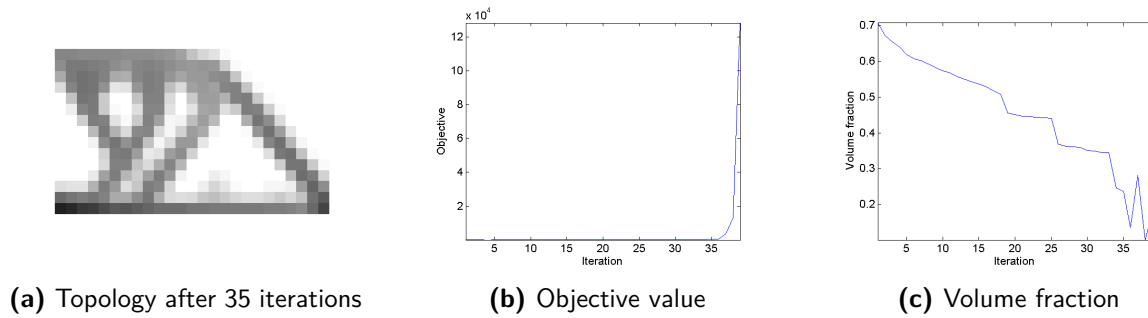


Figure C-65: Corner-loaded cantilever beam

C-3-2 Mid-loaded cantilever beam

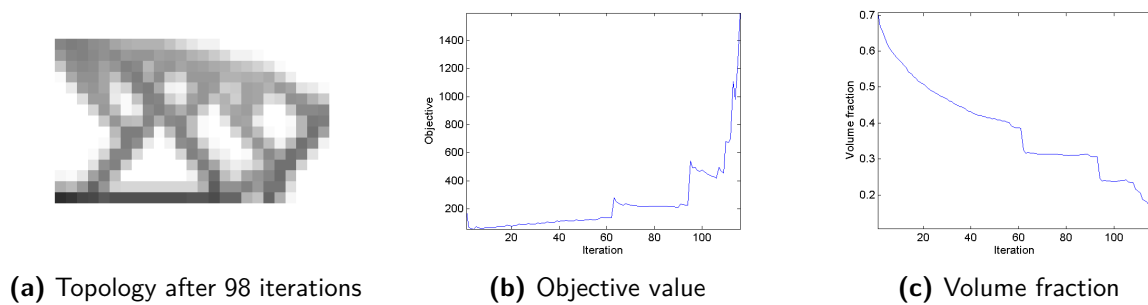


Figure C-66: Mid-loaded cantilever beam

C-3-3 Tension beam

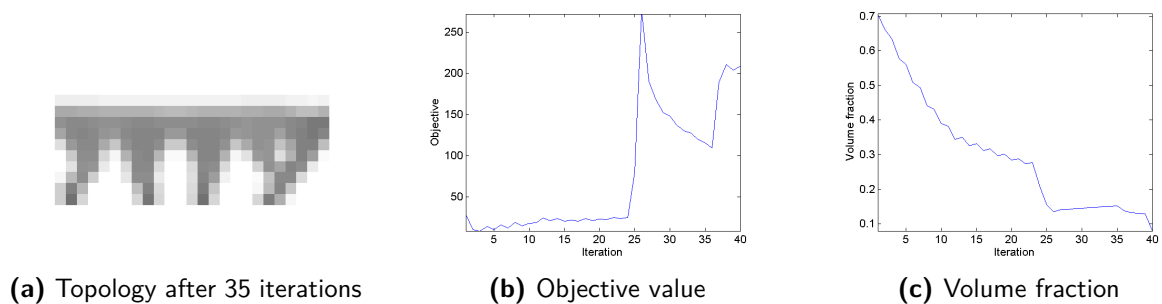


Figure C-67: Tension beam

Bibliography

- [1] W. Meiners, C. Over, K. Wissenbach, and R. Poprawe, “Direct generation of metal parts and tools by selective laser powder remelting (slpr),” *Proceedings of SFF, Austin, Texas*, 1999.
- [2] D. Thomas, *The development of design rules for selective laser melting*. PhD thesis, University of Wales, 2010.
- [3] M. R. Serphos, “Design of a metallic industrial part for selective laser melting.”
- [4] M. P. Bendsoe and O. Sigmund, *Topology optimization: theory, methods and applications*. Springer, 2003.
- [5] D. Brackett, I. Ashcroft, and R. Hague, “Topology optimization for additive manufacturing,” in *22nd Annual International Solid Freeform Fabrication Symposium*, pp. 348–362, 2011.
- [6] M. Zhou, R. Fleury, Y.-K. Shyy, H. Thomas, and J. Brennan, “Progress in topology optimization with manufacturing constraints,” in *Proceedings of the 9th AIAA MDO conference AIAA-2002-4901*, 2002.
- [7] E. Andreassen, A. Clausen, M. Schevenels, B. S. Lazarov, and O. Sigmund, “Efficient topology optimization in matlab using 88 lines of code,” *Structural and Multidisciplinary Optimization*, vol. 43, no. 1, pp. 1–16, 2011.
- [8] K. Svanberg, “The method of moving asymptotes—a new method for structural optimization,” *International journal for numerical methods in engineering*, vol. 24, no. 2, pp. 359–373, 1987.

Glossary

List of Acronyms

AM	Additive Manufacturing
SLM	Selective Laser Melting
FEA	Finite Element Analysis
CFRP	Carbon Fiber Reinforced Polymer
A-ADS	Antenna - Articulated Deployment System
S/C	spacecraft
TED	Thermo-elastic deformation
CTE	coefficient of thermal expansion
DfAM	design for additive manufacturing
SIMP	Solid Isotropic Material Penalization
MMA	Method of Moving Asymptotes

List of Symbols

c	Compliance of the material lay-out
U	Global displacement vector
F	Force vector
K	Global stiffness matrix
u_e	Element displacement vector

\mathbf{k}_e	Element stiffness matrix
$\boldsymbol{\rho}$	Vector of design variables
$\boldsymbol{\rho}_{min}$	Vector of minimum relative densities
N	Number of elements used to discretize design domain
p	Penalization power
$V(\boldsymbol{\rho})$	Material volume
V_0	Design domain volume
f	Prescribed volume fraction
ρ_{max}	The maximum value of the included density values
p_n	A parameter that influences how well the true maximum value is approximated
a	The element number for $a = 1 \dots k$
k	The number of elements being evaluated
ρ_i	The density value of element i
Ω_{tot}	A function that defines a value for the level of overhang
Ω_{fac}	A weight factor for the additional overhang term
M	A parameter that controls the steepness of the logistic function curve
x	The independent variable in the logistic function
\mathbf{F}	A convolution matrix representing a density filter
$\tilde{\boldsymbol{\rho}}$	Vector of filtered densities
err	Error introduced by P-norm
GL	Ghost-layer width
n_x	Number of elements along the x-axis of the design domain
n_y	Number of elements along the y-axis of the design domain
n_z	Number of elements along the z-axis of the design domain (in 3D)
S_i	The supportivity of element i
S_{max_i}	The maximum value of the supportivity of the candidate support elements for element i
ρ_{max_i}	The maximum density of the candidate support elements for element i